Site U1371[1]

Expedition 329 Scientists[2]

Chapter contents

Background and objectives

Integrated Ocean Drilling Program (IODP) Site U1371 (proposed Site SPG-12A) was selected as a drilling target because

- Its microbial activities and cell counts were expected to be characteristic of the upwelling zone just south of the southern gyre edge and
- Its basement age (~75 Ma) renders it a reasonable location for testing the extent of sediment-basement interaction in a moderately sedimented region of relatively old basaltic basement.

The principal objectives at Site U1371 were

- To document the habitats, metabolic activities, genetic composition, and biomass of microbial communities in subseafloor sediment with moderate microbial activity;
- To test how oceanographic factors control variation in sedimentary habitats, activities, and communities from gyre center to just outside the gyre margin;
- To quantify the extent to which these sedimentary microbial communities may be supplied with electron donors by water radiolysis; and
- To determine how sediment-basement exchange and potential activities in the basaltic basement vary with basement age and hydrologic regime (from ridge crest to abyssal plain).

Site U1371 (5301 meters below sea level [mbsl]) is in the South Pacific Gyre within a region of abyssal hill topography trending northeast–southwest (050°) with relief ranging from 50 to 100 m (Fig. **F1**). Abyssal hill spacing is ~5–8 km with very subdued fabric that has been smoothed by sedimentation. No obvious seamounts are observed, but a small conical feature ~200 m high is located ~4 km south-southeast of the coring site. The closest previous drilling site is Deep Sea Drilling Project Leg 29 Site 276, 800 nmi away.

The coring site is within magnetic polarity Chron 32n.2n, so the crustal age may range from 71.5 to 72.9 Ma (Gradstein et al., 2004). Based on a tectonic reconstruction of the region by Larson et al. (2002), the crust was accreted along the Pacific-Phoenix spreading center at ~73 Ma.

Many geological and geophysical characteristics of the target site were characterized by the Cruise KNOX-02RR site survey (**D'Hondt et al.,** 2011) (Figs. **F1, F2, F3, F4, F5, F6**). The shallow

[1] Expedition 329 Scientists, 2011. Site U1371. *In* D'Hondt, S., Inagaki, F., Alvarez Zarikian, C.A., and the Expedition 329 Scientists, *Proc. IODP,* 329: Tokyo (Integrated Ocean Drilling Program Management International, Inc.). doi:10.2204/iodp.proc.329.109.2011
[2] **Expedition 329 Scientists' addresses.**

doi:10.2204/iodp.proc.329.109.2011

sediment (0–5 meters below seafloor [mbsf]) consists of grayish brown to light yellowish brown siliceous ooze, with frequent burrows and bioturbation (D'Hondt et al., 2009). Smear slides contain abundant diatoms and some sponge spicules. D'Hondt et al. (2009) documented the presence of microbial cells throughout the uppermost 5 m of sediment at Site U1371. Dissolved oxygen was undetectable below ~1 mbsf (Fisher et al., 2009), and dissolved nitrate was undetectable below ~2.5 mbsf (D'Hondt et al., 2009). Cell concentrations were approximately two orders of magnitude higher at 5 mbsf than at similar depths in the South Pacific Gyre sites. Preliminary molecular study of archaeal 16S rRNA genes in three clone libraries (0.6, 1.5, and 2.1 mbsf) suggested the presence of Marine Crenarchaeota Group 1 (MG-1) and other non-MG-1 archaeal groups in shallow sediment (Durbin and Teske, 2010).

Operations

Transit to Site U1371

After a 51 h transit from Site U1370, covering 499 nmi and averaging 9.8 kt, the speed was reduced and thrusters were lowered. Dynamic positioning was initiated over Site U1371 at 0907 h on 2 December 2010. The position reference was a combination of GPS signals. No acoustic beacon was deployed, but a beacon remained on standby in the event of a loss of GPS satellite coverage. Whereas automatic input into the dynamic positioning system was not possible because of a system malfunction, it was possible to manually hold the vessel in position to clear the sea floor with the bottom-hole assembly (BHA) if necessary.

All times in this section are given in local ship time unless otherwise noted. For most of the expedition, local time was Universal Time Coordinated – 10 h.

Site U1371

Eight holes were drilled or cored at Site U1371 (Table T1). The first hole was a washdown hole drilled with the center bit in order to establish the sediment depth of 122.5 mbsf. The entire time on site was plagued by high vessel heave, which hindered the advanced piston corer (APC) coring. The first APC hole at the site came back with a disturbed mudline core and was abandoned. The second attempt at a mudline resulted in an over penetration without securing mudline and was abandoned as well. The following three APC holes were successfully cored to refusal. With the remaining time, an additional two holes were cored for mudline cores. The advanced piston corer temperature tool (APCT-3) was deployed five times in Hole U1371D. Perfluorocarbon tracer (PFT) was pumped from Hole U1371E onward until the last core was on deck. APC system recovery for Site U1371 was 94.9%. A total of 46 cores were attempted while coring 410.0 m. The total length of core recovered at Site U1371 was 389.01 m (94.9% recovery).

Hole U1371A

Rig floor operations commenced at 0907 h on 2 December 2010. The trip to the seafloor was uneventful. The top drive was picked up, the drill string was spaced out, and the hole was spudded at 1845 h on 2 December. The washdown hole was drilled to determine depth of basement. Mudline was established as 5316.0 meters below rig floor (mbrf) using the drill bit–tagged depth. There were no anomalies detected during the washdown to basement. After drilling down, basement was established at 5438.5 mbrf (122.5 mbsf). Total depth of the hole was 5439.5 mbrf after the bit was advanced into basement to verify basement contact. The bit was pulled back above the seafloor, clearing the seafloor at 2350 h on 2 December and ending Hole U1371A.

Hole U1371B

After clearing the seafloor, the center bit was pulled by wireline, the vessel was offset 20 m west, and the drill string was spaced out to spud Hole U1371B. After making up the first APC core barrel, the core barrel was run to bottom on the wireline and fired from 5310 mbrf. The core barrel came back empty and the bit was repositioned to 5315 mbrf. Hole U1371B was spudded at 0300 h on 3 December. Seafloor depth was established at 5316.4 mbrf (5305.1 mbsl) with a mudline core. Vessel heave during spud-in was ~4 m. The first mudline core was too disturbed for science and the hole was terminated. One core was taken with a total recovery of 8.15 m for an overall recovery in Hole U1371B of 100.6%. After Core 329-U1371B-1H, the vessel moved 20 m north, ending Hole U1371B at 0300 h on 3 December.

Hole U1371C

Hole U1371C began at 0300 h after abandoning Hole U1371B. After offsetting the vessel 20 m north, Hole U1371C was spudded at 0445 h. Core 329-U1371C-1H came back with a full core barrel and no obvious mudline. Shoot depth was 5312 mbrf, which was 3 m higher than the shoot depth for Hole U1371B. The best explanation for another mudline failure was the high heave (>4 m) at the time of spudding. One core was taken in Hole U1371C, with a total recovery of 9.85 m (103.5%). Hole U1371C was abandoned after the first core and the vessel

moved 20 m east on 3 December, ending Hole U1371C at 0445 h.

Hole U1371D

Hole U1371D was spudded 20 m east of Hole U1371C at 0635 h on 3 December. Seafloor depth was established with a mudline core at 5311.1 mbrf (5299.9 mbsl). Orientation with the Flexit tool was done on Cores 329-U1371D-1H through 11H. APCT-3 measurements were taken on Cores 4H–6H, 8H, and 10H. All temperature measurements returned good data. While pulling Core 6H, the coring line parted at the wire rope socket and the core barrel and sinker bars fell back inside the drill pipe. The wireline was removed from the hole and reheaded at surface. The aft sinker bars were installed and a rotary core barrel was dropped to "fish" the forward sinker bars. The sinker bars were recovered by wireline, and Core 6H was recovered. Total time from the incident to resumption of coring was 5.5 h. Coring continued until refusal on Core 14H. The APC system was used to take 14 cores to 126.0 mbsf with 126.87 m recovery (100.7%). After Core 14H, the bit was advanced and rotated into basement to verify basement depth. The bit was tripped back to just above the seafloor, ending Hole U1371D at 1330 h on 4 December.

Hole U1371E

Hole U1371E began with the ship offset 20 m east of Hole U1471D. Hole U1371E was spudded at 1605 h on 4 December. Seafloor depth was established with a mudline core at 5310.2 mbrf. The APC system was used to take 14 cores to 128.2 mbsf with a 118.16 m recovery (92.2%). Nonmagnetic core barrels were used for the first 12 cores. PFT was mixed with the drilling fluid (seawater) and pumped on all cores for contamination testing. After Core 329-U1371E-14H, the bit was advanced and rotated into basement to confirm basement depth and tripped back to just above the seafloor, ending Hole U1371E at 1100 h on 4 December.

Hole U1371F

Hole U1371F was offset 20 m south of Hole U1371E. After making up the first APC core barrel, it was run to bottom on the wireline and Hole U1371F was spudded at 1205 h on 5 December. Seafloor depth was established with a mudline core at 5308.3 mbrf. The APC system was used to take 14 cores to 130.6 mbsf with a 118.44 m recovery (90.7%). PFT was mixed with the drilling fluid (seawater) and pumped on all cores for contamination testing. After Core 329-U1371F-14H, the bit was advanced and rotated into basement to verify basement depth and APC advance. The drill string was tripped to just above the seafloor, ending Hole U1371F at 0655 h on 6 December.

Hole U1371G

Hole U1371G was offset 20 m south of Hole U1371F. After making up the first APC core barrel, the core barrel was run to bottom on the wireline and Hole U1371G was spudded at 0755 h on 6 December. Seafloor depth was established with a mudline core at 5314.1 mbrf. The APC system was used to take a single core to 1.4 mbsf with a 1.37 m recovery (97.9%). PFT was mixed with the drilling fluid (seawater) and pumped in for contamination testing. After taking mudline Core 329-U1371G-1H, a second core (test Core 329-U1371G-2H) was taken for training purposes. The drill string was tripped to just above the seafloor, ending Hole U1371G at 0945 h on 6 December.

Hole U1371H

Hole U1371H was offset 20 m west of Hole U1371G. After making up the first APC core barrel, the core barrel was run to bottom on the wireline and Hole U1371H was spudded at 1030 h on 6 December. Seafloor depth was established with a mudline core at 5310.3 mbrf. The APC system was used to take a single core to 6.2 mbsf with a 6.19 m recovery (99.8%). PFT was mixed with the drilling fluid (seawater) and pumped in for contamination testing. After taking mudline Core 329-U1371H-1H, the drill string was tripped to the surface, clearing the rotary table at 2326 h on 6 December. The rig floor was secured for the 1172 nmi transit to Auckland, New Zealand, ending the final hole and site of Expedition 329 at 2326 h on 6 December.

Lithostratigraphy

The sediment at Site U1371 consists of ~130 m of diatom ooze and pelagic clay (Fig. **F7**). The strata of the site's seven APC-cored holes are divided into two lithologic units based on their markedly different mineralogy. Here we will describe the sediment that was recovered from Holes U1371D–U1371F. Because they represent full penetrations of the sediment, shipboard sedimentologists, geochemists, and microbiologists relied on these holes primarily to characterize the subseafloor environment at Site U1371. Consequently, detailed descriptions of sediment recovered in Holes U1371B, U1371C, U1371G, and U1371H will not be included. See **"Core descriptions"** for images, basic visual descriptions, and data pertaining to the sediment in those holes.

The two lithologic units at Site U1371 have sharply contrasting mineralogies. Unit I is ooze with average

diatom and clay content of 56% and 17%, respectively. It is 104–107 m thick and contains numerous ash layers and multiple thin hardgrounds. Unit II is a blend of clay (32%), zeolite (30%), and red-brown to yellow-brown semiopaque iron manganese oxides (RSO; 15%). It contains an average modal abundance of up to 26% diatoms, but only in the upper 5 m of the unit where the lithology transitions from ooze to clay. Other minor constituents of the sediment include quartz, pyrite, manganese oxide/hydroxide, and biogenic particles including radiolarians, spicules, and silicoflagellates.

The clay-bearing diatom ooze and pelagic clay at Site U1371 form interbedded intervals of highly fossiliferous and clay-rich layers. Bioturbation is a prominent feature of the sediment and causes diffuse boundaries on most beds. Numerous coring-related disturbances and whole-round core sampling affect our ability to correlate specific intervals among the holes of Site U1371. In a broad sense, however, the overall sediment thickness and composition appear to be very uniform (Fig. **F8**).

Description of units

Unit I

Intervals: 329-U1371D-1H-1, 0 cm, to 12H-2, 20 cm; 329-U1371E-1H-1, 0 cm, to 12H-1, 100 cm; 329-U1371F-1H-1, 0 cm, to 12H-3, 76 cm

Depths: Hole U1371D = 0–104.10 mbsf, Hole U1371E = 0–104.20 mbsf, Hole U1371F = 0–107.96 mbsf

Lithology: clay-bearing diatom ooze

Unit I consists of three end-member colors: gray, olive, and brown (Fig. **F9A, F9B**). Pale olive-gray and greenish gray colors (5Y 6/2 and 5G 5/1 through 10GY 6/1 to 5GY 5/1) constitute the majority of Unit I's color. The two colors frequently blend together and change gradationally. The longest interval between color changes is ~5.5 m and occurs in the middle of the unit (e.g., Sections 329-U1371D-6H-3 through 6H-7). All olive and gray intervals are interrupted by numerous black (5GY 2.5) laminations, beds, and irregular lenses that are between ~1–2 mm and 6 cm thick. Brown sediment (10YR 5/3 through 2.5Y 6/3) is most common in the uppermost 6 m, the middle 7.5 m, (e.g., Sections 329-U1371D-4H-5 through 5H-3), and the lowermost 6 m of Unit I. Approximately 15 short brown intervals of 0.1–1 m fall between thicker layers of gray and olive ooze throughout the remainder of Unit I. Similar to the gray and olive intervals, the brown layers are interbedded with dark laminations, beds, and irregular patches. The dark sediment lying within the brown layers is dark gray (5Y 4/1). Thin (<5 cm) white, pink, dark green, and very dark brown layers are associated with ash beds and hardgrounds that are described below.

Smear slide analyses identify diatoms as the major component of Unit I (Fig. **F10A**); they constitute 31%–85% of the modal abundance of particles and are present in all layers except those that are >90% volcanic glass. Other biogenic particles in Unit I include siliceous spicules, radiolarian tests, and silicoflagellates. Like diatoms, spicules are present in all but the most volcanic of layers. Where present, their abundance ranges between 2% and 21% in roughly inverse proportions to diatom values. Average radiolarian abundance is 4.5% of the particles identified in smear slides. Radiolarians are present throughout the unit but are slightly more common (by 6%–10% above their average abundance) in the uppermost 6 m and in two very thin beds at 87 and 92 mbsf in Hole U1371D. Silicoflagellates are found above 8.5 mbsf and below 30.5 mbsf in Hole U1371D.

Clay, RSO, and quartz are the majority of accessory minerals at Site U1371. X-ray diffraction (XRD) analyses of samples drawn from clay-rich intervals in the uppermost part of Unit I reveal well-defined illite and chlorite patterns (Fig. **F11A**). Smectite is also present but only above 12 mbsf. The average modal abundance of clay in Unit I is ~18%. Although clay abundance varies from 5% to 30%, no clear trends are apparent. On the other hand, RSO demonstrates a clear pattern of decreasing abundance with increasing core depth. Maximum RSO abundance (47%) occurs in the uppermost 2 m below mudline, decreases sharply to ~10% at 3–4 mbsf, and is absent below 12 mbsf. All RSO grains are small (<50 µm) and subangular. Quartz grains have similar sizes and shapes but occur throughout Unit I. They occur in 85% of all smear slides with low modal abundances (<1%–7%).

Other accessory minerals are rare, restricted vertically, or exist in minute proportions. For example, pyrite is found only in the uppermost 10 m of Unit I and typically constitutes <2% of the sediment. Pyrite crystals are very small (<10–20 µm) and form euhedral pyritohedrons. The manganese oxyhydroxide nodules commonly associated with surface and shallowly buried sediments in the South Pacific were not observed in Unit I. However, black laminations (1–3 mm thick) occurring regularly throughout Unit I are composed of clay-sized particles that are probably manganese oxides or oxyhydroxides. The common zeolite, phillipsite, was not observed in smear slides; however, XRD analyses of clay-rich sediment in the uppermost 10 m of core contain peaks at 26.8° and 8.9°2θ that are strongly suggestive of phillipsite.

Unit I contains a minimum of 20 pumice and ash layers and 6 hardgrounds (Tables **T2, T3**). Pumice layers have low clay content and exhibit grainy tex-

tures and distinctive white to light gray color. Volcanic glass shards in the pumice are large (as large as 200 µm), highly angular, and possess smooth surfaces and edges that are free of discoloration, pits, or other obvious signs of alteration. Ash layers have smooth, claylike texture and variable colors that include white, green, and red-brown. Dark greenish gray hardgrounds consist of clay and biogenic debris. The debris consists of diatom girdles (very few valves were observed), fragmented radiolarian tests, and spicules.

Sediment consolidation increases with depth. Clay-bearing diatom ooze in the uppermost 10 mbsf is highly cohesive but easily deformed. Below 75 mbsf, sediment is very firm and brittle. Hardgrounds are particularly compact and difficult to divide for sampling purposes. Regardless of the vertical position of the ash and pumice layers, they are easily disaggregated into individual clay particles and glass shards.

Bedding and bioturbation structures are the dominant features of Unit I. Bedding exists across a broad spectrum of thicknesses from ~1 mm ashy laminations to 1.5 m sections of uninterrupted diatom ooze. Bedding contacts range from sharp, horizontal transitions that are common in clay-rich portions of Unit I to diffuse, barely perceptible transitions among adjacent layers of diatom ooze. The sediment lacks other primary sedimentary structures (e.g., cross-laminations, graded bedding, and so on).

Burrowing organisms impacted most sedimentary layers. With a frequency of at least one per core, extensive bioturbation created thick beds (10 cm to 1.5 m) of homogenized clay-bearing diatom ooze. On a much finer scale (1–3 cm), burrowing organisms blended and broadened bedding contacts among diatom, clay, ash, and other mineral components of individual layers. Although few burrows are distinct, large (~2 cm), subhorizontal, elliptical *Planolites* are evident in the uppermost 10 m, and small (~2–4 mm), subvertical *Chrondrites* burrows are faintly visible in the lower diatom ooze. The *Chondrites* burrows are especially well defined in the 2–10 cm of sediment that lies beneath thick ash layers in Section 329-U1371D-3H-6. The further redistribution of volcanogenic sediment is illustrated by a pair of glass-filled burrows in the lower part of Unit I (Section 329-U1371D-11H-3). These large (1.5 cm diameter × 8 cm length) horizontal and vertical burrows are part of a *Thalassinoides* network and are filled with light gray volcanic glass. The volcanogenic fill in these burrows is particularly interesting given that the nearest overlying ash layer is ~6 m upcore.

Sediment structures related to the volcanogenic sediment in Unit I are generally the most well preserved. The basal contacts of many ash layers are sharp despite disturbances by small burrowing organisms. The upper contacts of the ash/pumice layers typically show more significant bioturbation. The absence of detectable ash layers in the middle of Unit I (Table T2) is likely related to bioturbation given the following three reasons:

- The absence of an ash layer in the middle of Unit I is anomalous compared to the high frequency of ash layers in the uppermost third and lowermost sections of Unit I,
- Preserved burrows in the uppermost and lowermost parts of Unit I contain ash/pumice, and
- Smear slide analyses show minor amounts of volcanic glass in many slides prepared from the mottled diatom ooze found throughout Unit I.

Unit II

Intervals: 329-U1371D-12H-2, 20 cm, to 14H-4, 130 cm; 329-U1371E-12H-1, 100 cm, to 14H-5, 80 cm; 329-U1371F-12H-3, 76 cm, to 14H-5, 10 cm

Depths: Hole U1371D = 104.10–127.2 mbsf, Hole U1371E = 104.20–129.0 mbsf, Hole U1371F = 107.96–129.12 mbsf

Lithology: clay (including pelagic clay, zeolitic pelagic clay, and diatom-bearing clay)

Unit II includes a variety of brown colors that become increasingly darker with depth (Fig. F9C–F9E). At its uppermost contact, the unit consists of a mixture of medium brown (2.5Y 6/2) clay with thin layers and irregular lenses and ellipses of very pale brown (10YR 8/4). The clay that forms the majority of the sediment darkens to dark grayish brown (10YR 4/2) and eventually very dark gray (10YR 3/1) in the 2 m that overlies the lowest recovered sediment. The very pale brown lenses and ellipses become less common and darken to light yellowish brown (10YR 6/3) in the lower part of Unit II. Black sediment occurs as small (~1–20 mm), spherical, granular masses that occur irregularly throughout the entire unit and in five large (4–7 cm) nodules found in Holes U1371E and U1371F (Fig. F9D). Light red (2.5YR 7/6) clay fills 7 burrows found in Section 329-U1371D-12H-1 and >20 burrows found in Sections 329-U1371F-12H-1 and 12H-2.

Smear slide analyses show that Unit II is clay with varying amounts of phillipsite, RSO, volcanic glass, and biogenic particles and minor amounts of quartz and manganese oxide (Fig. F10B). On average, clay comprises the majority component of Unit II. Modal concentrations range from 0%–11% to 68%–77%. Where lower concentrations exist, RSO, phillipsite, or volcanic glass are the dominant particles. Clay mineralogy changes slightly through Unit II. In the uppermost 6 m, XRD results show well-defined illite

peaks (Fig. F11B). In the lowermost 12 m, diffraction peak intensities corresponding to illite decrease by 50% and peak areas broaden by ~2°2θ, changes that are somewhat suggestive of smectite.

Phillipsite is a major component of Unit II that is unevenly distributed. Although it is visibly absent from the uppermost 6 m, distinctive diffraction peaks from Sample 329-U1371D-12H-5 indicate phillipsite is probably a minor constituent of this interval (Fig. F11B). A similar set of conflicting results exists in the lower half of Unit II, where smear slide analyses indicate phillipsite is the majority (~60%) component of the clay, whereas XRD diffractograms show decreased (~30%) phillipsite peak intensities. Where visible, the phillipsite crystals are single laths and twinned crosses that are typically <10 µm × 40–60 µm and subhedral. The phillipsite crystals are heavily pitted (Fig. F10B).

Unit II clay is moderately metalliferous, containing both RSO and manganese oxide-oxyhydroxide. RSO is not present in the uppermost 8 m of Unit II. Through the middle 10 m of Unit II, RSO abundance fluctuates erratically between <1% and 100%. In the lowermost 4 m, RSO maintains a constant presence with a range of modal abundance between 30% and 42%. Although RSO is amorphous and thus difficult to quantify using XRD (Kastner, 1986), diffractograms from five samples spanning Unit II support smear slide results. Specifically, the characteristic broad hump (between 20.5° and 22°2θ) that is associated with RSO is not present in the samples drawn from the uppermost 10 m of Unit II but is present in the XRD patterns from the samples drawn from the lowermost 4 m of Unit II (Fig. F11B).

Manganese oxide-oxyhydroxide grains and nodules occur between ~110 and 120 mbsf. In the upper part of this interval, small (1–2 mm) spherical to medium (2 cm) elliptical black granular masses lie along burrow walls, bedding surfaces, and randomly in the intervening sediment. The masses are aggregated clay-sized grains. XRD analyses included one of the masses as part of the bulk sediment sample. Diffraction patterns for typical manganese oxides and oxyhydroxides (e.g., ramsdellite, manganite, romanèchite, etc.) could not be resolved in the resulting diffractograms. Five manganese nodules were recovered in Holes U1371E and U1371F. The nodules range in size from 2 to 4 cm and are situated between horizontal burrows and bedding planes.

Volcanogenic components of Unit II include glass shards and ash. Volcanic glass shards are small (<10 µm × <30 µm), angular, and exhibit pitted surfaces and edges. The glass particles demonstrate a nearly symmetrical distribution of abundance. They are absent in the uppermost and lowermost 1 m and increase in abundance toward the midpoint of the unit, where their abundance peaks at 29% to 37% of the sediment. Light red clay, likely the alteration product of volcanic ash, fills 7 *Planolites* burrows in Core 329-U1371D-12H and >20 burrows in Core 329-U1371F-12H. A second ash layer, very pale brown and moderately indurated, lies ~4 m above the lowest recovered sediment and separates overlying medium brown and underling very dark brown sediment.

Quartz is a relatively minor constituent of Unit II. Its abundance is distributed unevenly, with 8%–11% in the uppermost 8 m and 0% through the remainder of Unit II, except for the lowermost recovered in situ sedimentary layer where its abundance jumps to 100% of the particle abundance.

Biogenic particles, including diatoms, radiolarians, spicules, and silicoflagellates, are present in the transitional interval that separates Units I and II. In the uppermost 2 m of Unit II, they constitute as much as 47% of the sediment. However, their overall abundance in Unit II is ~5% because they are entirely absent below the upper 3 m that makes up the transition zone.

The upper half of Unit II is firm and pliable. The clay in the lower half of the unit is stiff and crumbly.

Bioturbation effects are the most pronounced sedimentary structures in Unit II. Throughout the uppermost 6 m, the diatom-bearing clay is mottled. Although their ichnofacies association is indeterminate, the numerous elliptical burrows (1–2 cm diameter) in the uppermost 50 cm of this interval are distinct because they are filled with red ash. Individual burrows become easily distinguishable ~7.5 m below the upper contact. Traces in this interval are transverse and longitudinal cross-sections through *Planolites* burrows. The increased visibility of the burrows is largely attributable to the development of "halo burrows" caused by reduction and loss of clay-bound iron associated with respiration of the burrowing animals (Ekdale, 1977). *Planolites* halos continue to be prominent in the lower third of Unit II, although they become far less common. The lowermost 60–80 cm of sediment has a mottled structure and a few small (1–4 mm diameter) burrows exhibiting both horizontal and vertical aspects (*Chondrites*?).

Bedding in Unit II is rare. The three different types of bedding observed in Unit II and the intervals they cover are as follows:

- Very pale brown layers (e.g., intervals 329-U1371D-12H-6, 60–73 cm; 13H-3, 0–16 cm; 13H-4, 87–92 cm; and 14H-4, 65–72 cm) are much thicker (5–10 cm average) and more uni-

form than any of the burrows in Unit II. Thus, they are likely primary bedding sedimentary structures although they contain evidence of being bioturbated.
- Thin, indurated, granular ash beds in Sections 329-U1371D-14H-1, 329-U1371E-14H-3, and 329-U1371F-14H-2 are disturbed by bioturbation but maintain distinctly horizontal bedding attitudes.
- Numerous very thinly bedded (2 cm thick) light brown and medium brown laminations (<1 cm thick) form bedding couplets in the interval between 113 and 119 mbsf. Many couplets are accompanied by manganese oxide-oxyhydroxide laminations. The couplets have diffuse boundaries and contain frequent thickenings and terminations indicative of bioturbation. However, given their frequency (>30 couplets), similarity, and horizontal attitude, it is likely that the couplets are depositional bedding features.

Sediment/Basalt contact

Individual vitric grains and clusters of vitric grains were recovered in Holes U1371D–U1371F. In all holes, the grains lie in long (1–2 m) intervals of flow-in. The flow-in material is similar to the lowermost sediment of Unit II, very dark brown zeolitic metalliferous clay. The distribution of the grains along vertical streaks of deformed clay suggests the grains were created by the impact of the APC shoe on basement basalt and were subsequently sucked into the core barrel during recovery operations. Consequently, the sedimentary characteristics of the sediment/basalt contact could not be discerned at Site U1371.

The igneous grains are glassy and possess alternating bands of red-brown and olive-yellow. They are translucent to semiopaque and are accompanied by thin coatings of yellow clay. These characteristics suggest that the material is altered basalt originating from an exterior position on an eruptive basaltic unit (e.g., pillow lava or sheet flow).

Interhole correlation

Lithologic units were correlated among holes at Site U1371 to facilitate the integration of physical property, geochemical, and microbiological data. The stratigraphic correlation panel for Site U1371 is presented in Figure **F8.** Correlations shown in this figure are based on principal characteristics of the sediment, including

- Strongly contrasting lithologies between Unit I diatom ooze and Unit II zeolitic clay,
- Numerous ash layers in Unit I that appear in all Site U1371 holes,
- Characteristically very high natural gamma ray emanations occurring just below the mudline in Holes U1371D and U1371F, and
- Correlative magnetic susceptibility responses associated with hardgrounds in Unit I and the transition from low susceptibility in diatomaceous sediment to significantly greater susceptibility in Unit II clay.

Correlations show that strata at Site U1371 have uniform unit thickness and composition.

Physical properties

At Site U1371, physical properties measurements were made to provide basic information characterizing lithologic units. After sediment cores reached thermal equilibrium with ambient temperature at ~20°C, gamma ray attenuation (GRA) density, magnetic susceptibility, and *P*-wave velocity were measured with the Whole-Round Multisensor Logger (WRMSL) on whole-round core sections. After WRMSL scanning, the whole-round sections were logged for natural gamma radiation (NGR). Thermal conductivity was measured using the full-space method on sediment cores. Discrete *P*-wave measurements were made on split sediment cores using the Section Half Measurement Gantry. Moisture and density (MAD) were measured on discrete subsamples collected from the working halves of the split sediment cores. Additional discrete measurements of electrical resistivity were made on the split sediment sections to calculate formation factor. The Section Half Image Logger and Section Half Multisensor Logger (SHMSL) were used to collect images and color spectrometry of the split surfaces of the archive-half cores. Three holes targeted the sedimentary cover, Holes U1371D–U1371F. The most complete hole for logging physical properties was Hole U1371D. The holes have not been correlated and offsets exist.

Density and porosity

Bulk density values at Site U1371 were determined from both GRA measurements on whole cores and mass/volume measurements on discrete samples from Hole U1371D from the working halves of split cores (see **"Physical properties"** in the "Methods" chapter [Expedition 329 Scientists, 2011a]). A total of 66 discrete samples were analyzed for MAD.

Bulk density values in Hole U1371D are relatively constant with depth through lithologic Unit I (clay-bearing diatom ooze) (Fig. **F12A**). Density in Unit II (clay) increases and then decreases with depth. Bulk density discrete values are consistent with GRA den-

sity values through Unit I but are significantly lower than GRA density values in Unit II.

Grain densities have a mean value of 2.64 g/cm^3 in lithologic Unit I and 2.40 g/cm^3 in Unit II (Fig. F12B). Porosity generally decreases with depth and varies between ~80% and 70% through Unit I (Fig. F12C). Porosity declines rapidly in Unit II, with minimum values of ~55%.

Bulk density GRA values in Holes U1371E and U1371F show similar patterns to those observed in Hole U1371D (Fig. F13). Whole-round sampling prior to WRMSL measurements caused edge effects, leading to noisier records.

Magnetic susceptibility

Volumetric magnetic susceptibilities were measured using the WRMSL and point measurements were made on the SHMSL in all recovered cores from Site U1371. Uncorrected values of magnetic susceptibility are presented for Holes U1371D–U1371F (Fig. F14). Point measurements from archive halves are much more scattered than whole-core measurements, and peak-to-peak variability is greatly subdued in the point measurements. Notably, point measurements of magnetic susceptibility in areas of core disturbance show the largest scatter, with means that are either high or low relative to the bulk of the data. The spatial resolution of the WRMSL magnetic susceptibility loop is ~5 cm, and the observed ringing in Holes U1371C and U1371E is due to edge effects.

Magnetic susceptibility of the clay-bearing diatom ooze (lithologic Unit I) lies within a relatively narrow range. Local highs in this unit correlate to zones of hardground (see **"Lithostratigraphy"**). Magnetic susceptibility of clay (Unit II) generally increases with depth. The high magnetic susceptibility values in Unit II are likely due to the RSO content of the clay.

Natural gamma radiation

NGR results are reported in counts per second (Fig. F15). NGR counting intervals were ~30 min per whole-core interval for Hole U1371D and decreased to 20 min per whole-core interval for Holes U1371E and U1371F. NGR counts are considered reliable. NGR counts at the tops of Holes U1371D and U1371F are high, indicating that the sediment/water interface was sampled. The top of Hole U1371E was sampled prior to NGR measurements.

In general, NGR counts increase slightly with depth through lithologic Unit I and increase at a greater rate through Unit II. These patterns are similar to those observed in the GRA density and magnetic susceptibility data. Ringing is more prevalent in cores from Holes U1371E and U1371F because only short core pieces remained after whole-round sampling prior to NGR measurements.

P-wave velocity

P-wave velocity at Site U1371 was determined from measurements on whole-round sediment cores (Fig. F16) and on discrete samples from the working halves of sediment split cores (see **"Physical properties"** in the "Methods" chapter [Expedition 329 Scientists, 2011a]). Only 11 discrete measurements of *P*-wave velocity were measured. These discrete values are somewhat higher than measurements made on whole-round core. This difference may be due to drying of core material. The mean *P*-wave velocity value of all whole-core measurements is ~1510 m/s (Fig. F16B). In Hole U1371D, compressional wave velocities are relatively uniform except in the upper portion of lithologic Unit I, where there is a conspicuous region of somewhat higher velocities.

Formation factor

Electrical conductivity was measured on working halves of the split sediment cores from Hole U1371D. Measurements in Hole U1371D were made at a nominal interval of 20 cm. For each measurement, the temperature of the section was also noted. Surface seawater was used as a standard and measured twice per section (Table T4), normally prior to making measurements for that section and then between sections. These measurements were used to compute the drift for this set of measurements (Fig. F17; Table T5). The first set of measurements through measurement 500 shows a sharp decline in values measured on the standard. This steep decline is attributed to the unusually rapid wear of the platinized electrodes caused by the abrasive lithologic character of Unit I. Near measurement number 500, the probe was replatinized and measurements of the standard briefly returned to high values. Following this return, the values measured on the standard again quickly dropped. This drift stabilized though lithologic Unit II. Because of the three distinct trends in measurements made on the standard, the drift is computed as three piecewise linear trends. The temperature dependence of electrical conductivity was corrected and all reported measurements correspond to a temperature of 20°C. Electrical conductivity measurements were transformed to a dimensionless formation factor by dividing the drift by the measurements (Table T6).

In general, formation factor in lithologic Unit I is relatively constant except for a conspicuous low between ~85 and 95 mbsf (Fig. F18). Formation factor

increases with depth in Unit II although conspicuous departures from this trend are present.

Thermal conductivity

Thermal conductivity measurements were conducted on sediment whole-round cores using the needle-probe method (see **"Physical properties"** in the "Methods" chapter [Expedition 329 Scientists, 2011a]). In general, measurements appear reliable, although values <0.6 W/(m·K) were culled from the analysis. Values <0.6 W/(m·K) are attributed to poor contact between the probe and the sediment or convection that leads to unreasonably low estimates of thermal conductivity by causing the thermal response to heating to depart from the theoretical prediction. Values are relatively constant with depth through lithologic Units I and II. The mean thermal conductivity is 0.7 W/(m·K) (Fig. **F19A**). For the uppermost ~3 mbsf, thermal conductivities collected during the Cruise KNOX-02RR site survey (R. Harris, unpubl. data) are somewhat more scattered than the values reported here; however, they also have a mean of 0.7 W/(m·K).

Downhole temperature

Downhole temperature was measured using the APCT-3. Five measurements were attempted between 35.9 and 92.9 mbsf in Hole U1371D (Table **T7**). All measurements were made in lithologic Unit I.

All temperature-time series were recorded with a sample interval of 1 s. The temperature tool was stopped at the mudline for up to 10 min prior to the first measurement and then for 5 min thereafter. The average bottom water temperature is 1.11°C (Table **T7**). All measurements were made in a moderate sea state (<3 m swell) and each temperature-time series suffers to some extent from the ship's heave (Fig. **F20**). Significant frictional heating occurred on all penetrations of the APCT-3, with the temperature-time records exhibiting characteristic probe penetration and subsequent decay. Tool movement was observed in all temperature records as sudden shifts in temperature both before and after the usable section of the temperature-time series. Tool movement is attributed to the ship's heave. The effective origin time of the frictional heat pulse was estimated by varying the assumed origin time until the thermal decay pulse best fit a theoretical curve. As a result of tool movement, delay times are quite large and fits to the equilibrium curve are short (Table **T7**). Nevertheless, all of the measurements appear to be reliable. Equilibrium temperatures plotted as a function of depth are relatively linear. Coupled with the average bottom water temperature, they give a least-squares gradient of 74.0°C/km (Fig. **F19B**).

Heat flow

Because thermal conductivity appears relatively constant in lithologic Unit I and the thermal gradient is linear, heat flow is computed as the product of the thermal conductivity 0.7 W/(m·K) and thermal gradient (74.0°C/km) yielding value of 52 mW/m^2. This value is a little less than conductive cooling models for crust of this age.

Color spectrometry

Spectral reflectance was measured on split archive-half sections from Holes U1371D–U1371F. Measurements from Hole U1371D are shown in Figure **F21.** Values for L* are generally constant through lithologic Unit I and decline through Unit II. Values for a* and b* are generally correlated through Units I and II. These values are well correlated with the redox potential.

Paleomagnetism

At Site U1371, we measured natural remanent magnetization (NRM) of all archive-half sections for Holes U1371B–U1371H using the three-axis cryogenic magnetometer at 2.5 cm intervals before and after alternating-field (AF) demagnetization. The archive-half sections were demagnetized by alternating fields of 10 and 20 mT. The present-day normal field in this region, as expected from the geocentric axial dipole model at Site U1371, has a negative inclination (approximately –64.2°), so positive remanence inclination indicates reversed polarity. Data from Hole U1371E provides only a partial record because whole-round core samples were taken from these holes for geochemical and microbiological analyses. The primary objective of the shipboard measurements for Site U1371 was to provide chronostratigraphic constraint by determining magnetic polarity stratigraphy. During coring operations at Site U1371, nonmagnetic core barrels were used for all holes to ~100 mbsf and the Flexit core orientation tool was used for Hole U1371D (see **"Operations"**).

Results

Paleomagnetic data for Holes U1371B–U1371F and U1371H are presented in Figures **F22, F23, F24, F25, F26,** and **F27,** together with the whole-core susceptibility data measured on the WRMSL (see **"Physical properties"**). The lithology at Site U1371 changed from clay-bearing diatom ooze (Unit I) at ~105 mbsf to zeolitic and metalliferous clays (Unit II) (see **"Lithostratigraphy"**).

Using magnetic susceptibility data, it was possible to correlate between Holes U1371B–U1371F (Figs. **F28,**

F29) in the 0–70 mbsf interval. This correlation was applied to the magnetic intensity data (Fig. F30). Postexpedition application of such correlations to declination and intensity will be used to test if changes in magnetic polarity (Figs. F30, F31) are consistent between the holes.

Assignment of polarity intervals to specific chrons must wait for postexpedition biostratigraphic work to provide general age control. The basement age at Site U1371 is ~73 Ma (Gradstein et al., 2004).

Biogeochemistry

Site U1371 is located just south of the South Pacific Gyre in a region of relatively high biological productivity compared to previous sites occupied during Expedition 329. Although it was the last site of the expedition, we were able to completely characterize the sequence. Sampling and analyses were performed to address

- How biogeochemical parameters in the sediment and interstitial water vary with oceanographic factors, such as ocean productivity and sedimentation rate, from gyre center (Site U1368) to outside the gyre's edge (Site U1371);
- The extent to which the sedimentary microbial community may be supplied with electron donors by water radiolysis; and
- How sediment-basement exchange and potential activities in the basaltic basement vary with basement age and hydrologic regime.

Site U1371 provided the thickest sediment sequence of the expedition, with the deepest interstitial water sample recovered from ~130 mbsf. Unlike any other site occupied during this expedition, the enhanced productivity in the overlying water causes oxygen to be depleted at a shallow sediment depth. Thus, anaerobic processes are more important at this site than at the other Expedition 329 sites. Furthermore, a clear signal of basement-associated processes includes a deep zone ~25 m above basement showing detectable oxygen, relatively high redox potential, and gradients in related biogeochemical constituents (e.g., Mn). Through this deepest interval, a strong signal of basement alteration exists (e.g., K).

Sampling strategy

Oxygen concentrations were measured on complete core sections from Cores 329-U1371B-1H, 329-U1371C-1H, and 329-U1371H-1H, all of which were mudline or attempted mudline cores (see "Operations"). Hole U1371D recovered the complete sequence (Cores 329-U1371D-1H through 14H) and was devoted to oxygen measurements, lithostratigraphy, and physical properties. Oxygen measurements of sections from Cores 329-U1371F-11H through 14H, the deepest core of Hole U1371D, were measured before the cores were sullied by microbiological sampling.

Samples for methane, both for safety and refined analysis (see "Biogeochemistry" in the "Methods" chapter [Expedition 329 Scientists, 2011a]), were obtained during sampling on the catwalk on section ends from Holes U1371D and U1371E.

Interstitial water samples were obtained through squeezing whole rounds gathered from Hole U1371E (67 samples) and through Rhizon sampling (103 samples) on sediment intervals from Holes U1371B, U1371E, and U1371H. With the exception of six interstitial water intervals from Core 329-U1371E-1H and four interstitial water intervals from Core 329-U1371E-14H cut in the core refrigerator on the Hold Deck, all of the interstitial whole-round cores were taken on the catwalk immediately after core recovery and directly delivered to the Geochemistry Laboratory for pore water squeezing. Interstitial water was extracted by Rhizon sampling after oxygen measurements on Holes U1371B and U1371H in the Geochemistry/Microbiology Laboratory cold room. Rhizon sampling of Hole U1371E occurred in the ship's core refrigerator on the Hold Deck.

Interstitial water extraction generally was easier at Site U1371 than at other sites during this expedition (see "Biogeochemistry" in the "Methods" chapter [Expedition 329 Scientists, 2011a]); we attribute this ease to increased permeability due to the greater biogenic content of the lithologic Unit I sediment (see "Lithostratigraphy"). Deeper in the section, however, within lithologic Unit II, permeability decreased and interstitial water extraction became extremely difficult. Through the deepest ~20 m, often no water was extracted by the Rhizon samplers even after 12 h of insertion and only ~20 mL from the squeezers over a ~2 h duration (see Fig. F11 in the "Methods" chapter [Expedition 329 Scientists, 2011a]).

Syringe sampling for dissolved hydrogen analysis was coupled to interstitial water whole-round sampling. Separate interstitial samples for He and ^{14}C-dissolved inorganic carbon (^{14}C-DIC) were also cut on the catwalk and delivered directly to the container laboratory on the deck above the bridge for immediate squeezing and sampling. These samples never entered the interior of the ship. For analysis of solid-phase C and N concentrations, 41 samples were taken from Hole U1371E.

Dissolved oxygen

Dissolved oxygen (O_2) was measured using electrodes and optodes on intact 1.5 m core sections from Holes U1371B–U1371D, U1371F (electrodes only), and U1371H after delivery from the catwalk to the Geochemistry/Microbiology Laboratory cold room (Fig. **F32**). Electrode-based measurements were performed at 10 cm intervals (Table **T8**) for the uppermost 2.9, 2.4, and 5.9 m in Holes U1371B, U1371C, and U1371H, respectively. Optode measurements were conducted in 10–30 cm intervals in the uppermost 4 m in Holes U1371B, U1371C, and U1371H (Table **T9**).

Electrode measurements in Hole U1371D were performed at 10 cm intervals in the uppermost 4 m (Table **T8**), followed by one measurement every 1.5 m (one per intact core section) to 110 mbsf. Toward the sediment/basement interface, higher resolution measurements of 10–30 cm intervals were taken to 125.7 mbsf. Optode measurements in Hole U1371D were measured at 10–30 cm intervals to 4 mbsf and from 115 to 125 mbsf. In Cores 329-U1371D-2H through 6H, 2–5 measurements were made per core. The optode signal stabilized very slowly (up to 30 min) in the consolidated sediment near the basement (Cores 13H and 14H), making quantification of oxygen concentration by optode difficult.

For Holes U1371D and U1371F, oxygen was measured with two different electrodes; the data for both profiles are recorded in parallel for most of the same depth intervals (Table **T8**). Intact core sections of Cores 329-U1371F-11H through 14H were directly brought from the catwalk to the Geochemistry/Microbiology Laboratory cold room and measured at the intervals marked by cutting lines drawn by microbiologists before being sectioned for microbiological whole-round core sampling. Electrode measurements were performed every 1.5 m (every core section) for Cores 329-U1371F-11H and 12H, in 20–50 intervals for Sections 329-U1371F-13H-2 through 13H-7, and at 20 cm resolution for Sections 14H-1 through 14H-6 (Table **T8**).

Dissolved oxygen concentrations measured by electrode decrease rapidly below the seafloor (Table **T8**). Near-surface values are 75, 33, and 60 µM for Holes U1371B, U1371C, and U1371H, respectively. Values approach the detection limit of oxygen measured by electrodes at ~1–1.3 mbsf for Holes U1371B and U1371C. For Hole U1371H, oxygen measurements are above the detection limit throughout the entire core (0–6 mbsf); however, very high but relatively constant values in Sections 329-U1371H-1H-2 and 1H-4 relative to Sections 1H-1 and 1H-3 suggest that large section-to-section variations in calibration affected this record.

For Hole U1371D, dissolved oxygen measured by electrode declines rapidly from a near-surface value of 82 to 2.5 µM at 1 mbsf and gradually decreases to <0.1 µM at 2.7 mbsf. Below this depth, values stay at this detection limit until ~110 mbsf, at which point oxygen becomes again detectable and gradually increases to 3–4 µM toward the basaltic basement. In Cores 329-U1371F-11H through 14H, electrode-based oxygen concentration values are close to the detection limit until 113.5 mbsf. They then increase with depth to ~11 µM with ~2 µM variability.

Oxygen measured by optode decreased rapidly from 180 to <5 µM in the uppermost 50 cm below the sediment surface (Hole U1371D). Below, oxygen was present at low and decreasing concentrations to 5–6 mbsf. No oxygen was detected (detection limit ~ 0.4 µM; see Table **T9**) between 10 and 45 mbsf. Oxygen again appeared in low (<2 µM) concentrations above the basement (115–125 mbsf). Oxygen measurements in both Holes U1371D and U1371F indicate a diffusive flux of oxygen upward into the sediment from the basement.

Redox potential

Redox potential (mV) was measured using needle electrodes (see **"Biogeochemistry"** in the "Methods" chapter [Expedition 329 Scientists, 2011a]) in 1–3 intervals per core section from all of Hole U1371D and the lowermost 4 cores in Hole U1371F (Cores 329-U1371F-11H through 14H). As shown in Figure **F33** and Table **T10,** redox potentials in the uppermost ~6 mbsf are positive and only slightly decrease from 199 mV at 0.7 mbsf to 153 mV at 6.68 mbsf. These are typical values for an oxidizing environment (ZoBell, 1946). Below 7 mbsf, the redox potential quickly decreases to –208 mV at 16.9 mbsf, which indicates the presence of dissolved reduced substances in the interstitial waters. This 16.9 mbsf minimum is the first of three or four local minima in redox potential in this sediment column. Neither the peaks nor the valleys forming the pattern seem to be associated with individual core breaks or other potential handling artifacts. The pattern may be related to zones of greater biogeochemical activity within discrete layers of the sequence (see **"Lithostratigraphy"**).

Redox potential reaches its most negative value (–554 mV) at 87.9 mbsf. Below 100 mbsf, redox potential exhibits a linear increase toward higher redox values and reaches values similar to, or even slightly more positive (>200 mV) than, those observed in the surface sediments. This deep (deeper than 100 mbsf) in-

crease in redox potential to highly oxidizing values was replicated in measurements performed on the lowermost four cores of Hole U1371F (Fig. F33). These observations underscore the finding that dissolved oxygen is present in the lowermost part of the Site U1371 sediments and that lithologic Unit II is in a relatively oxidizing environment.

Dissolved hydrogen and methane

Dissolved hydrogen (H_2) concentrations were quantified in 71 samples collected in Hole U1371E from 0.3 to 130.2 mbsf (Fig. F34; Table T11). The maximum H_2 concentration in the sediment column was 10.4 nM in the uppermost sample (0.3 mbsf). Hydrogen concentrations remain at or below 2 nM for most of the sediment column, followed by a slight increase near the sediment/basalt interface. Seven samples were taken in the core refrigerator on the Hold Deck, whereas the remaining samples were collected on the catwalk. Based on the average of 13 blanks, the detection limit at this site was calculated as 1.4 nM.

Methane concentrations are below the detection limit (<0.98 µM) in all 14 samples from Hole U1371E, as measured by the IODP standard safety protocol. The detection limit is defined here as three times the standard deviation of the blank (ambient air). However, with the refined protocol, one sample (Section 329-U1371E-2H-5; 15.35 mbsf) reveals a methane concentration slightly above the detection limit (6.8 µM).

Interstitial water samples

A total of 90 Rhizon samples for dissolved nitrate analyses were obtained from Holes U1371B, U1371E, and U1371H. Profiles of dissolved nitrate concentration exhibit variations between the holes (Fig. F35A; Table T12). Nitrate concentrations in Hole U1371B are not discernible even at 0.2 mbsf. Nitrate concentrations decrease to below detection limit at 1 mbsf in Hole U1371E and drop below the detection limit in Hole U1371H at 2.5 mbsf. Vertical profiles of nitrate in Hole U1371H, in which nitrate samples were taken at high resolution (10–30 cm interval) through the uppermost 6 mbsf, were similar to those reported from the site survey cruise (D'Hondt et al., 2009). The results suggest that the near-surface sediment in Holes U1371B and U1371E may not have been recovered during coring. Nitrate concentration near the sediment/water interface in Hole U1371H is 41 µM (Sample 329-U1371H-1H-1, 18–20 cm), which is ~8 µM higher than local bottom water (Talley, 2007). This increase of nitrate is in conjunction with the steep decrease of oxygen (Fig. F32) in the uppermost 0.2 mbsf and indicates aerobic respiration of organic nitrogen (nitrification) near the seafloor at this site. Below 0.2 mbsf in Hole U1371H and for the first time during Expedition 329, nitrate concentrations continuously decrease to 2.1 µM at 2.53 mbsf (Sample 1H-2, 98–100 cm), implying microbial nitrate reduction (e.g., denitrification) in the suboxic condition with oxygen concentrations below 5 µM. Another unique feature of the nitrate profile is that ~2–5 µM of nitrate was observed above the sediment/basalt interface, between 105 and 120 mbsf.

Ammonium was measured on Rhizon-sampled interstitial waters. The concentration at 0.15 mbsf in Hole U1371E is 0.35 µM (Fig. F35A). Concentrations then rise steeply with a convex-upward profile, reaching a maximum of ~55 µM between 30 and 65 mbsf. Below 65 mbsf, concentration decreases slightly to 40 µM at 97 mbsf.

The dissolved phosphate profile, measured on 55 interstitial water samples obtained through squeezing from Hole U1371E, exhibits a similar pattern as at Site U1370, but its concentration range is approximately an order of magnitude greater here at Site U1371 (Table T13; Fig. F35B). Phosphate concentrations start at 9.9 µM at 0.05 mbsf and increase with a straight gradient to 22.6 µM at 1.45 mbsf. Peak concentrations occur at 4.95 mbsf and a peak of net release into interstitial water is apparent between 4.95 and 12.65 mbsf. This peak is attributed to microbially mediated oxidation of organic matter under anoxic conditions. Below this depth, the phosphate profile shows a slight concave-upward pattern as the phosphate concentrations decline to below 3 µM at 98.15 mbsf. The lowest concentrations range between 1.2 and 1.7 µM in the lithologic Unit II sediment. Adsorption or removal into mineral phases is expected to control the phosphate flux into the deep sediments. The pooled standard deviation (1σ; see "Biogeochemistry" in the "Methods" chapter [Expedition 329 Scientists, 2011a]) on triplicate measurements of the phosphate concentration is 0.066 µM.

In contrast to the previous Expedition 329 sites, dissolved silica shows greater and increasing concentrations with depth in Hole U1371E (Table T13; Fig. F35C). The dissolved silica concentration at 0.05 mbsf is 533 µM and increases to 759 µM by 12.5 mbsf. Below this depth, concentrations remain between 700 and 750 µM until they gently increase to above 800 µM at depths below 80 mbsf. The profile within the uppermost 100 m of sediment is typical for the dissolution of amorphous silica in siliceous sediment, coupled to equilibrium control of dissolved silica concentration. However, below 101 mbsf, dissolved silica concentrations show a striking

and monotonic decrease toward basement, with a concentration of 383 µM at 128 mbsf. The pooled standard deviation (1σ; see "Biogeochemistry" in the "Methods" chapter [Expedition 329 Scientists, 2011a]) for duplicate measurements is 12.8 µM.

Alkalinity sharply increases from 3.0 mM at seafloor to 3.2 mM at ~2 mbsf and gradually decreases to 2.1 mM to the bottom of the hole (Fig. F35D). The maximum value at Site U1371 was higher than at previous sites, and may be due to more active oxidation of organic matter. No obvious offset was observed between the alkalinity of the samples taken on the catwalk and those taken in the Hold Deck's core refrigerator (see "Biogeochemistry" in the "Methods" chapter [Expedition 329 Scientists, 2011a]). The standard deviation and error of alkalinity measurements on standard seawater CRM104 are 0.018 and 0.005 mM (N = 14), respectively.

Dissolved inorganic carbon (DIC) increases from 2.89 mM at the sediment surface to 3.1 mM at 1.45 mbsf (Fig. F35E) and remains stable to 5.95 mbsf, where it starts to decrease, reaching 2.1 mM at 130.31 mbsf. Between 50 and 70 mbsf, DIC content again remains stable. The range in DIC values is 0.79 mM. The average standard deviation of triplicate injection of the samples is 0.023 mM.

Chloride was determined from the squeezed interstitial water samples (Table T13; Fig. F35F). The chloride concentration near the seafloor is indistinguishable from local bottom water but monotonically increases by ~12 mM at ~35 mbsf. This 2% increase may be due to relict higher salinity seawater. Below this depth, there is no significant gradient until 100 mbsf, at which point chloride concentration decreases toward 552.8 mM (at 127.65 mbsf; interval 329-U1371E-14H-4, 40–50cm).

Sulfate was determined in the squeezed interstitial water samples. Sulfate concentrations begin at the surface sediment at 28.5 mM (Fig. F35G), which is close to the 28.6 mM concentration of sulfate in local bottom water. Sulfate concentrations increase to 28.6 mM at ~4.5 mbsf and then decrease smoothly to 27.5 mM at 98 mbsf. A steeper decline follows with a concentration of 26.6 mM at 123.6 mbsf. A clearer understanding of sulfate reactivity may be seen in the plot of the sulfate anomaly (Fig. F35H; see "Biogeochemistry" in the "Methods" chapter [Expedition 329 Scientists, 2011a]). The sulfate anomaly decreases monotonically from –0.5% near the surface to –7.9% at 123.6 mbsf. The gradient of sulfate near the sediment/basalt interface may reflect removal of sulfate into authigenic minerals. There also appears to be some curvature in the sulfate profile that indicates microbial sulfate reduction.

As at previous sites, cations were measured for Site U1371 by both inductively coupled plasma–atomic emission spectroscopy (ICP-AES) and ion chromatography. Because of time constraints associated with the end of the expedition, not every sample was analyzed. The precision of cation measurements by ICP-AES was as follows, as quantified by multiple triplicate and quadruplicate analyses of International Association for the Physical Sciences of the Oceans (IAPSO) standard seawater and internal matrix-matched standards:

Ca = 0.8% of the measured value,
Mg = 0.4% of the measured value,
Na = 0.6% of the measured value,
K = 0.4% of the measured value,
Fe = 1% of the measured value, and
Mn = 1%.

Because of end-of-expedition instrumentation constraints, B and Sr were not analyzed. Accuracy of the ICP-AES results, as quantified by comparison to multiple replicate analyses of IAPSO standard seawater not included in the calibration, was within precision of the measurement. For the ion chromatography analyses, precision (pooled standard deviation, 1σ) was

Ca = 0.8%,
Mg = 0.5%,
Na = 0.4%, and
K = 0.4%.

The shape of the concentration profiles determined by ICP-AES and ion chromatography agree well. As was the case at previous sites, the absolute values of the concentrations differ by an amount that is minimally greater than the analytical precision(s). The ion chromatography data at Site U1371 are slightly higher than the ICP-AES data. This contrast is most pronounced in the relative sense for Ca and less so for Na, Mg, and K. We favor the ICP-AES data for Ca because the shallowest samples measured by ICP-AES are closer to seawater values than the Ca data determined by ion chromatography. We favor the ion chromatography data for Na because they are closer to the expected seawater value for the shallowest samples. We emphasize this is a judgment determination at this point because the cause of this discrepancy remains unclear, even though the ICP-AES and ion chromatography protocols were both rigorously calibrated against multiple replicate analyses of IAPSO standard seawater, with identical items analyzed by both instruments and with detailed determinations of analytical precision. Postcruise shore-based analyses will aim to resolve this slight ambiguity (Table T13; Figs. F35I, F35J, F35K, F35L).

Both the ion chromatography and ICP-AES profiles of dissolved Ca show a consistent and linear increase of ~1 mM to ~70 mbsf. Between ~70 mbsf and the bottom of Hole U1371E, Ca concentrations are essentially constant. From the surface sediment to ~100 mbsf, Mg concentrations remain constant before increasing by ~4 mM to basement. Like Mg, Na presents no change from the surface to ~100 mbsf before decreasing to the basement. K remains constant over the uppermost ~20 mbsf before decreasing by ~1 mM steadily to ~100 mbsf. Between ~100 mbsf and the basement, K decreases by ~2.5 mM. Decreases in Na and K concentration most likely represent uptake of these alkalis by basement alteration processes. The increase in Mg is more unusual because during basement alteration Mg is usually sequestered into authigenic clay phases. The increase in Mg may result from some type of cation exchange during alteration, perhaps with Na and/or K.

The concentration of dissolved Fe is only a few times that of its detection limit (~4 µM; Fig. **F35M**) and the concentration profile is consistent with the O_2-depleted nature of this site. Moreover, the observed concentrations are the highest observed during among the Expedition 329 sites. Although there is a great deal of scatter in the Fe profile, it generally mirrors the redox potential profile (Fig. **F33**), with local Fe minima at the top and bottom of the sediment column and local Fe maxima coinciding with the redox potential minima within the column. Postcruise analyses will address the distribution of dissolved Fe more completely.

Unlike the previous sites occupied during Expedition 329, the concentration of Mn reached relatively high values and is readily interpretable (Figs. **F35N, F35O**). Concentrations of Mn show a very strong increase to ~360 µM through the uppermost 3 mbsf before decreasing gradually to values of ~200 µM at ~110 mbsf. Below this depth, values of dissolved Mn decrease to ~70 µM in the deepest sample analyzed at ~128 mbsf. Strong minima in dissolved Mn concentration occur at the top and bottom of the sediment column. Weak local minima approximately correspond to the strong minima in redox potential within the sediment column (Fig. **F33**).

At Site U1371, only 10 interstitial water samples were processed in the Hold Deck core refrigerator. Nonetheless, comparison of the catwalk samples (squeezed immediately upon core recovery) to those samples stored in the core refrigerator on the Hold Deck shows no offset between the data sets for any cation (see **"Biogeochemistry"** in the "Methods" chapter [Expedition 329 Scientists, 2011a]).

Solid-phase carbon and nitrogen

Concentrations of total carbon, total organic carbon (TOC), total inorganic carbon (TIC), and total nitrogen were determined for 40 samples from Hole U1371E (Fig. **F36;** Table **T14**).

Total nitrogen shows a slow decrease from ~0.05 wt% at the seafloor to 0.005 wt% at 128.1 mbsf. TOC shows a downcore decrease similar to total nitrogen, from 0.22 wt% at the seafloor to 0.01 wt% at 128.1 mbsf. The almost linear decrease of TOC is interrupted by slightly elevated values between 50 and 60 mbsf and again between 85 and 95 mbsf (Fig. **F36**). Total carbon also shows a slight decrease with depth, from 0.28 wt% at 0.01 mbsf to 0.04 wt% at 128.1 mbsf. However, the total carbon profile shows more significant variations downhole, in particular with two maxima at 49.15 and 91.65 mbsf. These depths correspond to two clear minima in the redox potential profile (Fig. **F33**).

TIC and $CaCO_3$ values obtained by coulometry follow a different pattern from the total carbon content obtained from the CHNS elemental analyzer (Fig. **F36**). The $CaCO_3$ content oscillates around ~0.04 wt% in the uppermost 20 mbsf and then shows three maxima at 33.15, 49.15, and 91.65 mbsf (0.27, 0.78, and 0.52 wt%, respectively). Below 100 mbsf, $CaCO_3$ values gradually increases from 0.02 wt% at 101.15 mbsf to 0.25 wt% at 128.1 mbsf.

Microbiology

Sediment samples for microbiological studies were obtained by APC coring, primarily from Holes U1371E and U1371F. PFT was continuously injected into the drilling fluid for quantification of sample contamination. Samples for cell and virus-like particle (VLP) abundance were taken from the cut cores that face interstitial water whole-round samples and fixed for subsequent microscopic studies. After core recovery, core sections were transferred to the core refrigerator on the Hold Deck, where microbiological whole-round cores were sampled. The temperature of the core refrigerator during subsampling ranged from 7°–10°C. Microbiological whole-round cores were taken at a high depth resolution from the first core (1H) and the bottom core (14H) of Hole U1371F. All whole-round cores for cultivation were immediately transferred into N_2-flushed foil packs to prevent excess oxidation of fresh microbiological samples from the air and stored at 4°C before subsampling.

Cell abundance

Microbial cells were enumerated by direct counting using epifluorescence microscopy (Table T15; see "Microbiology" in the "Methods" chapter [Expedition 329 Scientists, 2011a]). Sediment subcores (2 cm^3) for shipboard analysis were taken using tip-cut syringes from Holes U1371E and U1371F. In addition, eighteen 10 cm whole-round cores were taken for postcruise analysis from Holes U1371E and U1371F and stored at –80°C.

Six blanks were prepared and counted during processing of the samples from Site U1371. As at the previous site, a slurry of heat-sterilized (4 h at 450°C) sediment was used as a blank instead of Tris-EDTA buffer. The mean blank value of the heat-sterilized blanks was 3.2×10^2 cells/cm^3 with a standard deviation of 2.5×10^2 cells/cm^3, resulting in minimum detection limit (MDL; blank plus three times standard deviation) of 1.1×10^3 cells/cm^3. As the blanks did not vary much between sites, they were pooled from all sites. At the end of the expedition, a single MDL for all sites (1.4×10^3 cells/cm^3) was calculated based on the extended database.

Cell abundance in the uppermost sample (329-U1371E-1H-1, 35–43 cm) is ~6×10^6 cells/cm^3 and gradually decreases to 28.55 mbsf. Below this depth, cell abundance is below the MDL or even below the blank, with two exceptions at 50 and 95 mbsf (Fig. F37). Because of the limited time before the end of the expedition, no samples from below 114 mbsf were counted and no samples without cell extraction steps were examined. These will be quantified postcruise. Only two samples were recounted by another shipboard microbiologist. These counts were in good agreement with the original counts, suggesting that differences in cell recognition among observers are small.

Virus abundance

Eighty samples for VLP enumeration were taken at a high depth resolution from Holes U1371E and U1371F (Table T16). All of these samples were preserved at –80°C for shore-based analyses.

Cultivation

Sediment samples

Sediment whole-round cores were subsampled aseptically with sterile, tip-cut syringes to make slurries for inoculation of a variety of media (Table T17). After aseptic slurry inoculation in the Microbiology Laboratory, the headspace in the vials containing culture medium for anaerobic microbes was flushed with N_2 and sealed with an autoclaved rubber stopper. Additional samples (referred to as SLURRY in Table T17) were stored in N_2-flushed serum bottles or in syringes packed in sterile foil packs and stored at 4°C for shore-based cultivation experiments.

Seawater control sample

A surface seawater sample was collected from Site U1371 with a sterile 500 mL glass bottle immediately after the R/V *JOIDES Resolution* arrived at the site. Aerobic heterotrophic bacteria were cultured on marine agar and marine R2A plates (see Table T8 in the "Methods" chapter [Expedition 329 Scientists, 2011a]) at 25°C. No visible colonies were observed on either marine agar or R2A plates after 5 days of incubation.

Bottom seawater was collected from the mudline of Core 1H in Holes U1371B and U1371G, placed in a sterile plastic bag and stored at 4°C. The water was filtered through 0.2 µm pore size polycarbonate filters into sterile 50 mL serum bottles and sparged with N_2 for 5 min. The bottles were capped with rubber stoppers and aluminum crimp caps and stored at 4°C for future preparation of liquid media on shore. Aerobic heterotrophic bacteria were cultured from the unfiltered sample at 25°C for 3 days. The abundances of cultivable aerobic heterotrophic bacteria on marine agar and R2A plates were ~2.5×10^3 and ~2.3×10^3 colony-forming units (cfu)/mL, respectively, which are in marked contrast to numbers obtained from surface seawater as described above. The estimated abundance of *Vibrio*-like species, based on selective enrichment for this genus on thiosulfate citrate bile salts sucrose agar, was ~2.5×10^3 cfu/mL.

Molecular analyses

Sediment samples

Whole-round cores were taken throughout the entire sediment column and transferred to –80°C freezers for storage. These samples will be used for shore-based molecular ecological studies (see "Microbiology" in the "Methods" chapter [Expedition 329 Scientists, 2011a]). Sixteen 10 cm whole-round core samples were taken from Hole U1371E as routine microbiology samples (curatorial code MBIO) and stored at –80°C. These samples will be stored at –80°C in the Gulf Coast Core Repository at Texas A&M University (USA) to accommodate future sample requests.

Deep seawater control sample

For shore-based molecular ecological studies, the bottom seawater was collected from the top part of mudline cores (1H) in Holes U1371B and U1371G. Approximately 300 mL of seawater was collected in a

sterilized plastic bag and stored at 4°C in the Microbiology Laboratory until further processing. The sample was then filtered through 0.2 µm pore size polycarbonate membrane filters under aseptic conditions and the filters stored at –80°C.

Fluorescence in situ hybridization analysis

Duplicate 10 cm^3 subcores of sediment from Sections 329-U1371E-3H-3, 5H-3, 7H-2, 9H-3, 11H-2, and 14H-3 and 329-U1371F-1H-1 through 1H-3, 14H-3, and 14H-4 were collected using sterile tip-cut syringes and fixed as described in "Microbiology" in the "Methods" chapter (Expedition 329 Scientists, 2011a) for shore-based fluorescence in situ hybridization analyses.

Radioactive and stable isotope tracer incubation experiments

Stable isotope (^{13}C and ^{15}N) experiments to measure carbon and nitrogen uptake activities were initiated on board in the Isotope Isolation Van. Sediment subcores (15 cm^3) were taken from the inner part of 20 cm whole-round cores, placed in sterile glass vials, flushed with N_2, sealed with a rubber stopper, and stored until processing in the core refrigerator on the Hold Deck (see "Microbiology" in the "Methods" chapter [Expedition 329 Scientists, 2011a]). Six whole-round cores from Sections 329-U1371E-5H-2, 8H-2, and 11H-2 and 329-U1371F-1H-2, 2H-2, and 14H-4 were processed for stable isotope tracer incubation experiments, as described in "Microbiology" in the "Site U1365" chapter (Expedition 329 Scientists, 2011b).

Whole-round interval 329-U1371E-1H-2, 110–120 cm (2.8 mbsf), was used for slurry experiments on metabolic activities using radioactive and stable isotopes. The whole-round core section had been stored in the core refrigerator on the Hold Deck until processing in the Microbiology/Chemistry Laboratory cold room. Incubation experiments were prepared in the Isotope Isolation Van using radioactive and stable isotope or a combination according to the methods described in detail (see "Microbiology" in the "Methods" chapter [Expedition 329 Scientists, 2011a]).

Seven sediment whole-round cores were collected from Hole U1371E (Samples 329-U1371E-1H-1, 20–30 cm; 2H-2, 50–60 cm; 5H-4, 90–100 cm; 7H-5, 20–30 cm; 9H-5, 10–20 cm; 11H-4, 0–10 cm; and 14H-4, 60–70 cm) for stable isotope probing and nuclear magnetic resonance biomass experiments. Subsamples were taken with 5 cm^3 tip-cut syringes and amended with stable isotope tracers dissolved in low-nutrient growth media (^{13}C-labeled sodium acetate, sodium benzoate, methanol, and methane sulfonic acid) and incubated at 4°C (see "Microbiology" in the "Methods" chapter [Expedition 329 Scientists, 2011a]). Four whole-round cores collected from Hole U1371E (Samples 329-U1371E-1H-1, 25–35 cm; 2H-4, 20–40 cm; 5H-4, 20–40 cm; and 9H-1, 40–60 cm) were simultaneously processed in a similar manner.

For sulfate reduction rate measurements, 24 whole-round cores were collected from Hole U1371E (Samples 329-U1371E-1H-4, 50–60 cm; 1H-5, 50–60 cm; 1H-6, 20–30 cm; 2H-1, 100–110 cm; 2H-2, 20–30 cm; 2H-3, 50–60 cm; 2H-4, 50–60 cm; 2H-5, 50–60 cm; 3H-2, 100–110 cm, 3H-3, 50–60 cm; 3H-4, 50–60 cm; 3H-5, 50–60 cm; 3H-6, 10–20 cm; 4H-1, 50–60 cm; 4H-2, 50–60 cm; 4H-3, 50–60 cm; 4H-4, 50–60 cm; 4H-5, 50–60 cm; 4H-6, 10–20 cm; 5H-2, 60–70 cm, 5H-4, 60–70 cm; 6H-4, 50–60 cm; and 6H-6, 50–60 cm). Five to seven subsamples (~2.5 cm^3) were collected directly from each whole-round core for the shore-based distillation analysis of ^{35}S-labeled reduced sulfur compounds (see "Microbiology" in the "Methods" chapter [Expedition 329 Scientists, 2011a]).

Contamination assessment

We used perfluoromethylcyclohexane tracer as PFT to monitor drilling fluid contamination in sediment cores. PFT was continuously injected into drilling fluids during APC coring in Hole U1371E. Subcore samples (3 cm^3) were taken from whole-round cores on the catwalk and stored in vials with 2 mL of water prior for postexpedition gas chromatography measurement (see "Microbiology" in the "Methods" chapter [Expedition 329 Scientists, 2011a]).

References

D'Hondt, S., Abrams, L.J., Anderson, R., Dorrance, J., Durbin, A., Ellett, L., Ferdelman, T., Fischer, J., Forschner, S., Fuldauer, R., Goldstein, H., Graham, D., Griffith, W., Halm, H., Harris, R., Harrison, B., Hasiuk, F., Horn, G., Kallmeyer, J., Lever, M., Meyer, J., Morse, L., Moser, C., Murphy, B., Nordhausen, A., Parry, L., Pockalny, R., Puschell, A., Rogers, J., Schrum, H., Smith, D.C., Soffientino, B., Spivack, A.J., Stancin, A., Steinman, M., and Walczak, P., 2011. KNOX-02RR: drilling site survey—life in subseafloor sediments of the South Pacific Gyre. *In* D'Hondt, S., Inagaki, F., Alvarez Zarikian, C.A., and the Expedition 329 Scientists, *Proc. IODP,* 329: Tokyo (Integrated Ocean Drilling Program Management International, Inc.). doi:10.2204/iodp.proc.329.112.2011

D'Hondt, S., Spivack, A.J., Pockalny, R., Ferdelman, T.G., Fischer, J.P., Kallmeyer, J., Abrams, L.J., Smith, D.C., Graham, D., Hasiuk, F., Schrum, H., and Stancine, A.M.,

2009. Subseafloor sedimentary life in the South Pacific Gyre. *Proc. Natl. Acad. Sci. U. S. A.*, 106(28):11651–11656. doi:10.1073/pnas.0811793106

Durbin, A.M., and Teske, A., 2010. Sediment-associated microdiversity within the Marine Group I Crenarchaeota. *Environ. Microbiol. Rep.,* 2(5):693–703. doi:10.1111/j.1758-2229.2010.00163.x

Expedition 329 Scientists, 2011a. Methods. *In* D'Hondt, S., Inagaki, F., Alvarez Zarikian, C.A., and the Expedition 329 Scientists, *Proc. IODP,* 329: Tokyo (Integrated Ocean Drilling Program Management International, Inc.). doi:10.2204/iodp.proc.329.102.2011

Expedition 329 Scientists, 2011b. Site U1365. *In* D'Hondt, S., Inagaki, F., Alvarez Zarikian, C.A., and the Expedition 329 Scientists, *Proc. IODP,* 329: Tokyo (Integrated Ocean Drilling Program Management International, Inc.). doi:10.2204/iodp.proc.329.103.2011

Ekdale, A.A., 1977. Abyssal trace fossils in worldwide Deep Sea Drilling Project cores. *In* Crimes, T.P., and Harper, J.C. (Eds.), *Trace Fossils 2*. Geol. J. Spec. Iss., 9:163–182.

Fischer, J.P., Ferdelman, T.G., D'Hondt, S., Røy, H., and Wenzhöfer, F., 2009. Oxygen penetration deep into the sediment of the South Pacific gyre. *Biogeosciences*, 6:1467–1478. http://www.biogeosciences.net/6/1467/2009/bg-6-1467-2009.pdf

Gradstein, F.M., Ogg, J.G., and Smith, A. (Eds.), 2004. *A Geologic Time Scale 2004:* Cambridge (Cambridge Univ. Press). http://cambridge.org/uk/catalogue/catalogue.asp?isbn=9780521781428

Kastner, M., 1986. Mineralogy and diagenesis of sediments at Site 597: preliminary results. *In* Leinen, M., Rea, D.K., et al., *Init. Repts. DSDP,* 92: Washington, DC (U.S. Govt. Printing Office), 345–349. doi:10.2973/dsdp.proc.92.116.1986

Larson, R.L., Pockalny, R.A., Viso, R.F., Erba, E., Abrams, L.J., Luyendyk, B.P., Stock, J.M., and Clayton, R.W., 2002. Mid-Cretaceous tectonic evolution of the Tongareva triple junction in the southwestern Pacific Basin. *Geology,* 30(1):67–70. doi:10.1130/0091-7613(2002)030<0067:MCTEOT>2.0.CO;2

Talley, L.D., 2007. *Hydrographic Atlas of the World Ocean Circulation Experiment (WOCE)* (Vol. 2): *Pacific Ocean.* Sparrow, M., Chapman, P., and Gould, J. (Eds.): Southampton, U.K. (International WOCE Project Office). http://www-pord.ucsd.edu/whp_atlas/pacific_index.html

ZoBell, C.E., 1946. Studies on redox potential of marine sediments. *Bull. Am. Assoc. Petrol. Geol.,* 30(4):477–513. http://search.datapages.com/data/bulletns/1944-48/data/pg/0030/0004/0450/0477.htm

Publication: 13 December 2011
MS 329-109

Figure F1. Multibeam bathymetry of the Site U1371 survey area with the KNOX-02RR survey track overlain. sol = start of seismic line, eol = end of seismic line, z = time (Greenwich Mean Time), sp = shotpoint.

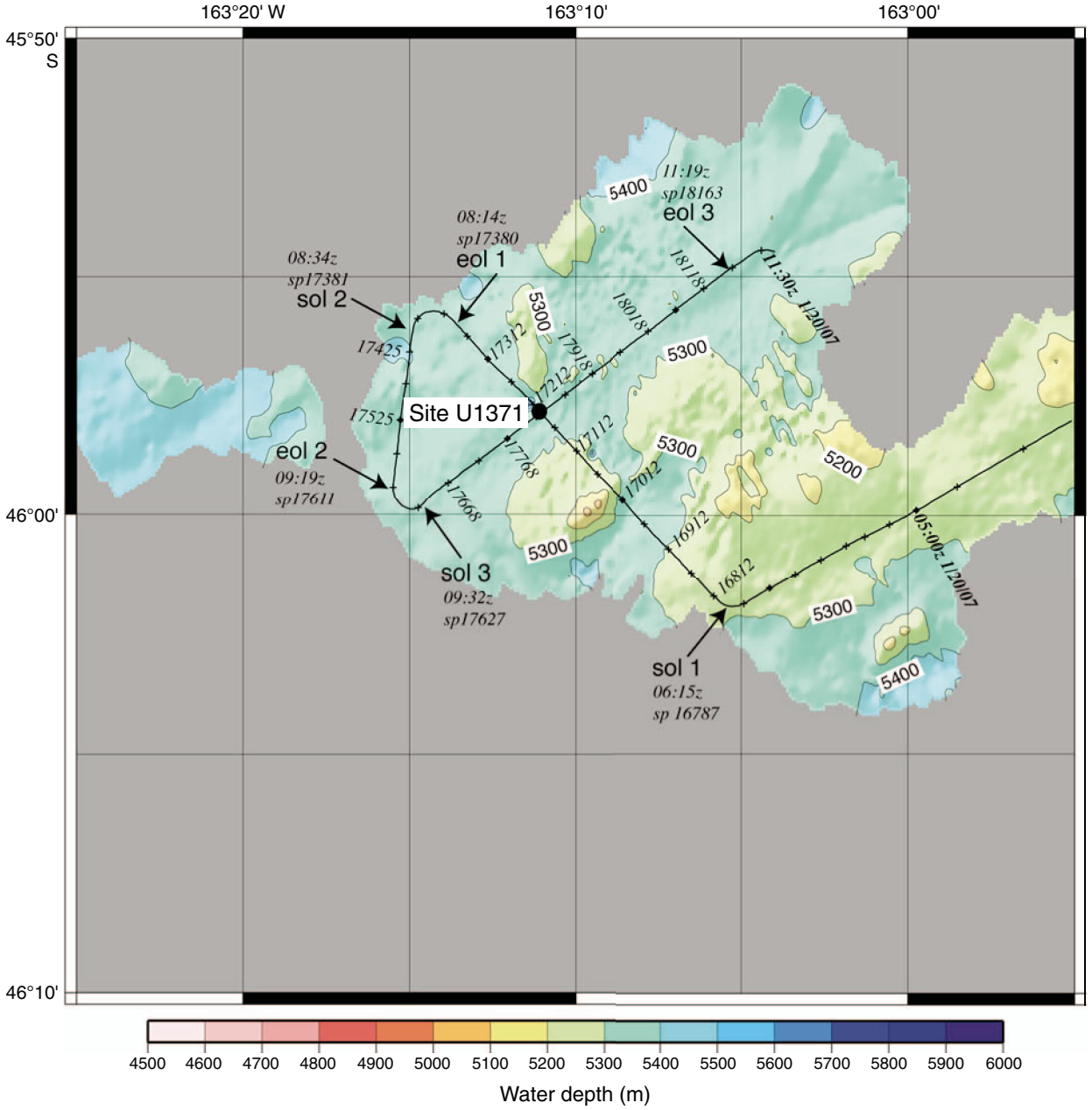

Figure F2. KNOX-02RR seismic survey track for Site U1371. sol = start of seismic line, eol = end of seismic line, z = time (Greenwich Mean Time), sp = shotpoint.

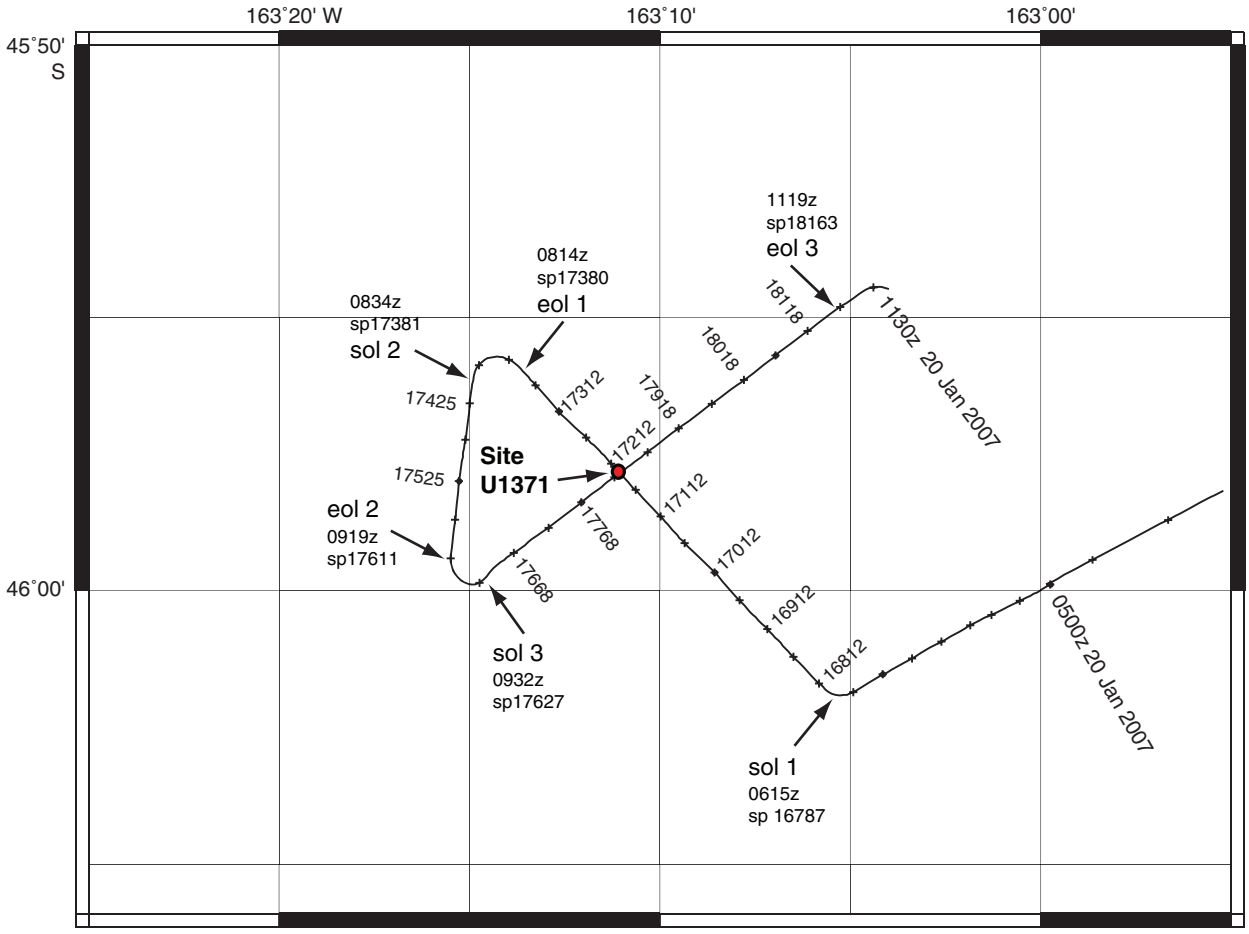

Figure F3. KNOX-02RR Channel 48 of MCS Line 1 across Site U1371. z = time (Greenwich Mean Time), SP = shotpoint, MORB = mid-ocean-ridge basalt, WD = water depth, SCS = single-channel seismic, BP = band-pass, AGC = automatic gain control, VE = vertical exaggeration.

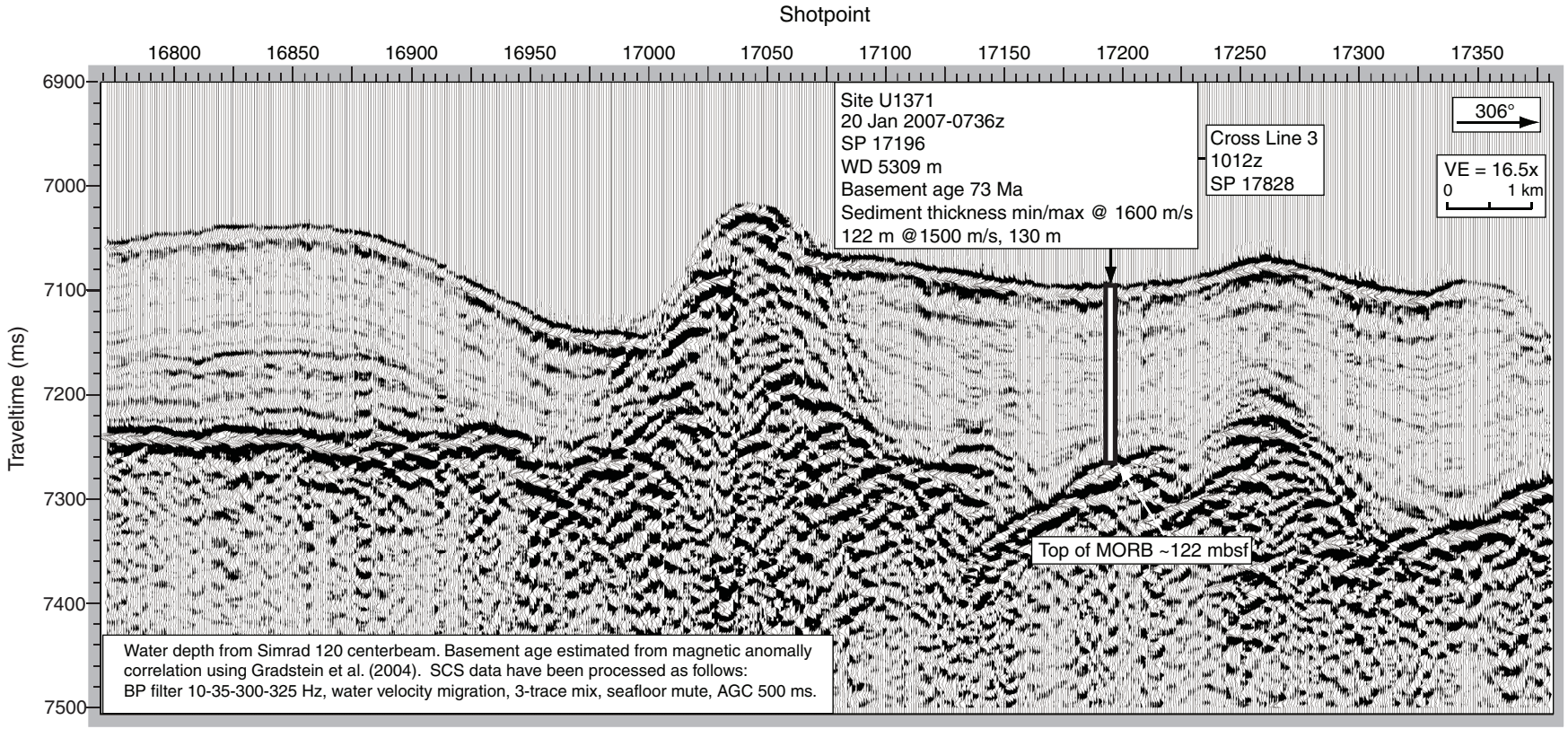

Figure F4. A portion of KNOX-02RR Channel 48 of MCS Line 3 crossing MCS Line 1, northeast of Site U1371. z = time (Greenwich Mean Time), SP = shotpoint, MORB = mid-ocean-ridge basalt, WD = water depth, SCS = single-channel seismic, BP = band-pass, AGC = automatic gain control, VE = vertical exaggeration.

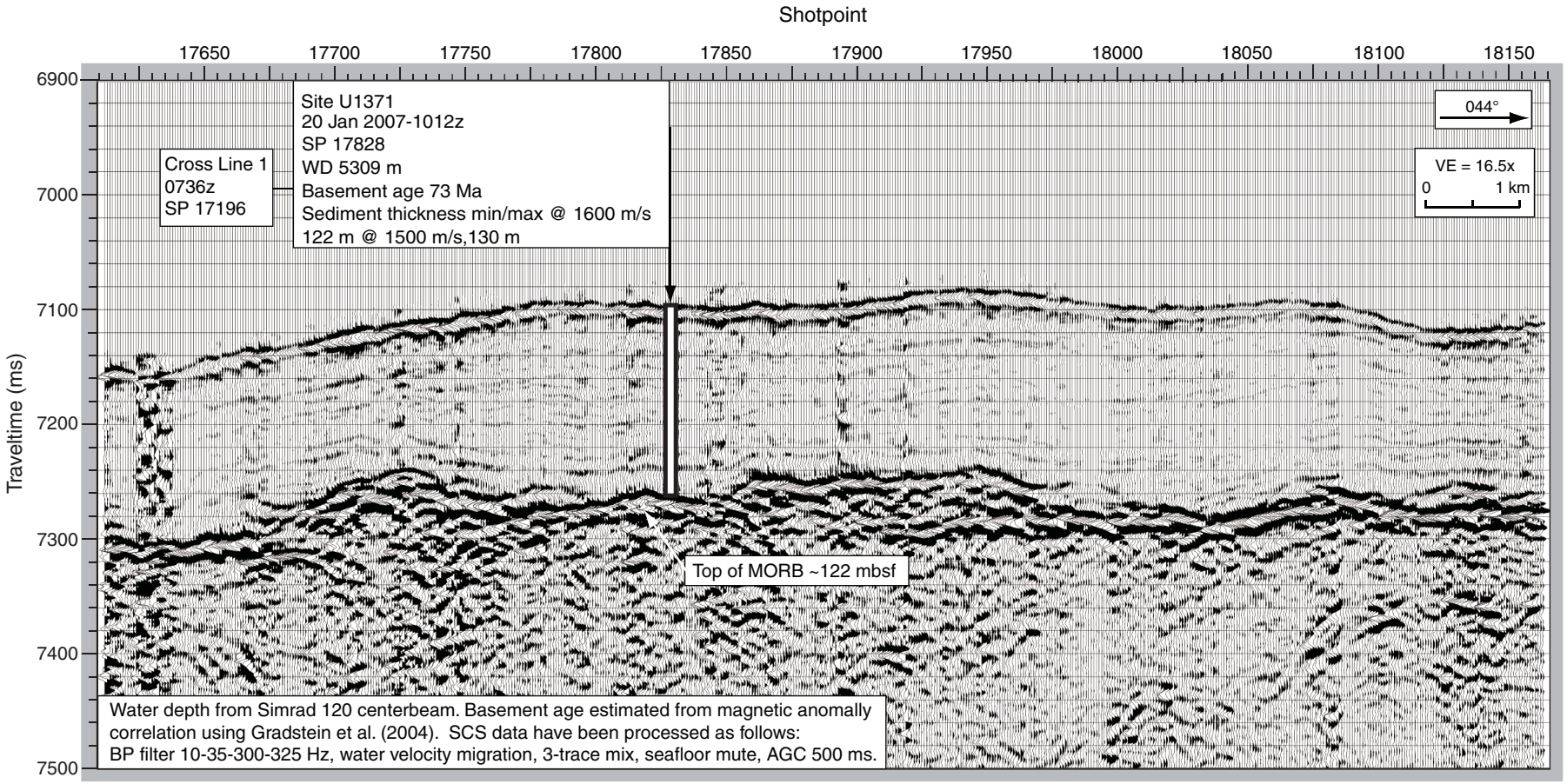

Figure F5. A portion of KNOX-02RR, 3.5 kHz seismic Line 1 across Site U1371.

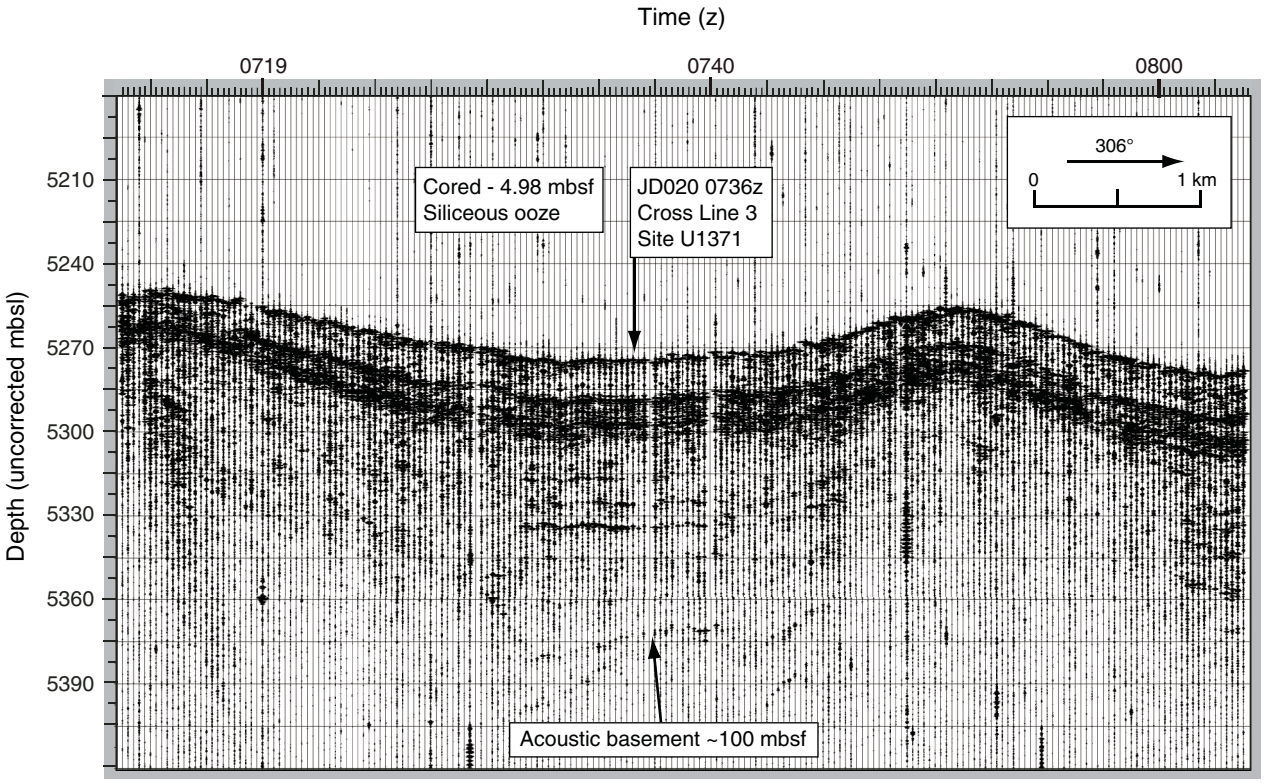

Figure F6. A portion of KNOX-02RR, 3.5 kHz seismic Line 3 across Site U1371.

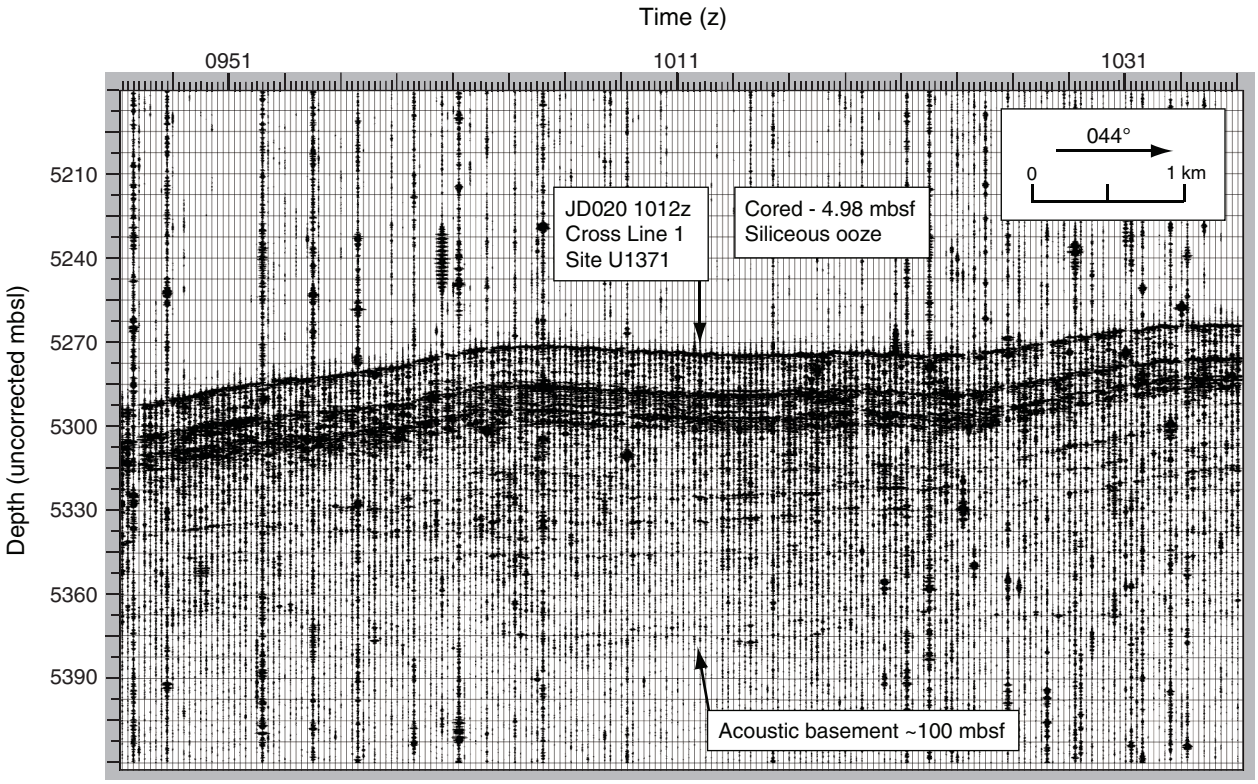

Figure F7. Summary of lithology and physical property data, Hole U1371D. MS = magnetic susceptibility, GRA = gamma ray attenuation, K = potassium content based on spectral gamma ray analyses, NGR = natural gamma radiation, RSO = red-brown to yellow-brown semiopaque oxide.

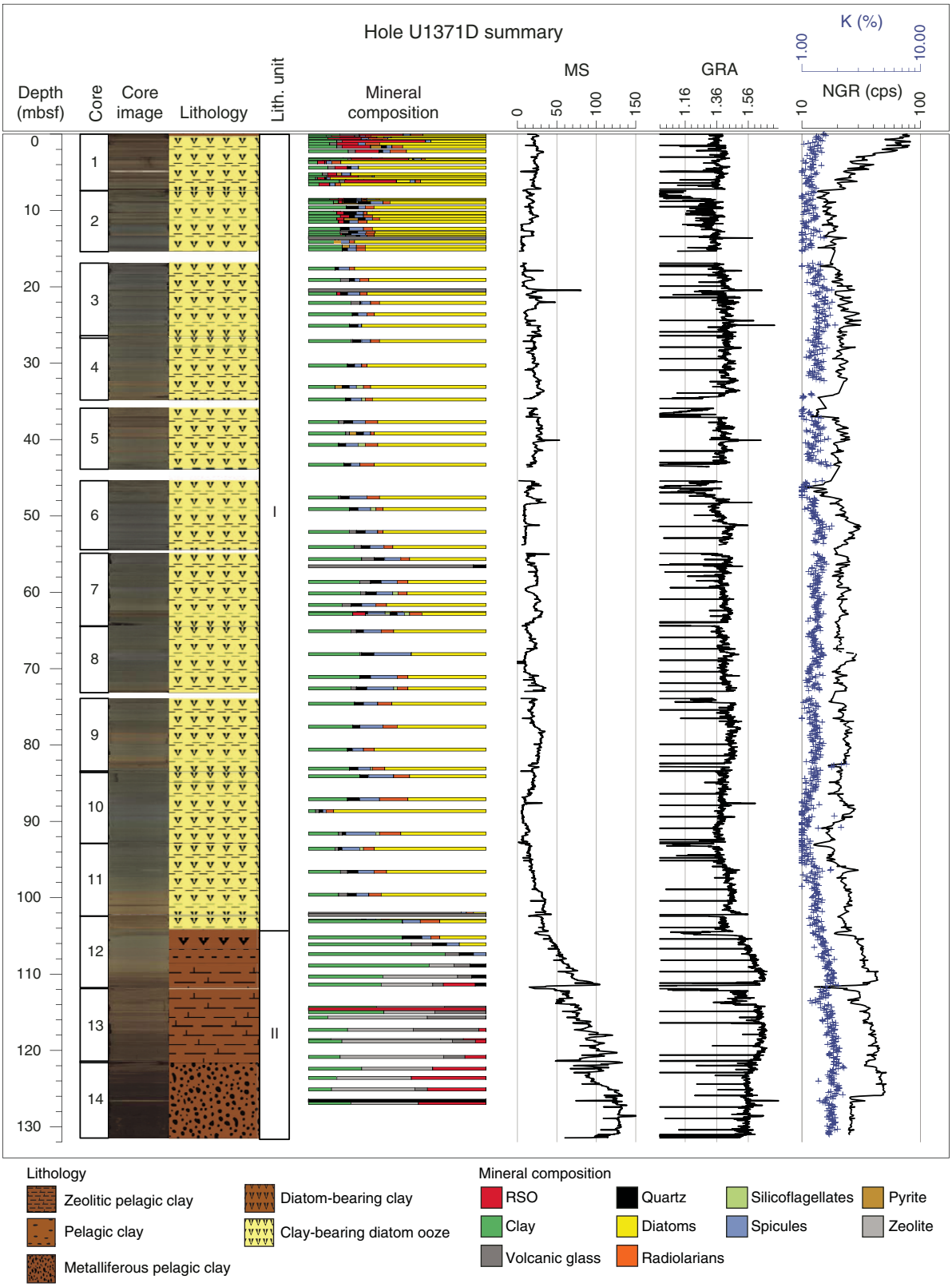

Figure F8. Lithostratigraphic correlations of holes at Site U1371.

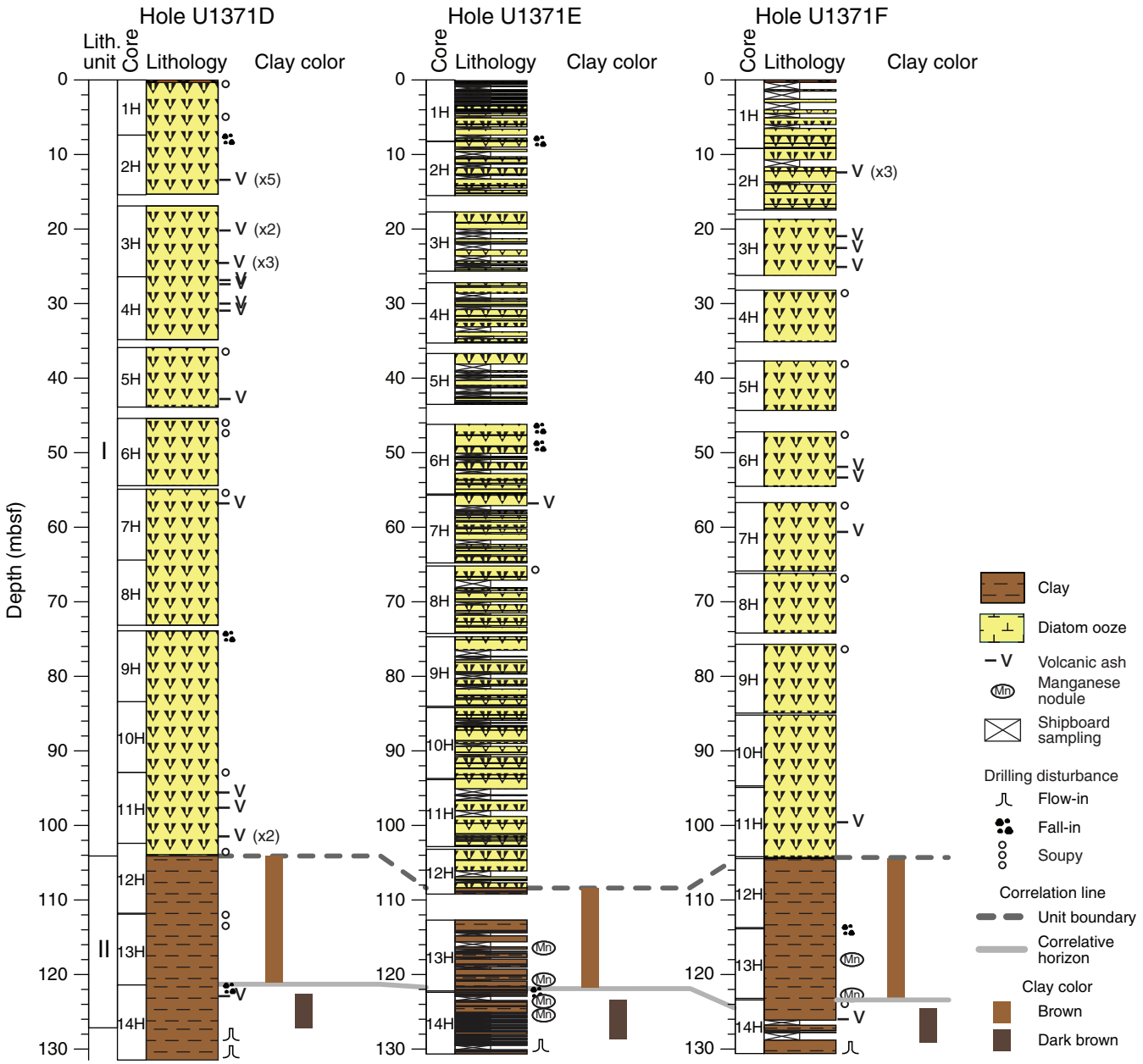

Figure F9. Representative core photographs of sediment, Site U1371. **A.** Olive-gray clay-bearing diatom ooze containing burrows at the top of Unit I (interval 329-U1371D-1H-1, 70–110 cm). **B.** Typical greenish gray clay-bearing diatom ooze containing an ash layer in Unit I (interval 329-U1371D-3H-6, 50–90 cm). **C.** Light olive-brown zeolitic pelagic clay containing burrows in the upper part of Unit II (interval 329-U1371D-12H-6, 90–130 cm). **D.** Manganese nodule and irregularly formed manganese-rich sediment in Unit II (interval 329-U1371D-13H-3, 60–90 cm). **E.** Very dark grayish brown zeolitic pelagic clay containing burrows and layers in the lower part of Unit II (interval 329-U1371D-14H-2, 110–150 cm).

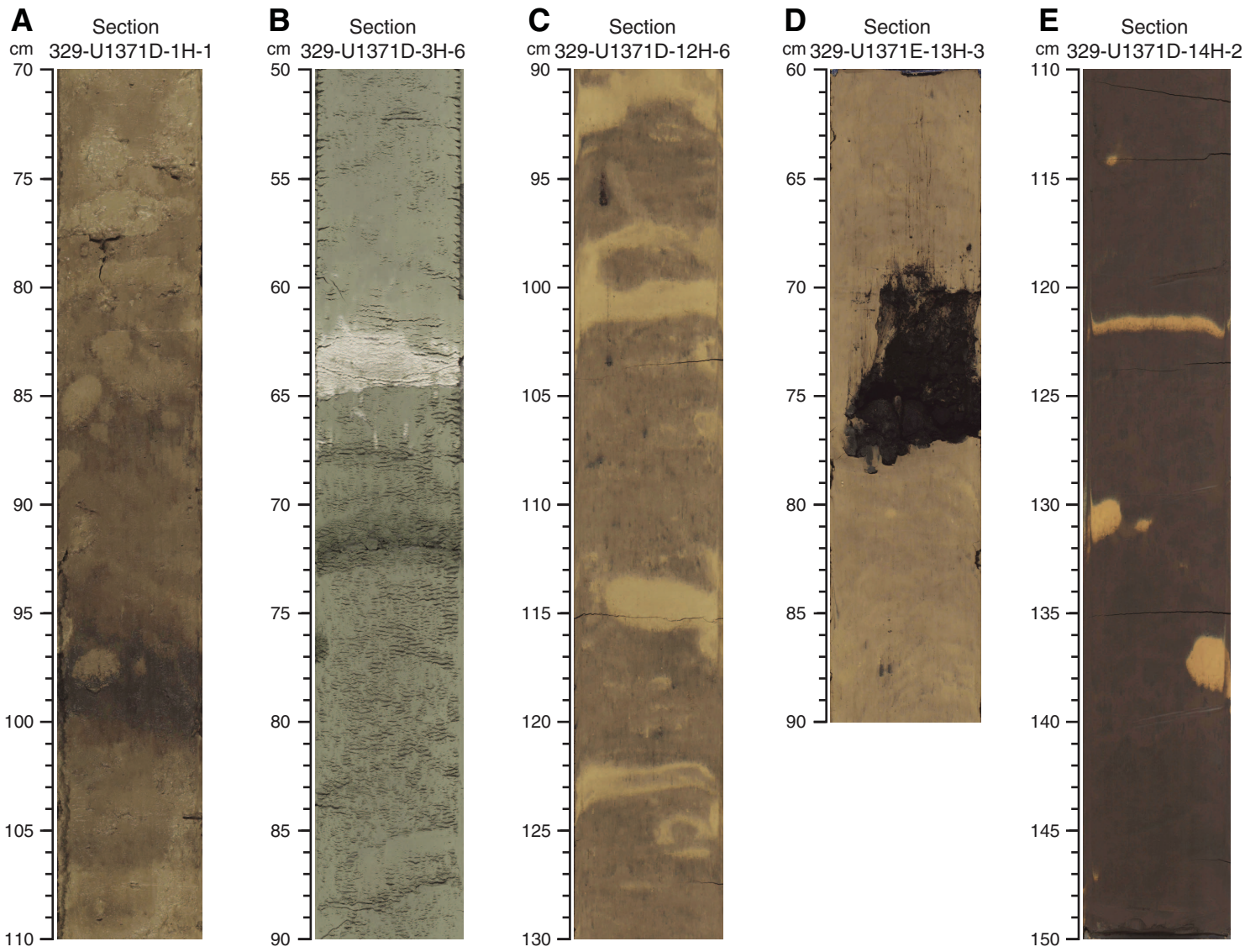

Figure F10. Selected smear slide photomicrographs of clay and ooze sediments, Site U1371. **A.** Clay-bearing diatom ooze in Unit I (Sample 329-U1371D-2H-1, 145 cm). **B.** Zeolitic metalliferous pelagic clay in Unit II (Sample 329-U1371D-14H-3, 70 cm).

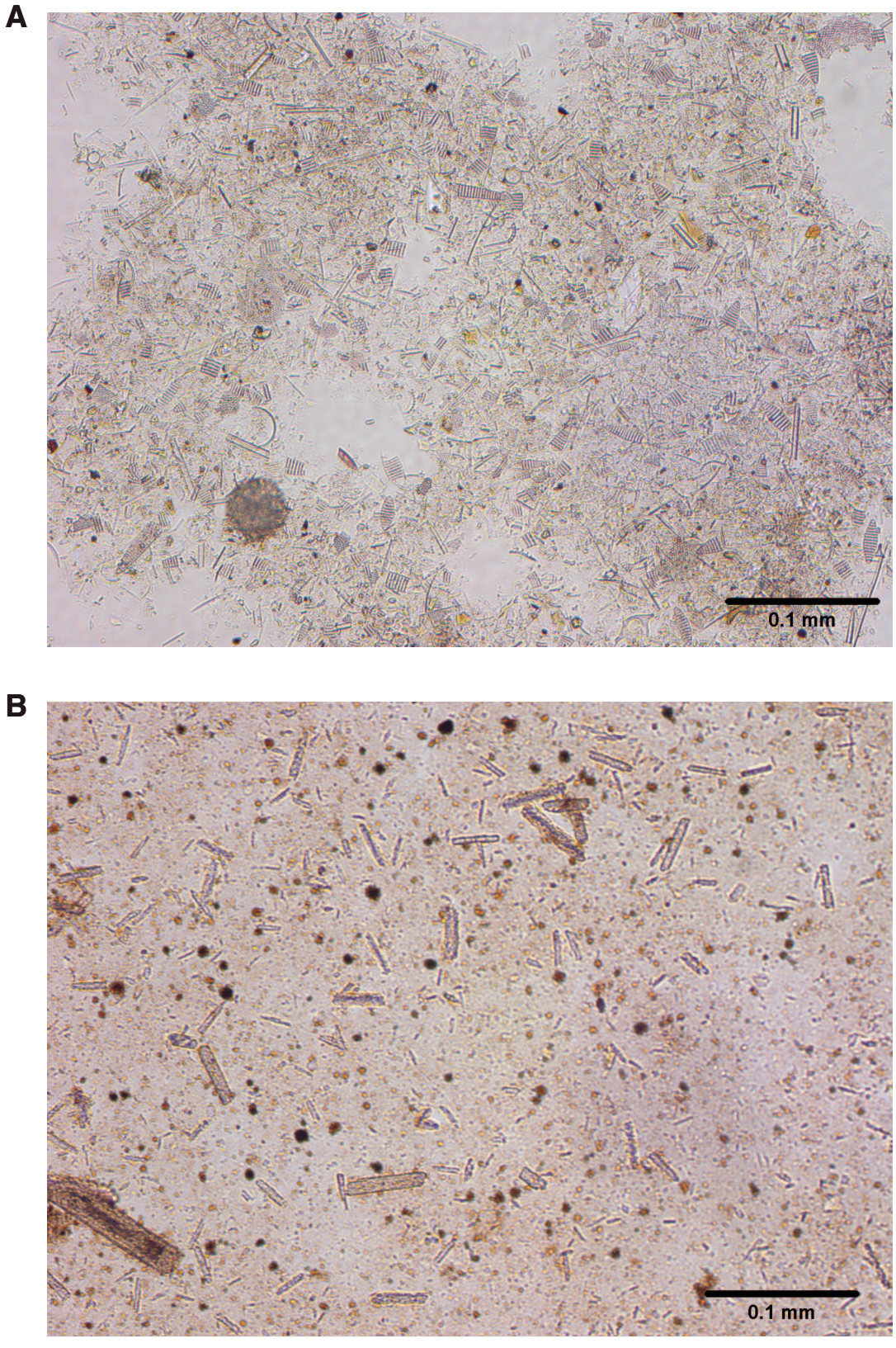

Figure F11. X-ray diffractograms of selected sediment, Site U1371. **A.** Characteristic diffraction peaks for quartz (Q), cristobalite (C), chlorite (Cl), illite (I), phillipsite (P), and halite (H) in Unit I. Peaks are labeled twice when the intensities from the upper (black) and lower (red) parts of the unit showed significant differences. **B.** Diffraction patterns illustrating differences among variable XRD mineralogy in samples from the upper (black) and lower (red) parts of Unit II. Notable changes in minerals common to the intervals (illite, cristobalite, quartz, and phillipsite) and unique occurrence of red-brown to yellow-brown semiopaque oxyhydroxides (RSO) distinguish the two patterns.

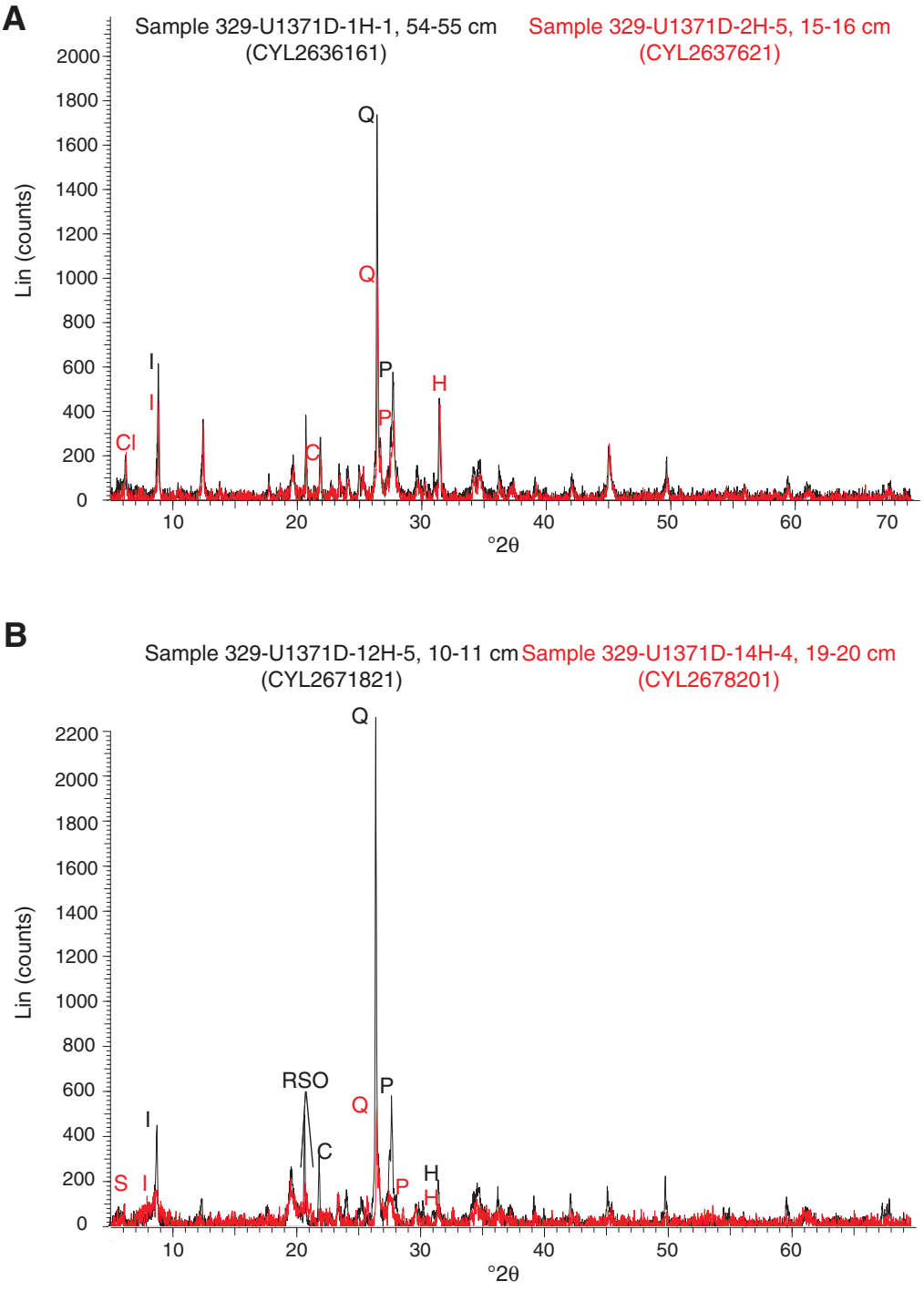

Figure F12. Plots of moisture and density (MAD) measurements, Hole U1371D. **A.** Bulk density. Red circles indicate bulk density derived from MAD Method C, blue circles indicate bulk density derived from gamma ray attenuation. **B.** Grain density. **C.** Porosity.

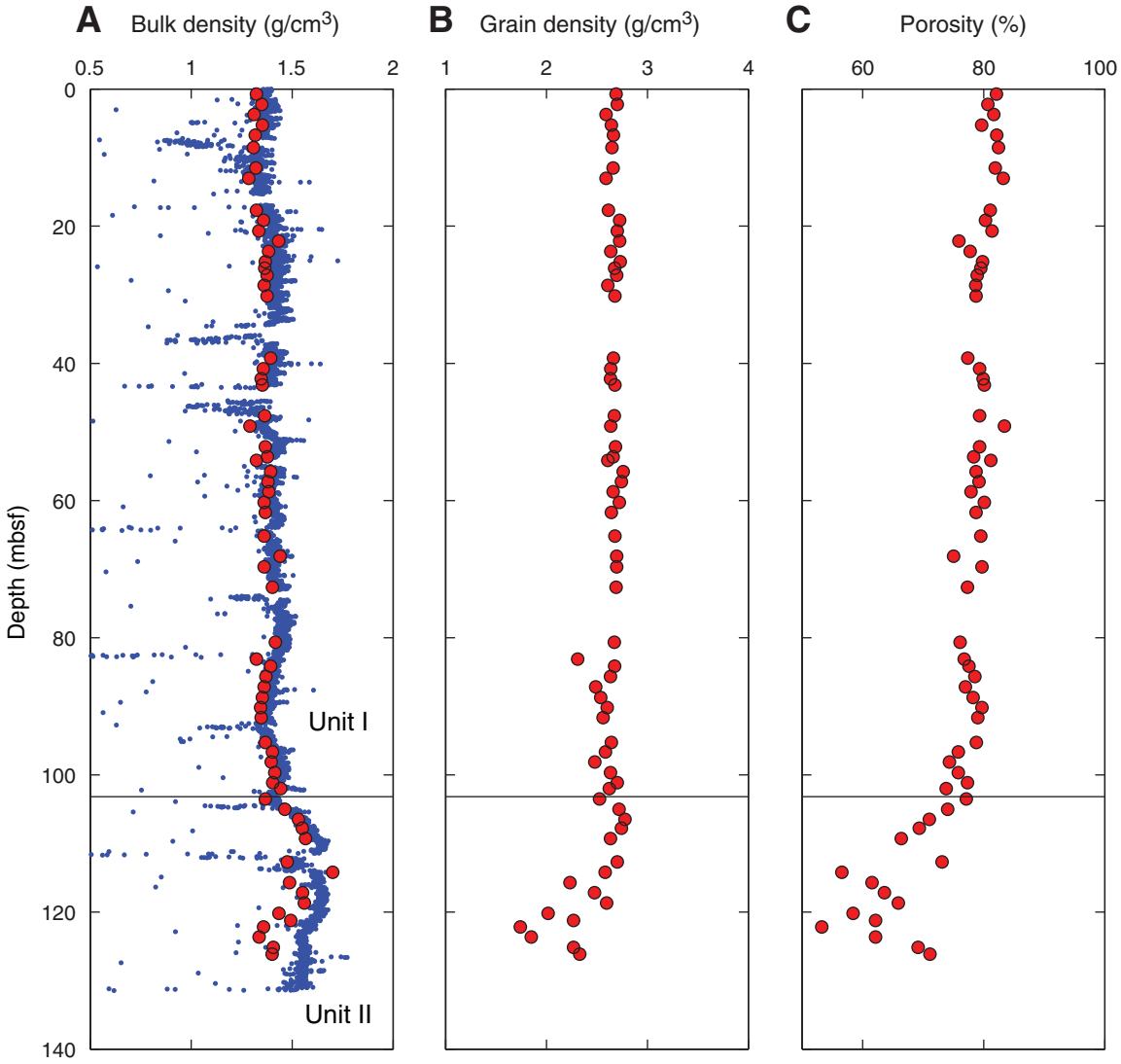

Figure F13. Plots of bulk density values determined by gamma ray attenuation, Site U1371. Red circles show bulk density derived from MAD measurements.

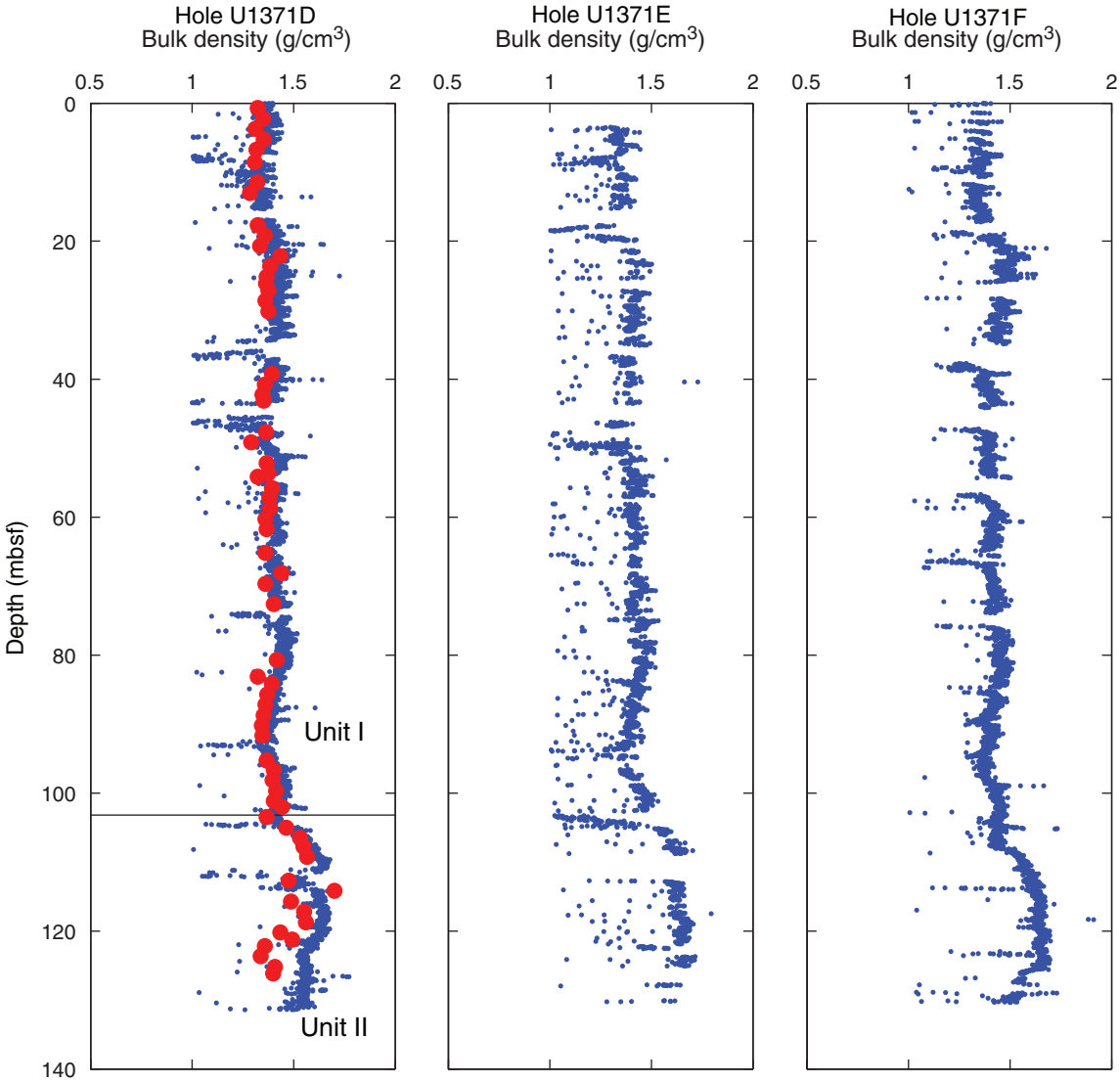

Figure F14. Plots of (**A–C**) magnetic susceptibility measurements made on the Whole-Core Multisensor Logger and (**D–F**) point magnetic susceptibility measurements made on the Section Half Multisensor Logger, Site U1371.

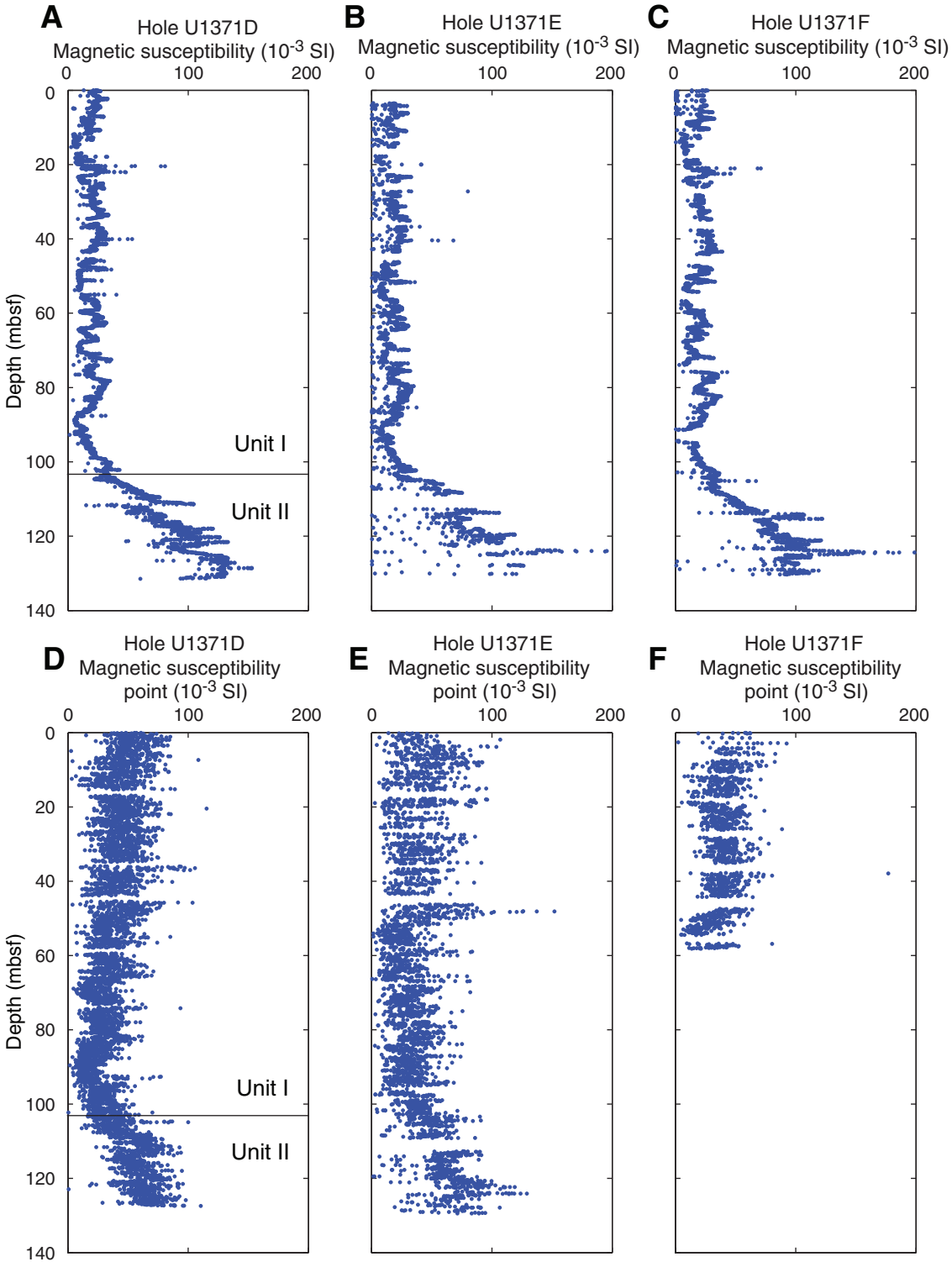

Figure F15. Plots of natural gamma radiation (NGR) as a function of depth, Site U1371.

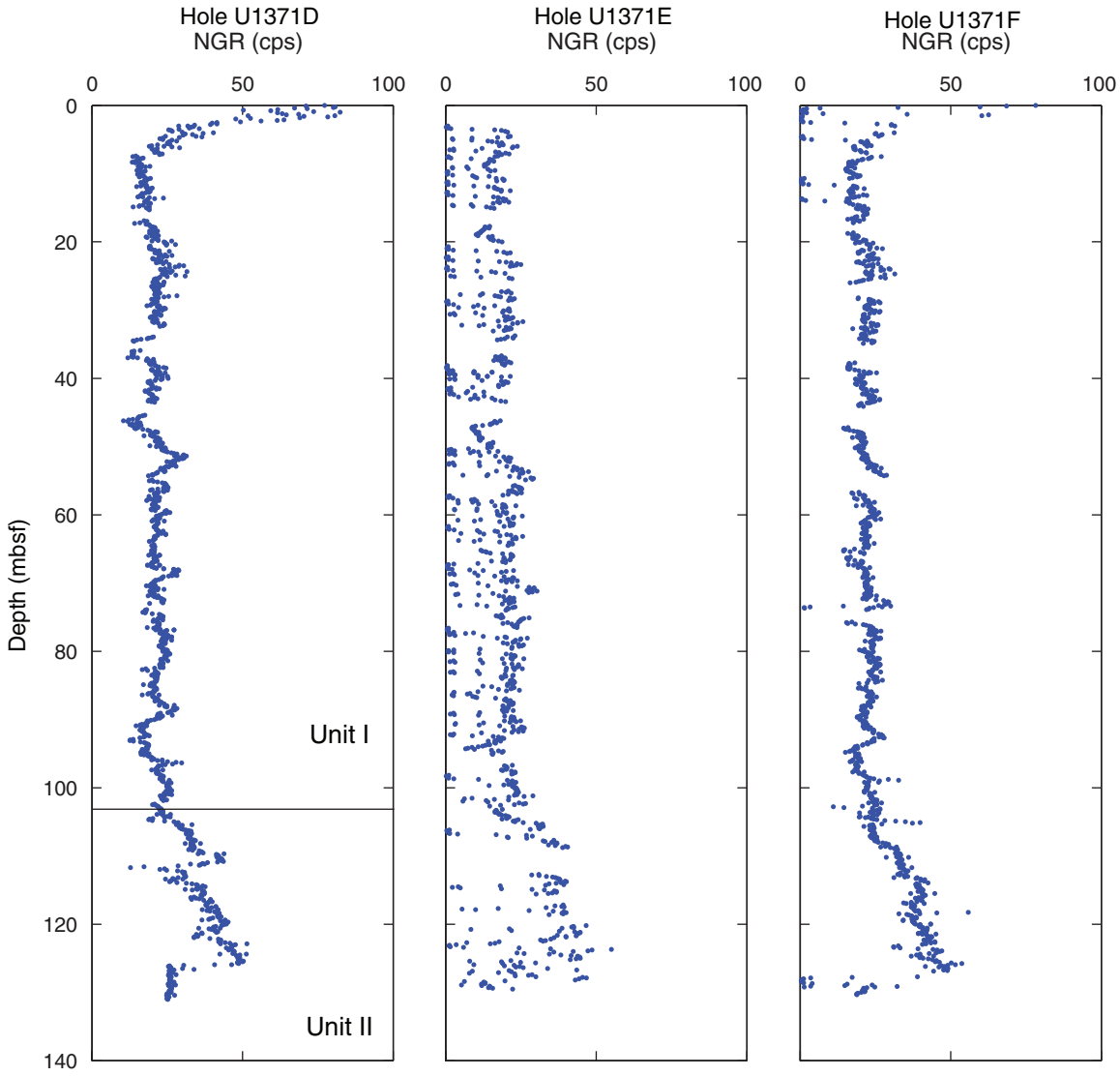

Figure F16. A. Plots of compressional wave velocity measured on the Whole-Round Multisensor Logger (WRMSL), Site U1371. Red circles indicate discrete measurements. **B.** Histogram of WRMSL *P*-wave velocity from all holes.

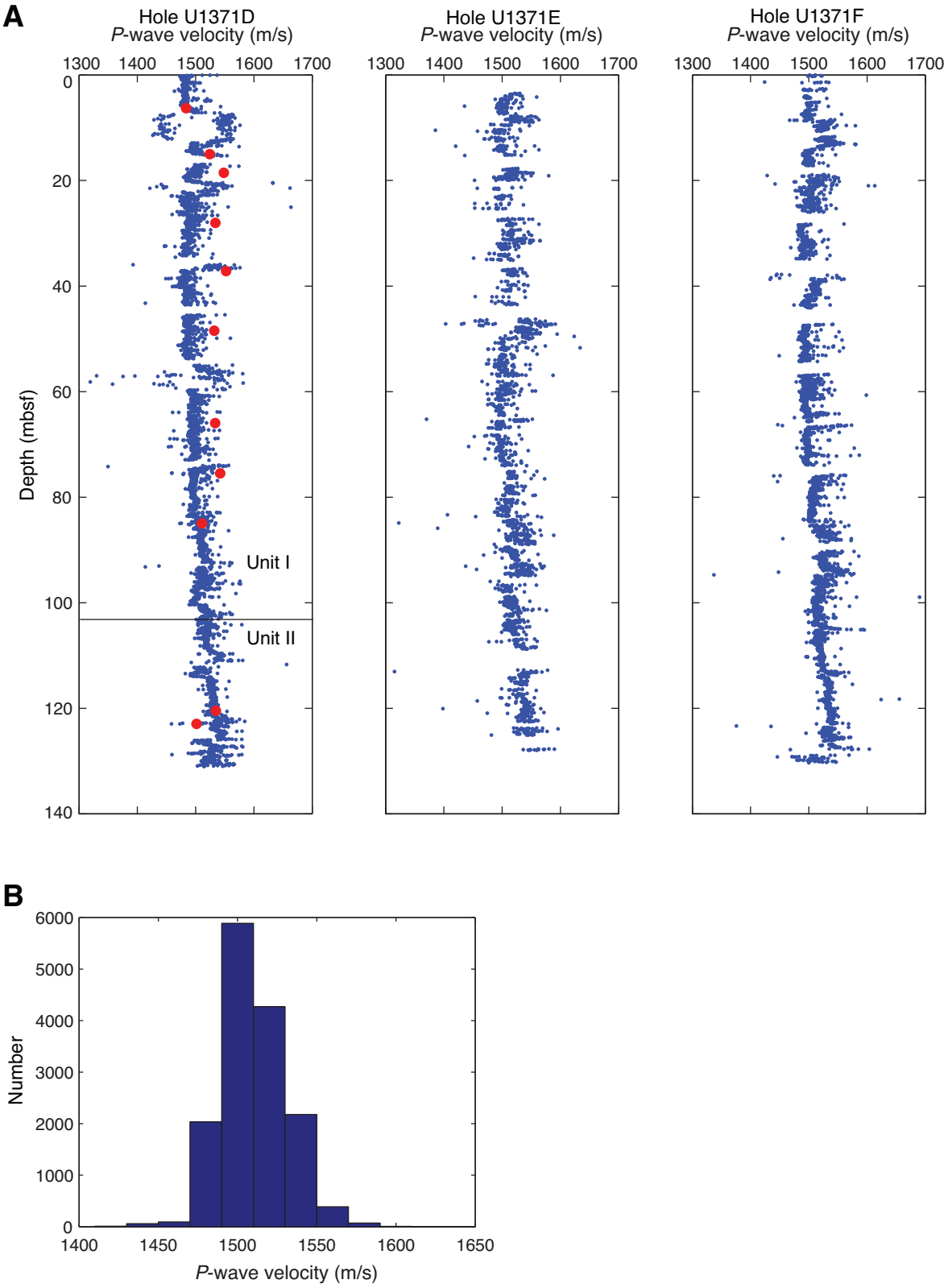

Figure F17. Plot of electrical conductivity measured on surface seawater standard, Site U1371. Lines show optimum linear fit to data.

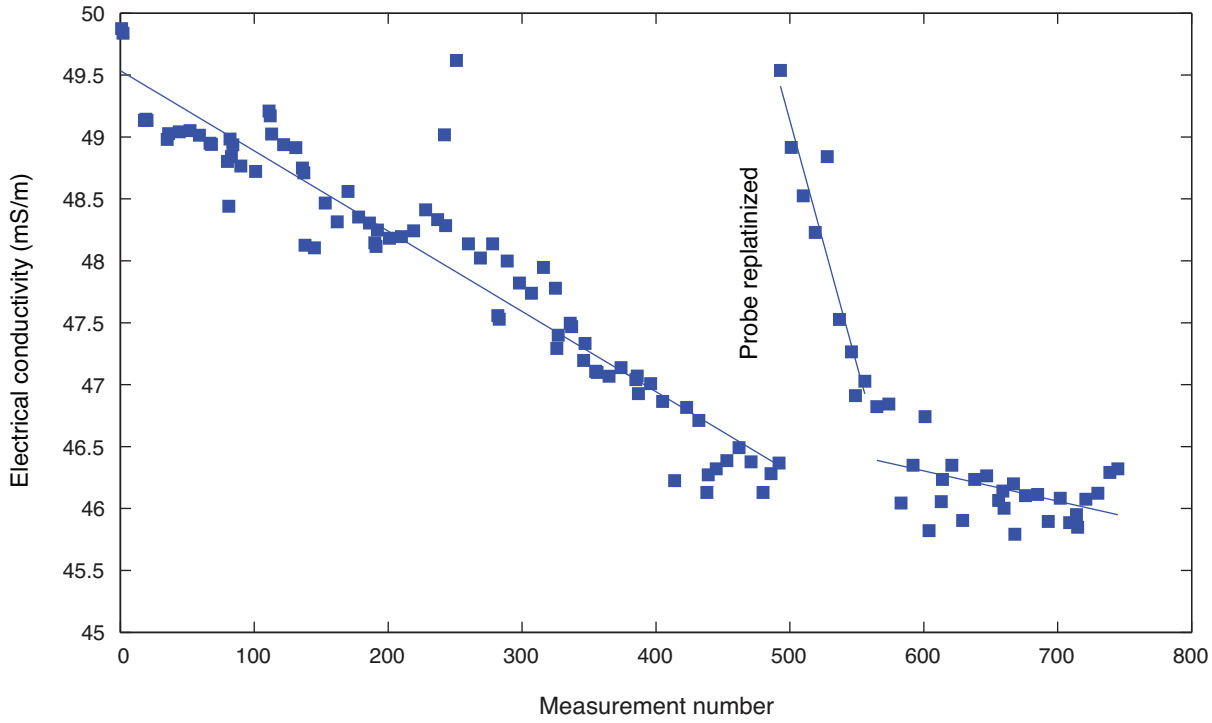

Figure F18. Plot of formation factor as a function of depth, Hole U1371D.

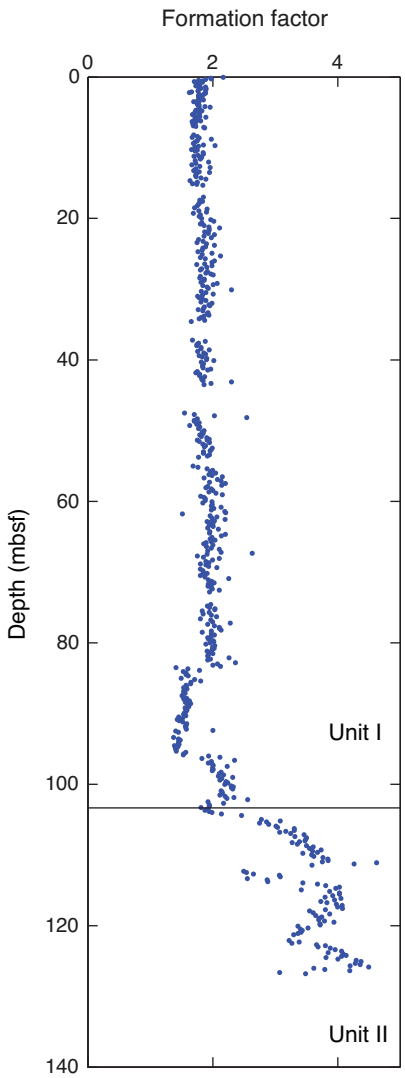

Figure F19. Plots of thermal data, Site U1371. **A.** Thermal conductivity values. Blue circles = full-space measurements from Expedition 329, black triangles = measurements from KNOX-02RR site survey (R. Harris, unpubl. data). **B.** Equilibrium temperatures.

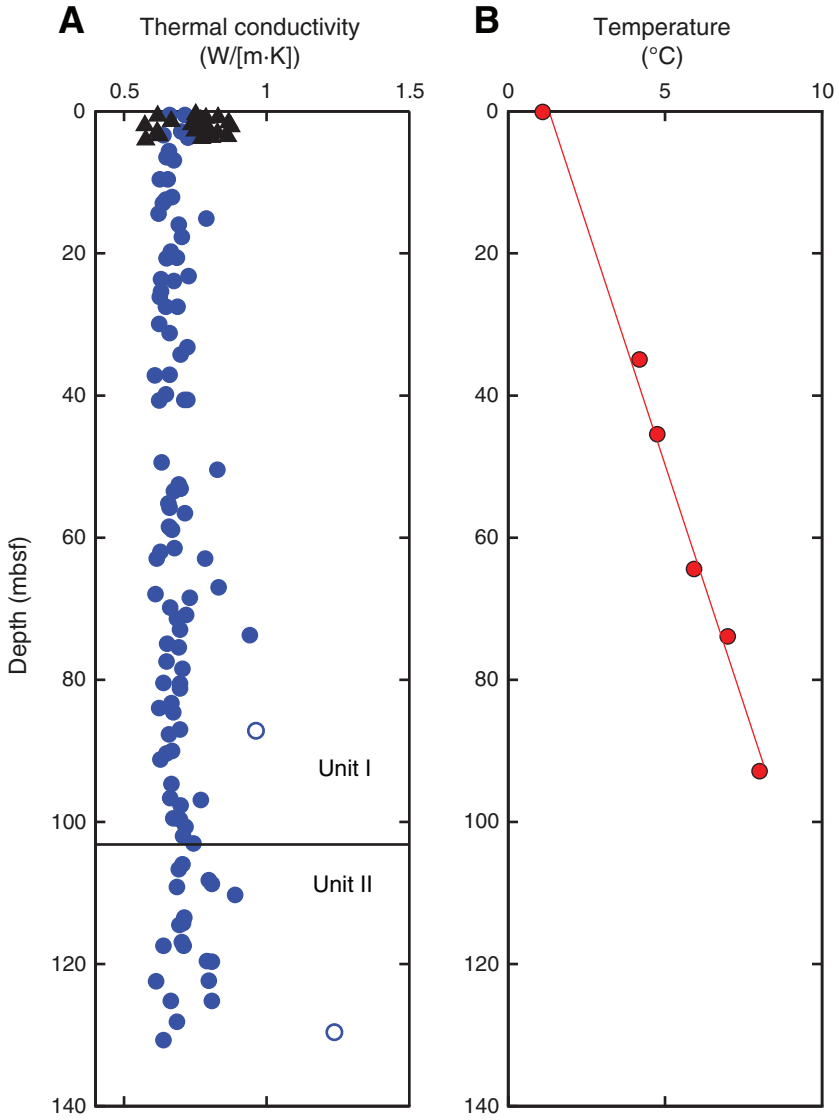

Figure F20. Temperature-time series measured during the deployment of APCT-3 (blue line), Site U1371. Unshaded area indicates data used for equilibrium temperature fit. Red line indicates theoretical equilibrium curve, triangle indicates beginning of fit, inverted triangle indicates end of fit. Dashed red line with circles indicates estimate of equilibrium temperature. (Continued on next page.)

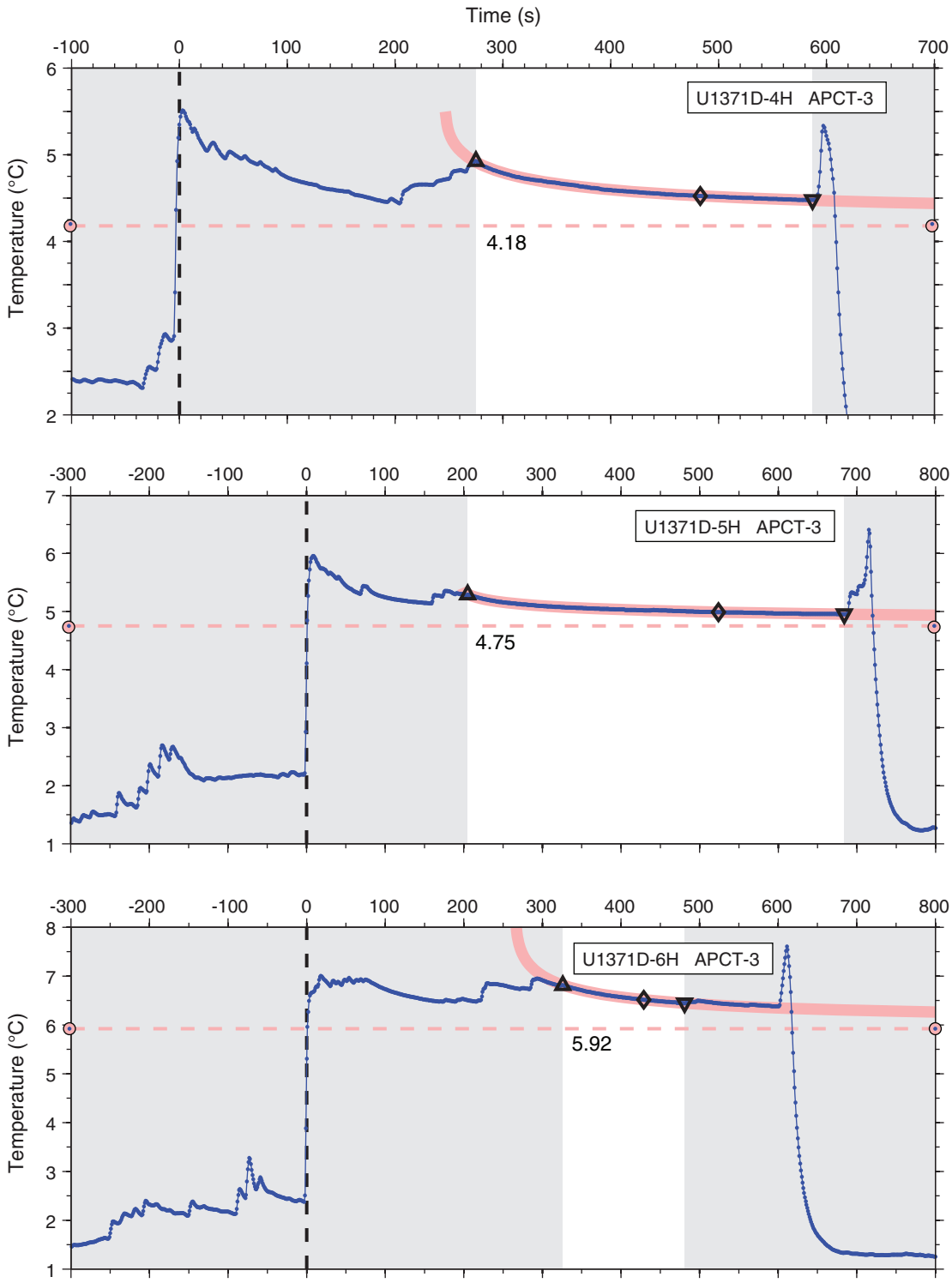

Figure F20 (continued).

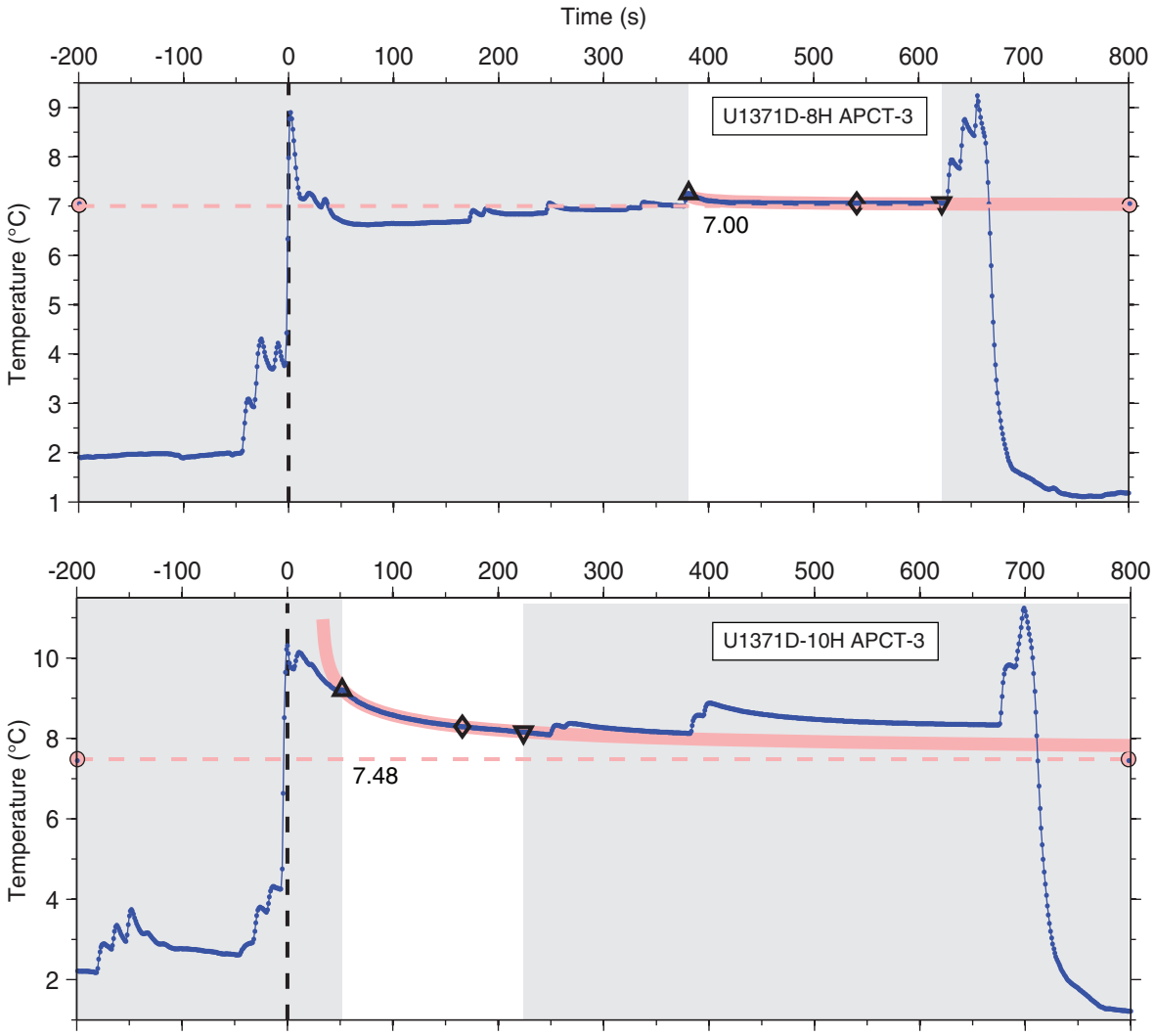

Figure F21. Plots of color spectrometry values, Hole U1371D.

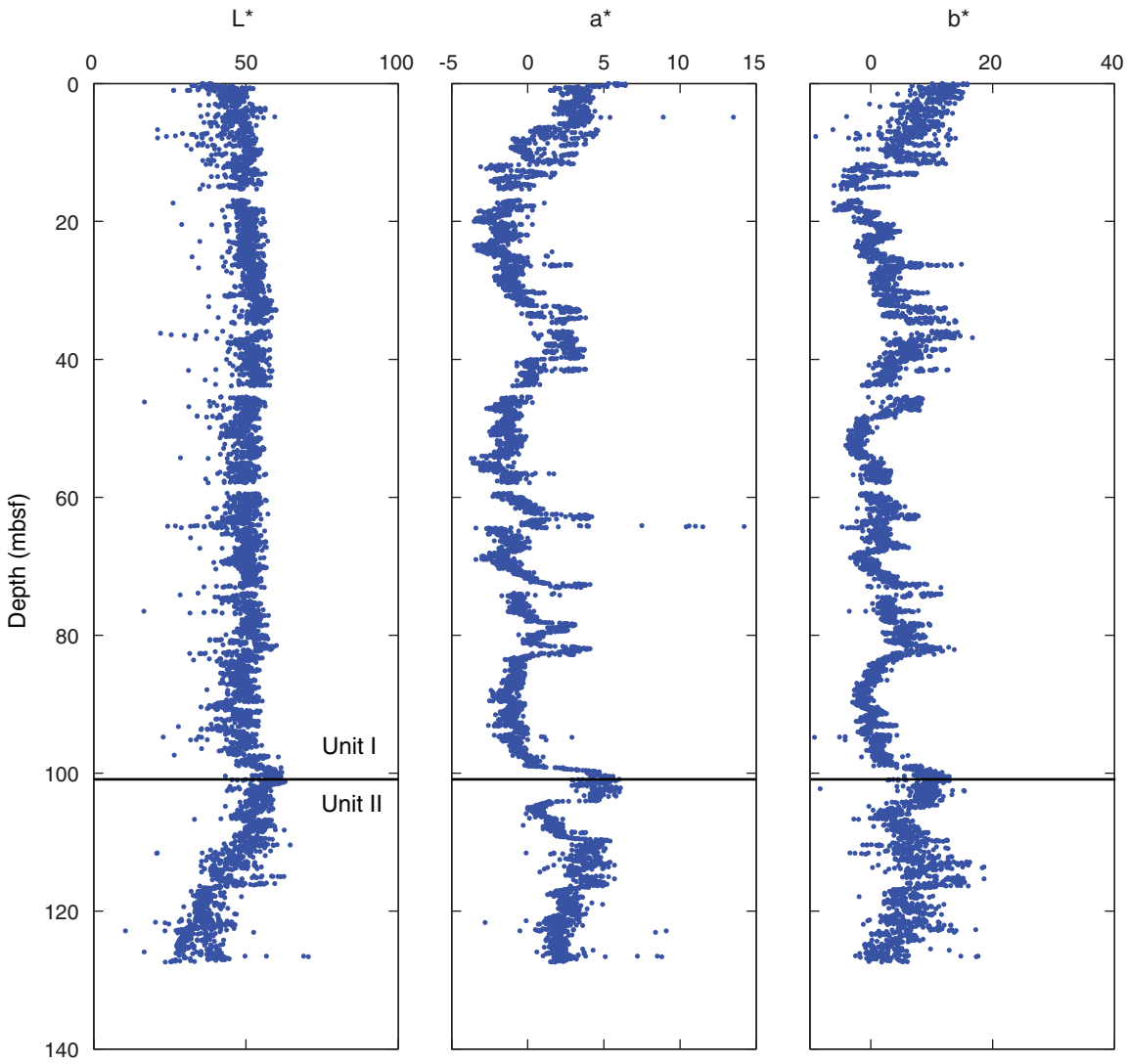

Figure F22. Summary of magnetic susceptibility and paleomagnetic intensity, Hole U1371B. Gray = measurement before demagnetization, red = measurement after 20 mT AF demagnetization step (inclination and intensity), blue = declination measurements, green = magnetic susceptibility data.

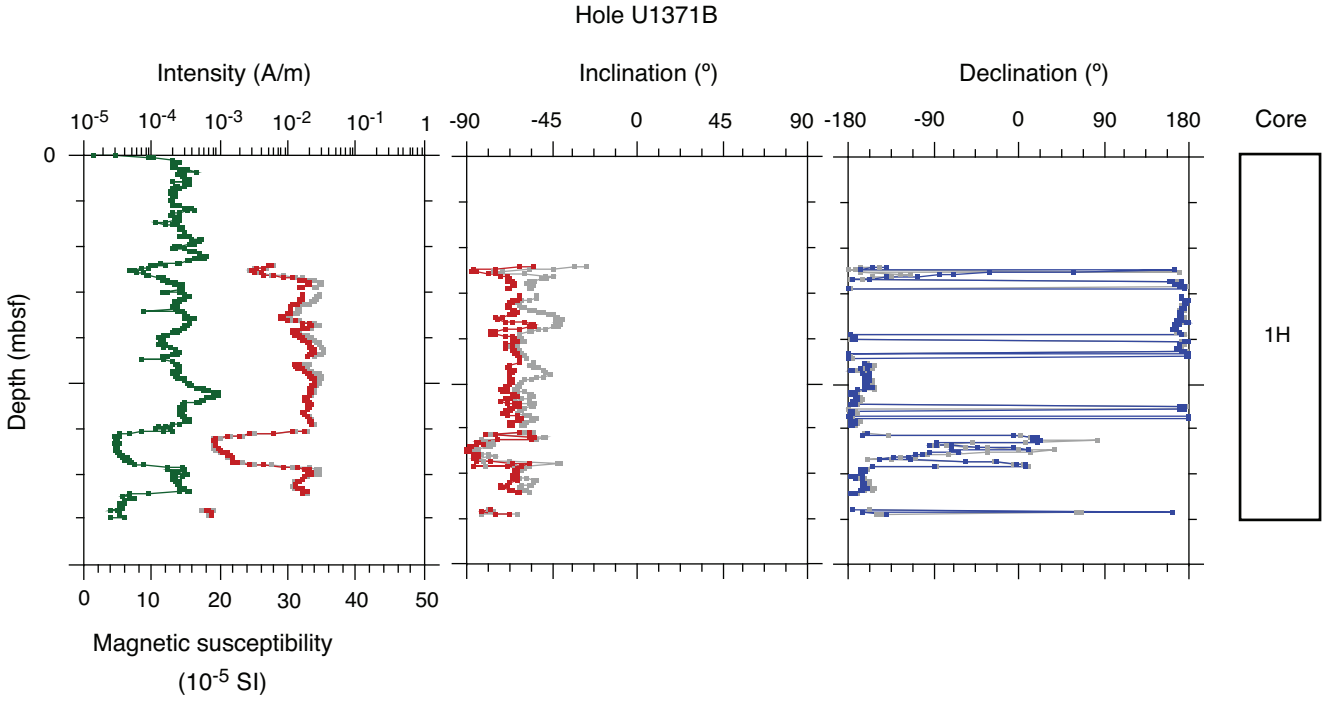

Figure F23. Summary of magnetic susceptibility and paleomagnetic results, Hole U1371C. Gray = measurement before demagnetization, red = measurement after 20 mT AF demagnetization step (inclination and intensity), blue = declination measurements, green = magnetic susceptibility data.

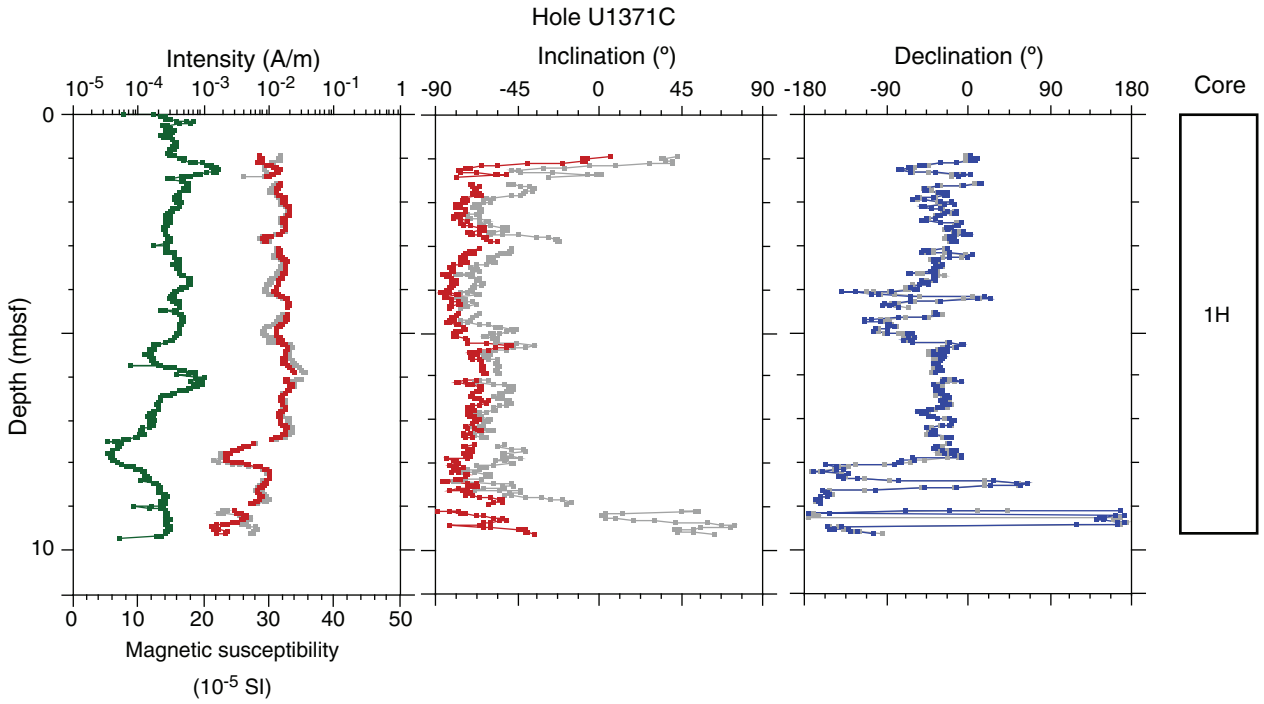

Figure F24. Summary of magnetic susceptibility and paleomagnetic results, Hole U1371D. Gray = measurement before demagnetization, red = measurement after 20 mT AF demagnetization step (inclination and intensity), blue = declination measurements, green = magnetic susceptibility data. Declinations are raw data before orientation using the Flexit tool.

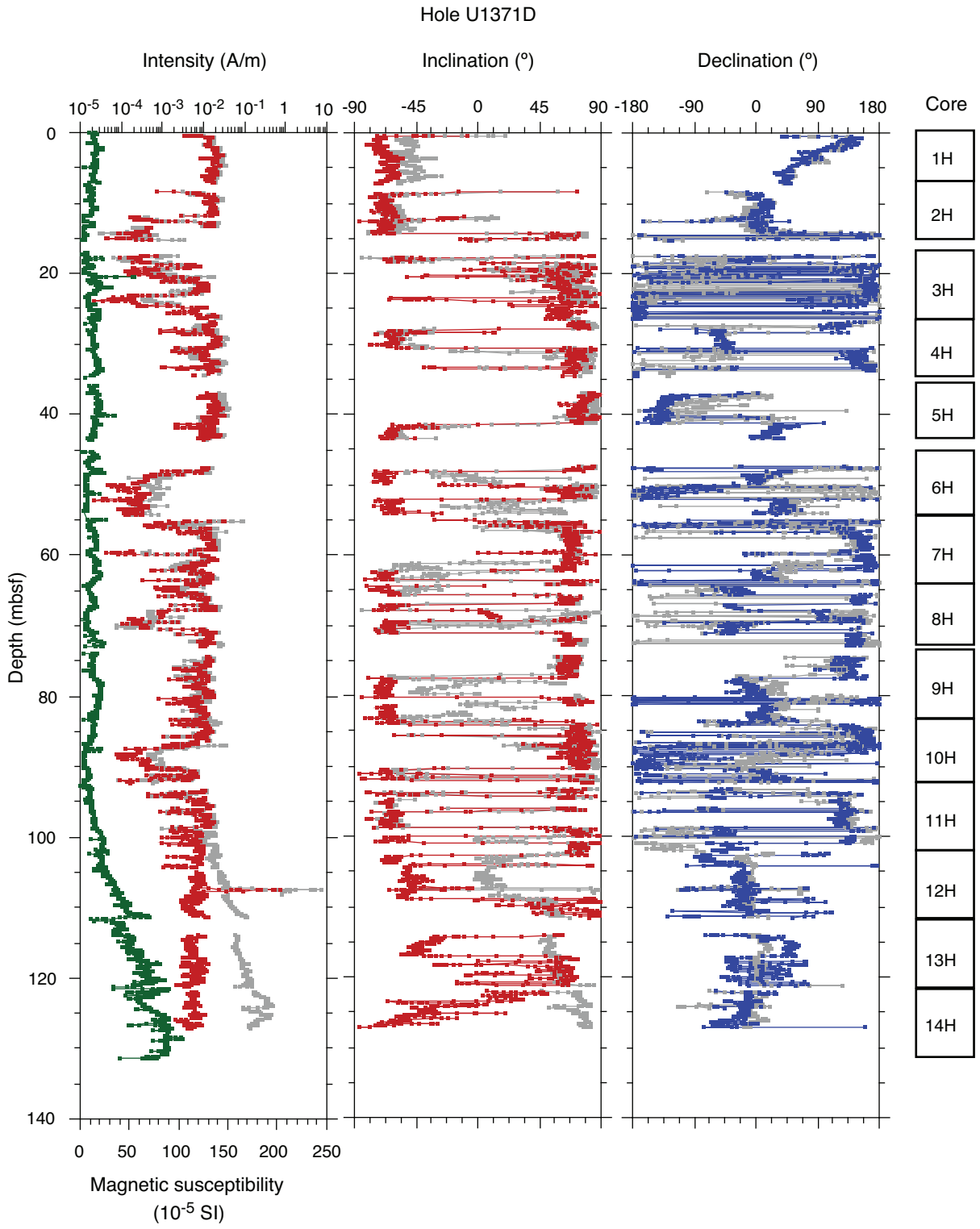

Figure F25. Summary of magnetic susceptibility and paleomagnetic results, Hole U1371E. Gray = measurement before demagnetization, red = measurement after 20 mT AF demagnetization step (inclination and intensity), blue = declination measurements, green = magnetic susceptibility data.

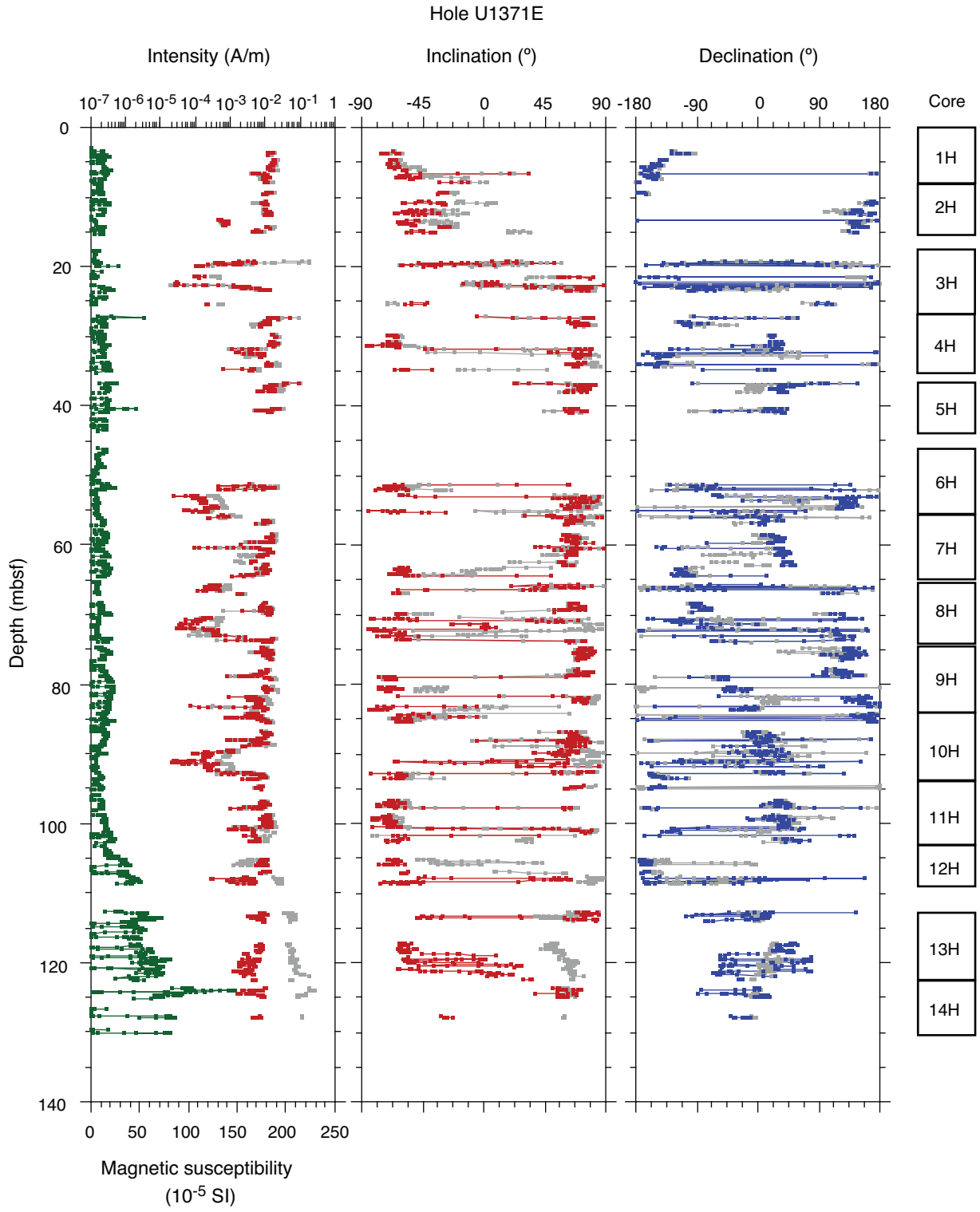

Figure F26. Summary of magnetic susceptibility and paleomagnetic results, Hole U1371F. Gray = measurement before demagnetization, red = measurement after 20 mT AF demagnetization step (inclination and intensity), blue = declination measurements, green = magnetic susceptibility data. Declinations are raw data before orientation using the Flexit tool.

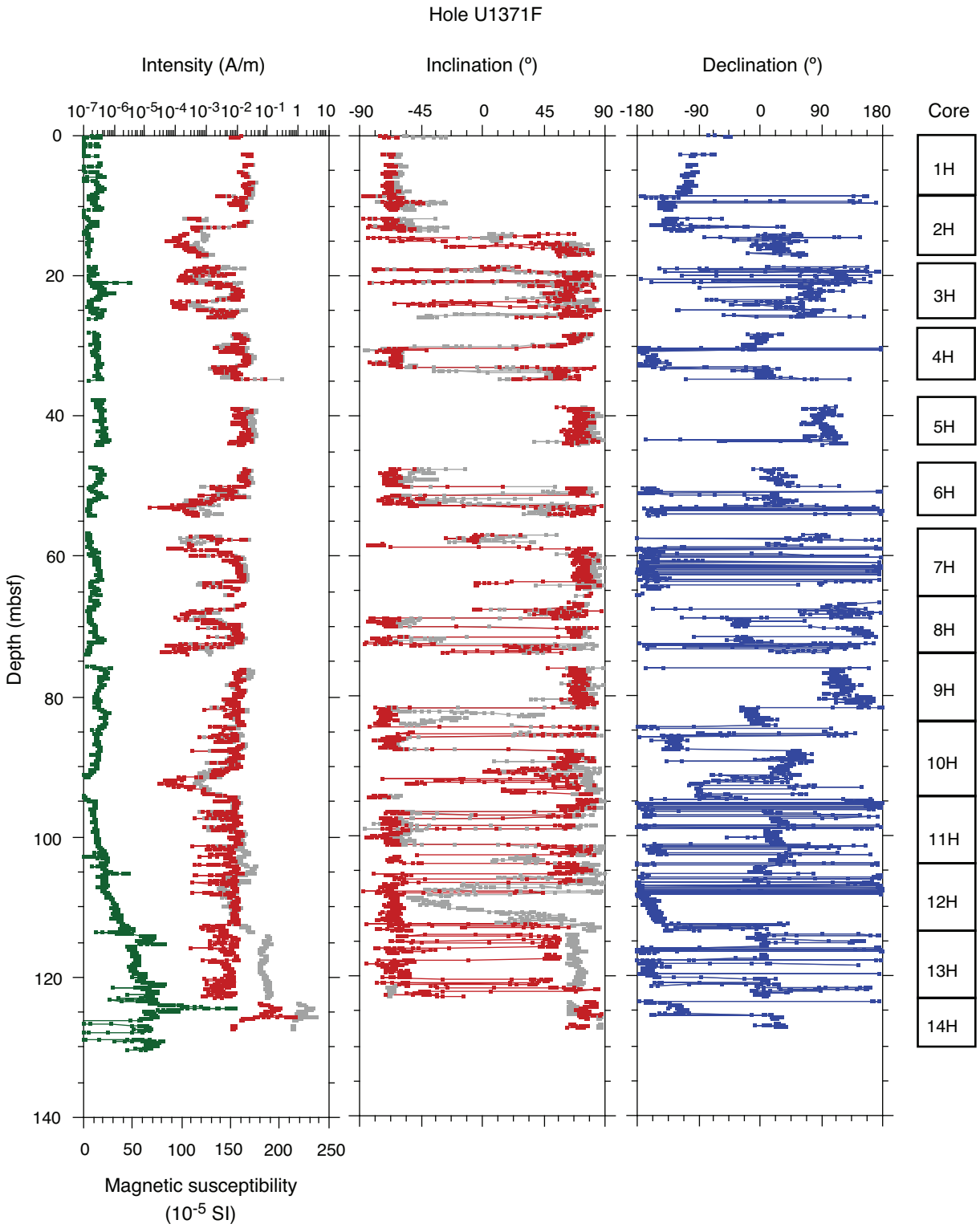

Figure F27. Summary of magnetic susceptibility and paleomagnetic results, Hole U1371H. Gray = measurement before demagnetization, red = measurement after 20 mT AF demagnetization step (inclination and intensity), blue = declination measurements, green = magnetic susceptibility data.

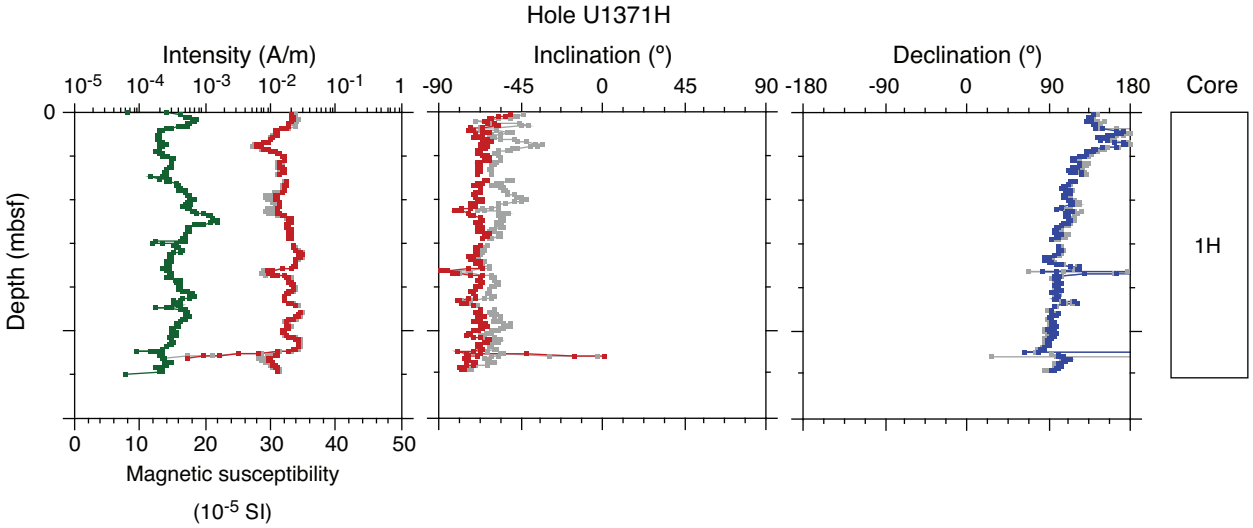

Figure F28. Results of hole-to-hole correlation using magnetic susceptibility (green) and magnetic intensity (red) data from Holes U1371B–U1371D. Black lines indicate correlation points between holes. Gray = measurement before demagnetization, red = inclination after 20 mT AF demagnetization step.

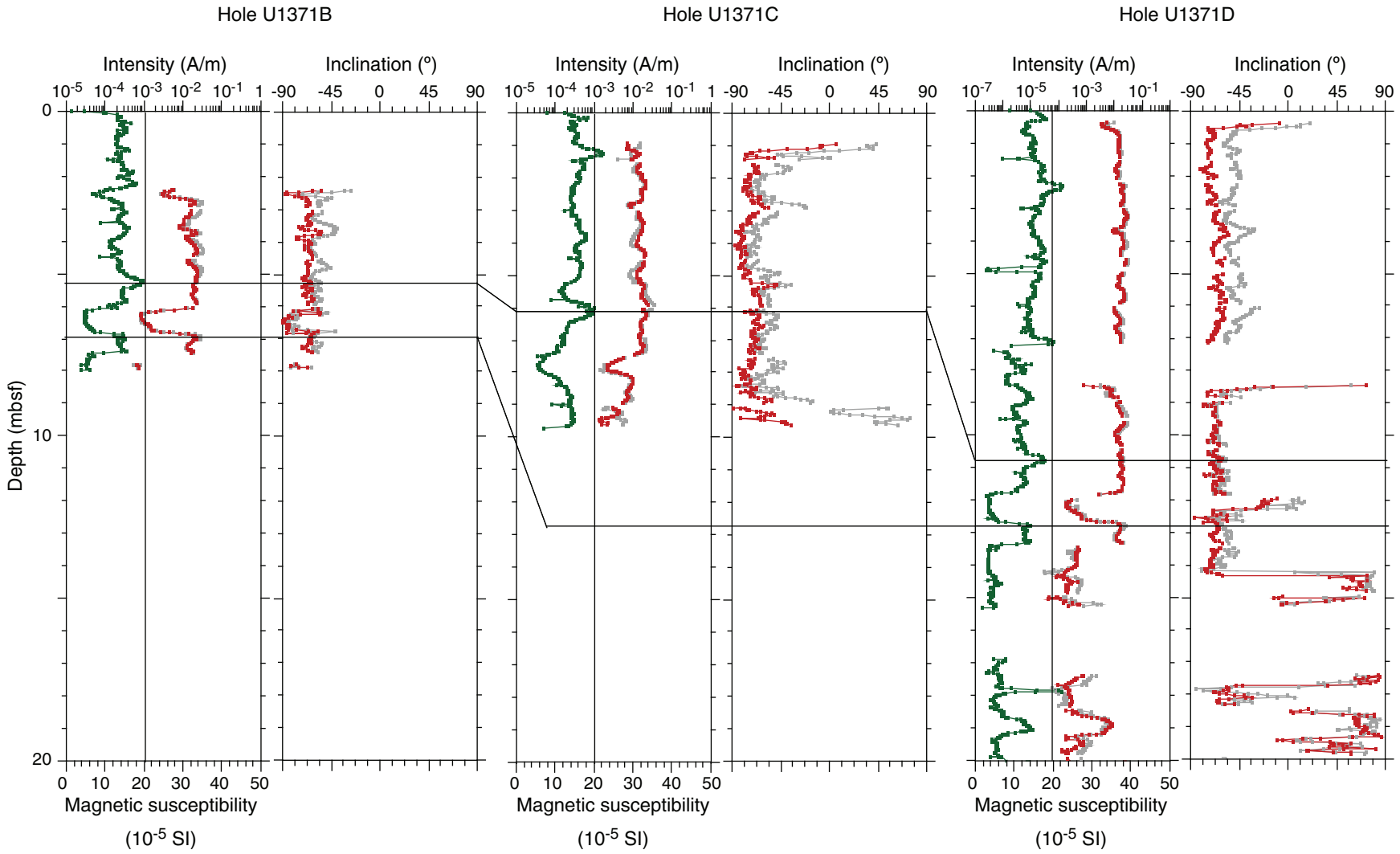

Figure F29. Results of hole-to-hole correlation using magnetic susceptibility (green) and magnetic intensity (red) data from Holes U1371D–U1371F. Black lines indicate correlation points between holes. Gray = measurement before demagnetization.

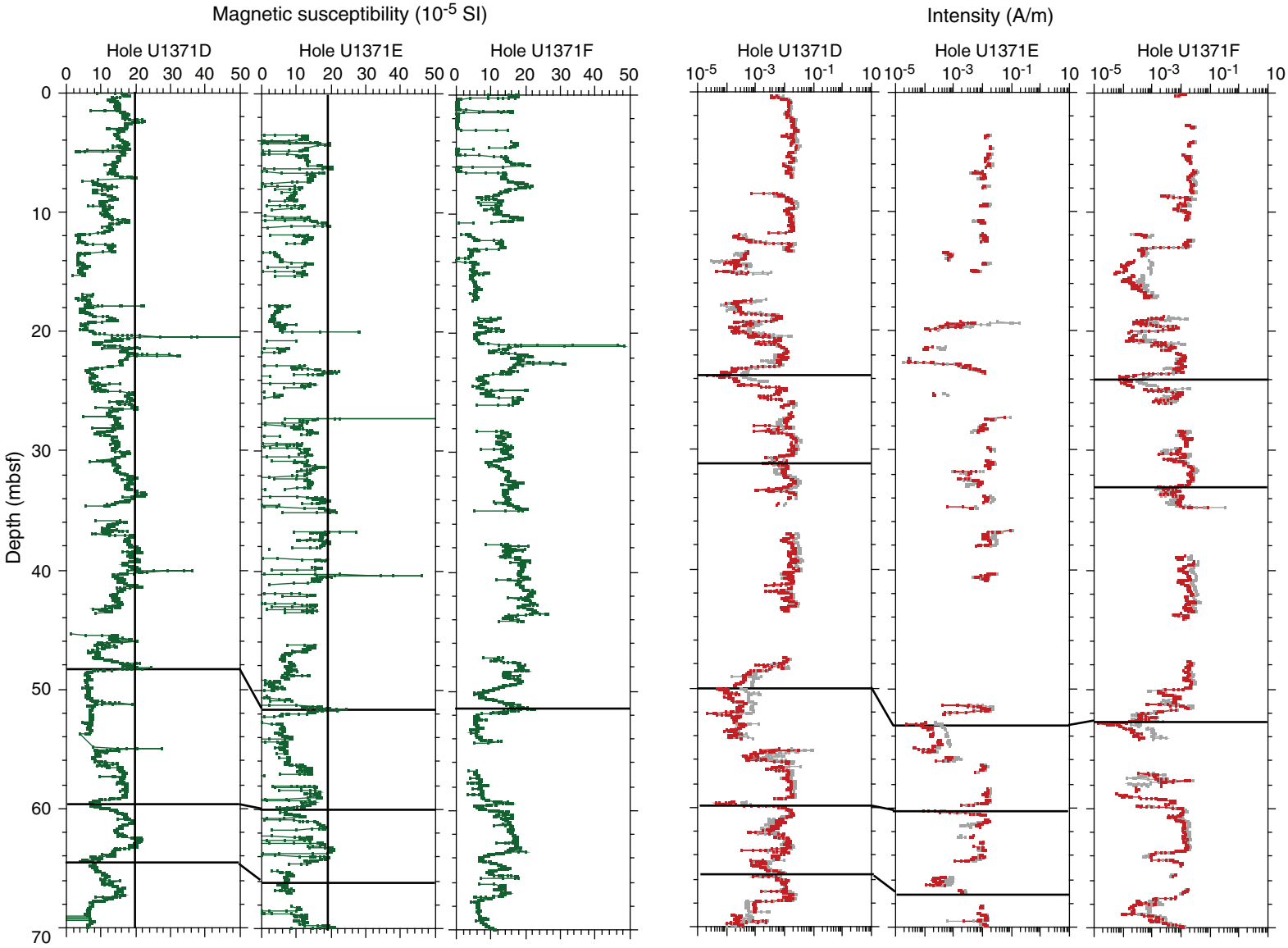

Figure F30. Comparison of polarity records between Holes U1371D and U1371F, 0–70 mbsf. Inclination (red) and declination (blue) data are after the 20 mT AF demagnetization step. Gray = measurement before demagnetization. Black indicates normal polarity, white reverse polarity.

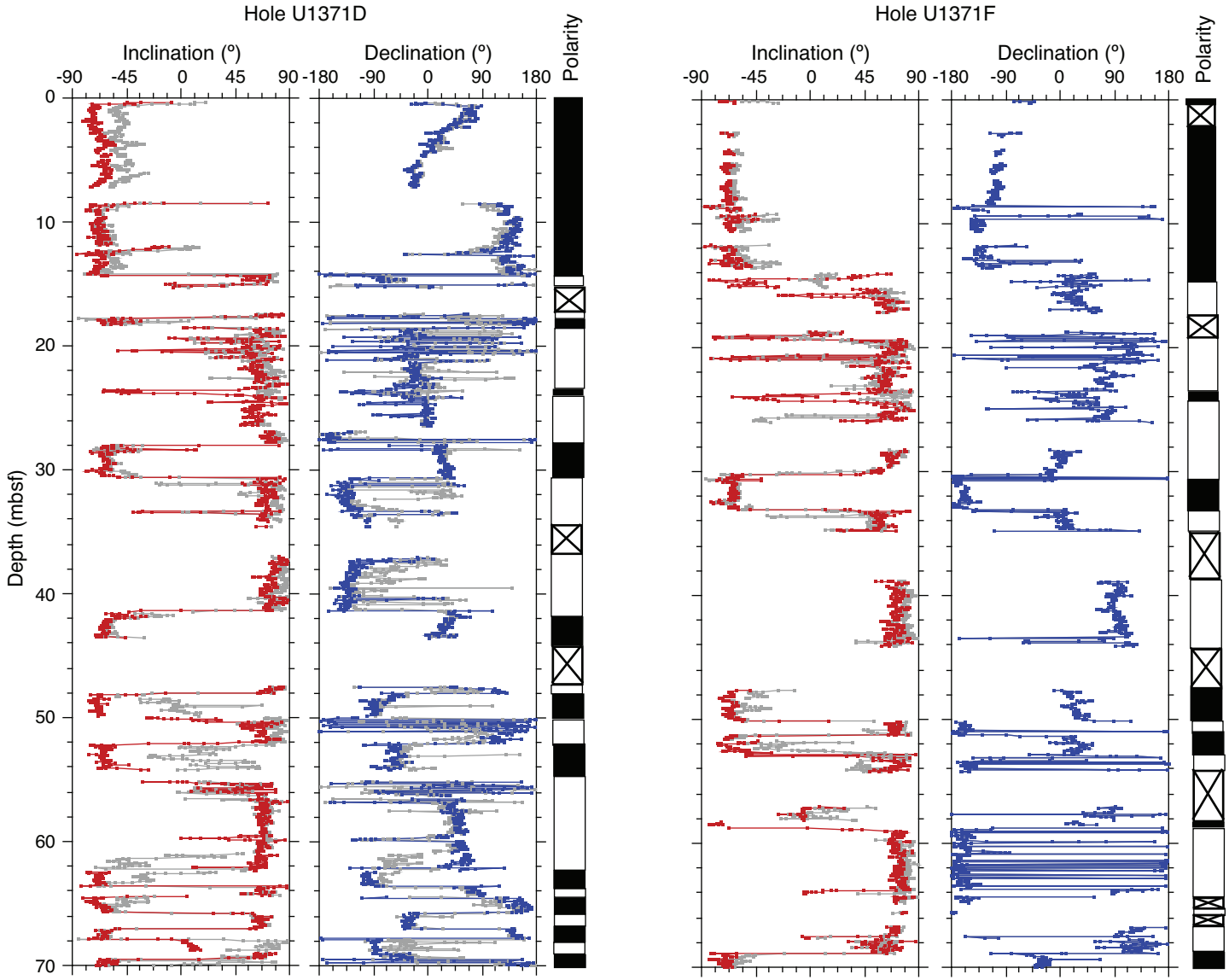

Figure F31. Comparison of polarity records between Holes U1371D and U1371F, 70–130 mbsf. Inclination (red) and declination (blue) data are after the 20 mT AF demagnetization step. Gray = measurement before demagnetization. Black indicates normal polarity, white reverse polarity.

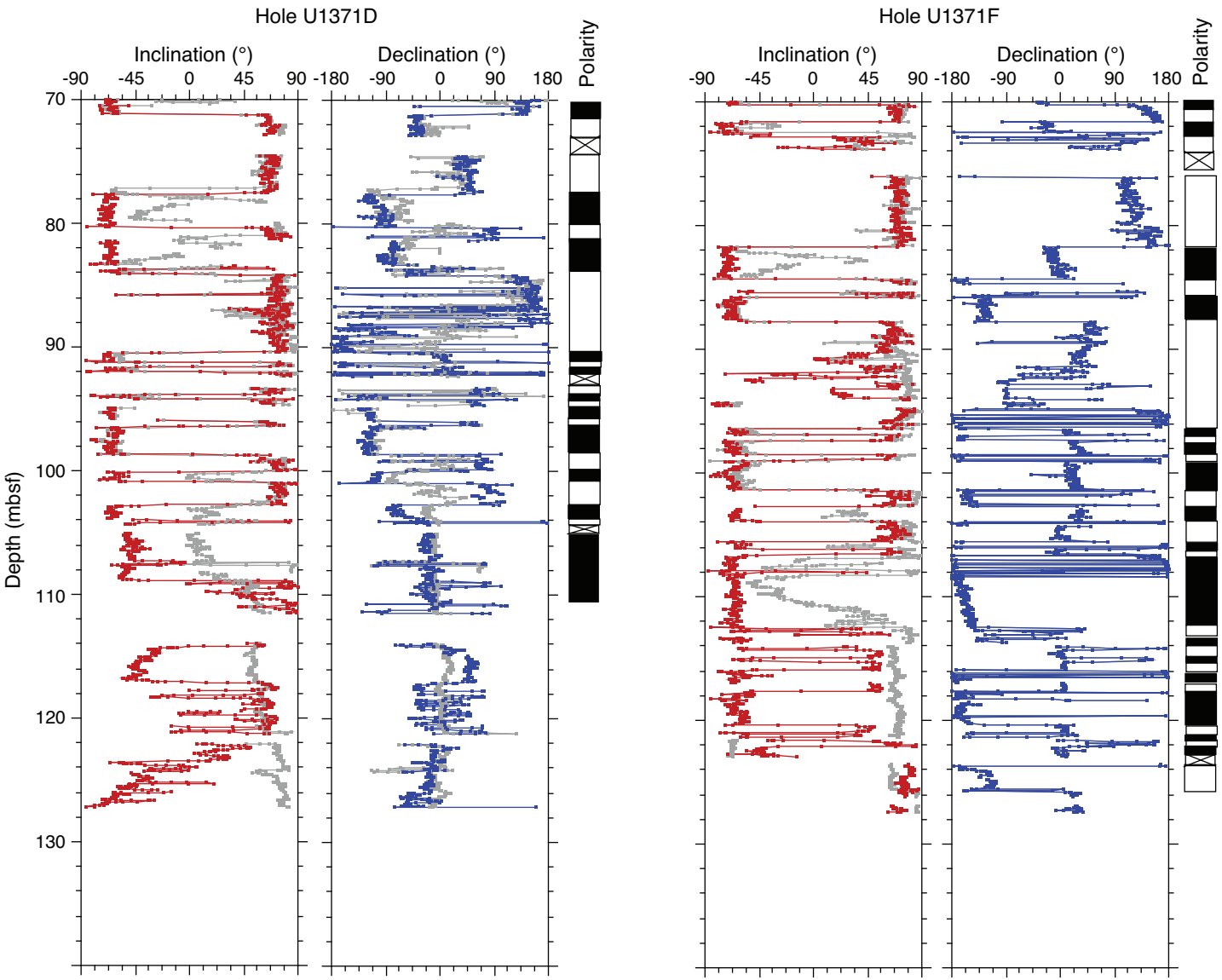

Figure F32. Plots of dissolved oxygen concentration, Site U1371. **A.** Optode measurements. **B.** Electrode measurements. **C.** Optode measurements in the uppermost 10 m of sediment. **D.** Electrode measurements in the uppermost 10 m of sediment. (Continued on next page.)

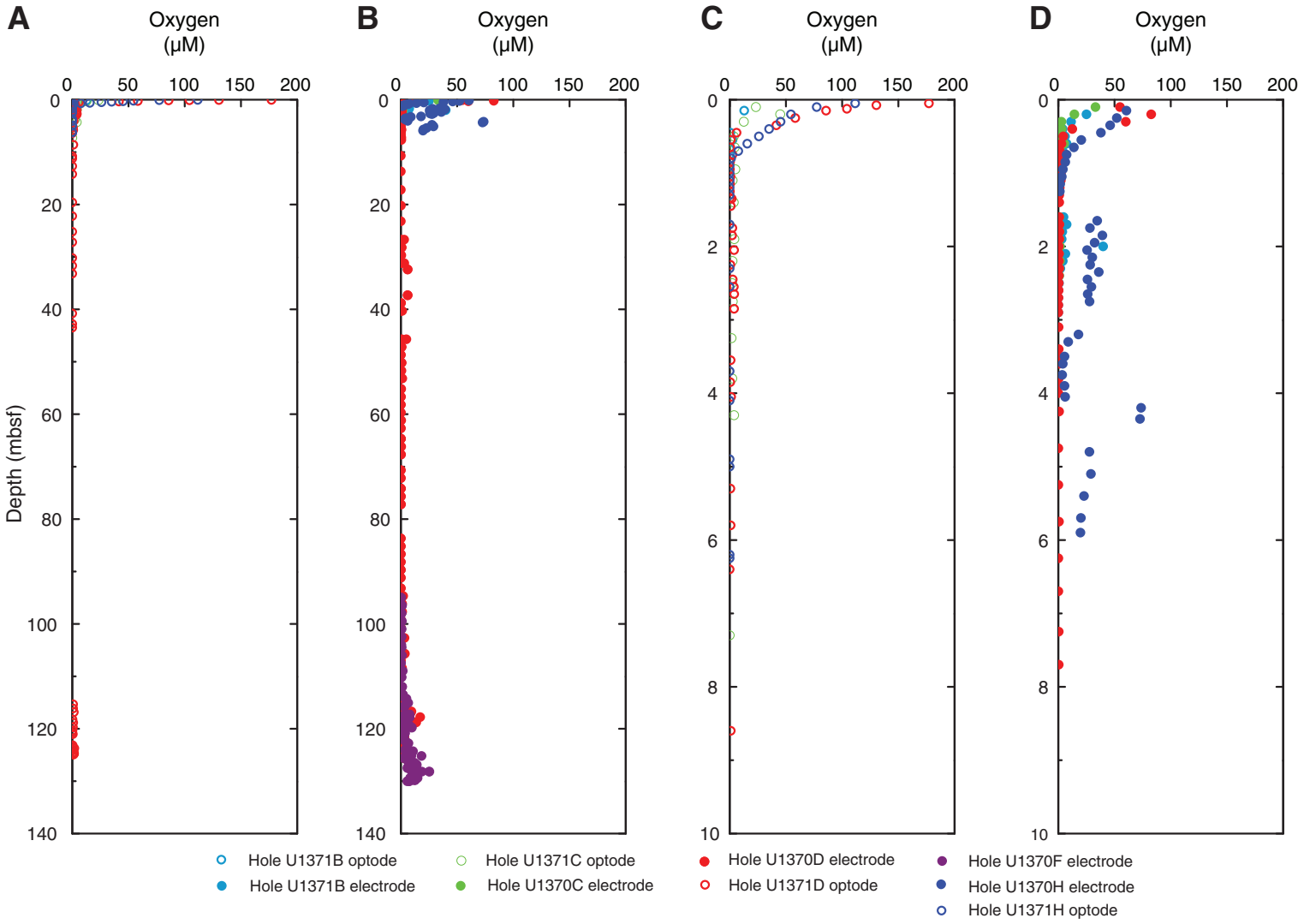

Figure F32 (continued). **E.** Optode measurements in uppermost 10 m of sediment with an expanded O_2 scale. **F.** Electrode measurements in uppermost 10 m of sediment with an expanded O_2 scale. **G.** Optode measurements in lowermost 115–135 mbsf of sediment with an expanded O_2 scale. **H.** Electrode measurements in lowermost 115–135 mbsf of sediment with an expanded O_2 scale.

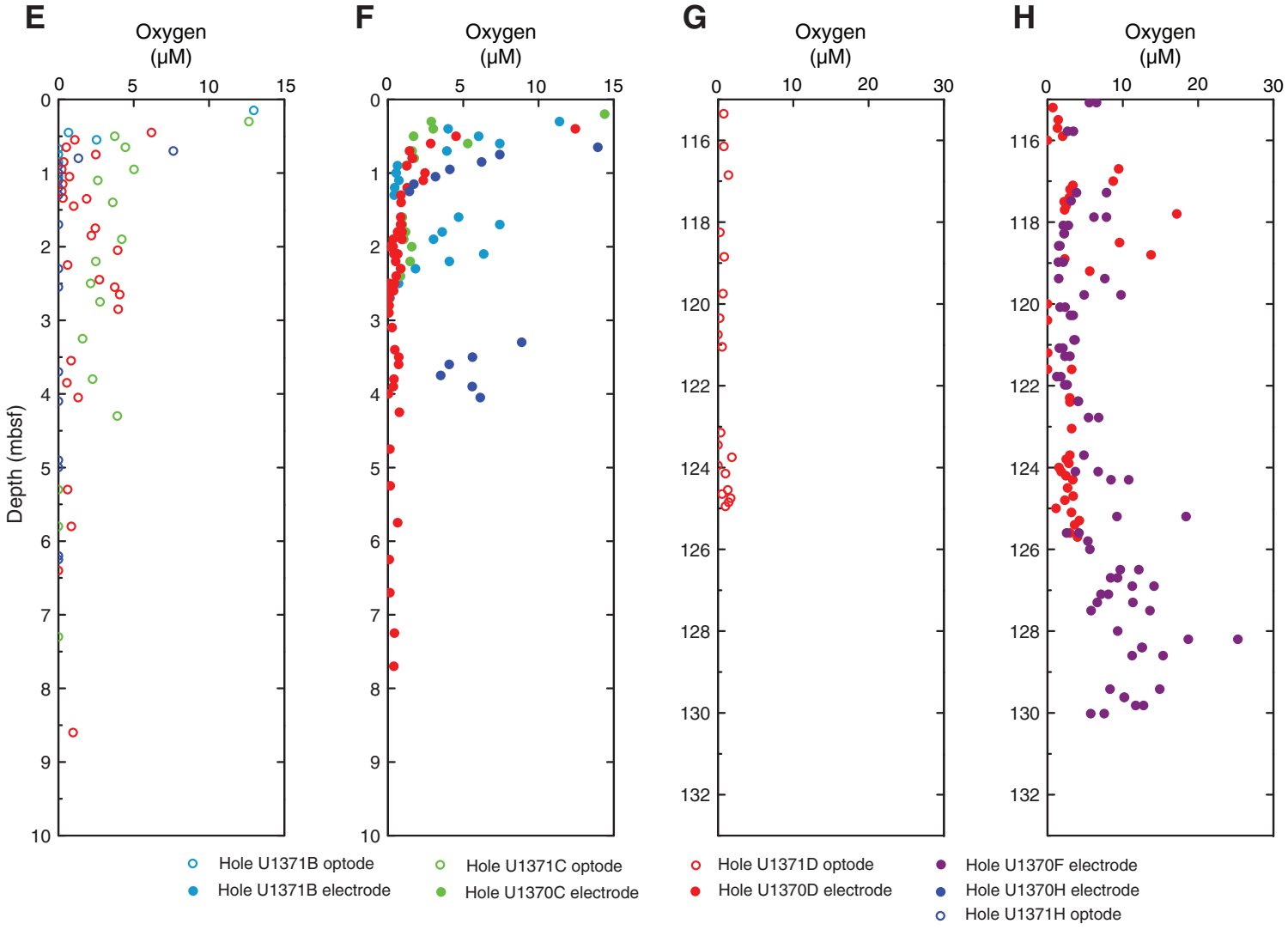

Figure F33. Plot of redox potential as measured by needle electrode, Site U1371.

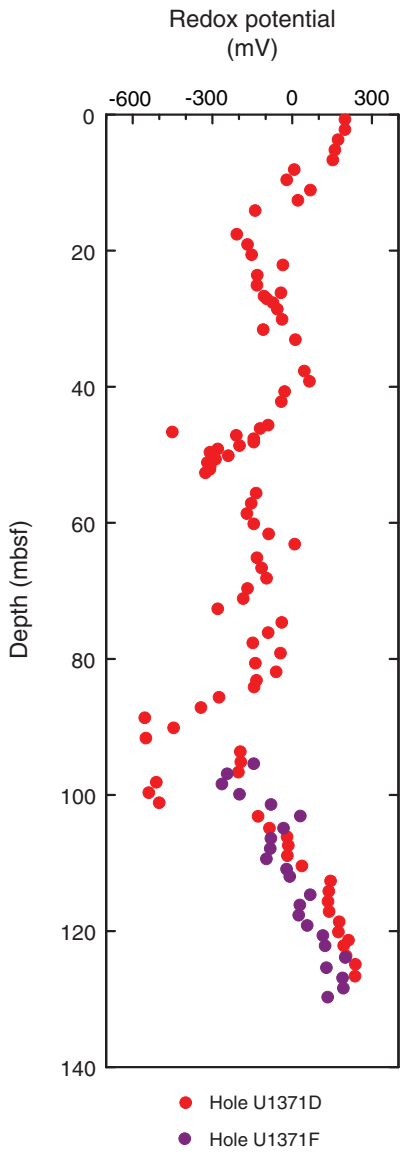

Figure F34. Plot of dissolved hydrogen concentrations, Hole U1371E.

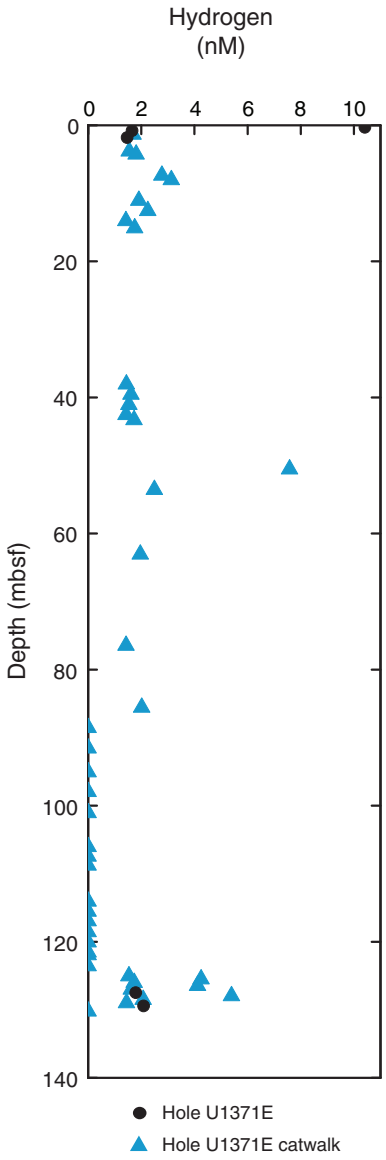

Figure F35. Plots of dissolved interstitial water constituents, Site U1371. IC = ion chromatography, ICP = inductively coupled plasma–atomic emission spectroscopy. **A.** Nitrate and ammonium. **B.** Phosphate. **C.** Silica. **D.** Alkalinity. **E.** Dissolved inorganic carbon (DIC). (Continued on next two pages.)

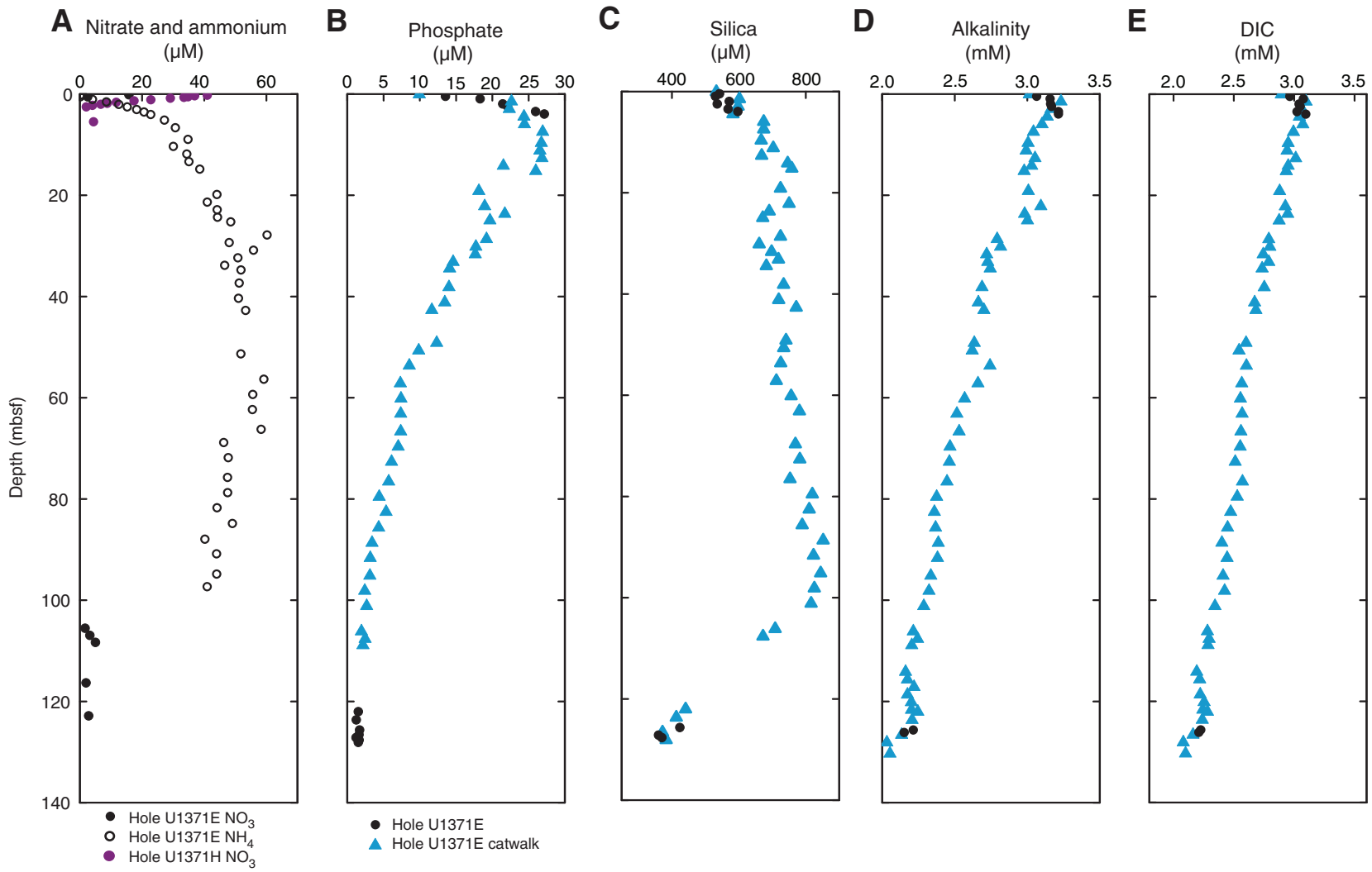

Figure F35 (continued). **F.** Chloride. **G.** Sulfate. **H.** Sulfate anomaly. **I.** Calcium. **J.** Magnesium. (Continued on next page.)

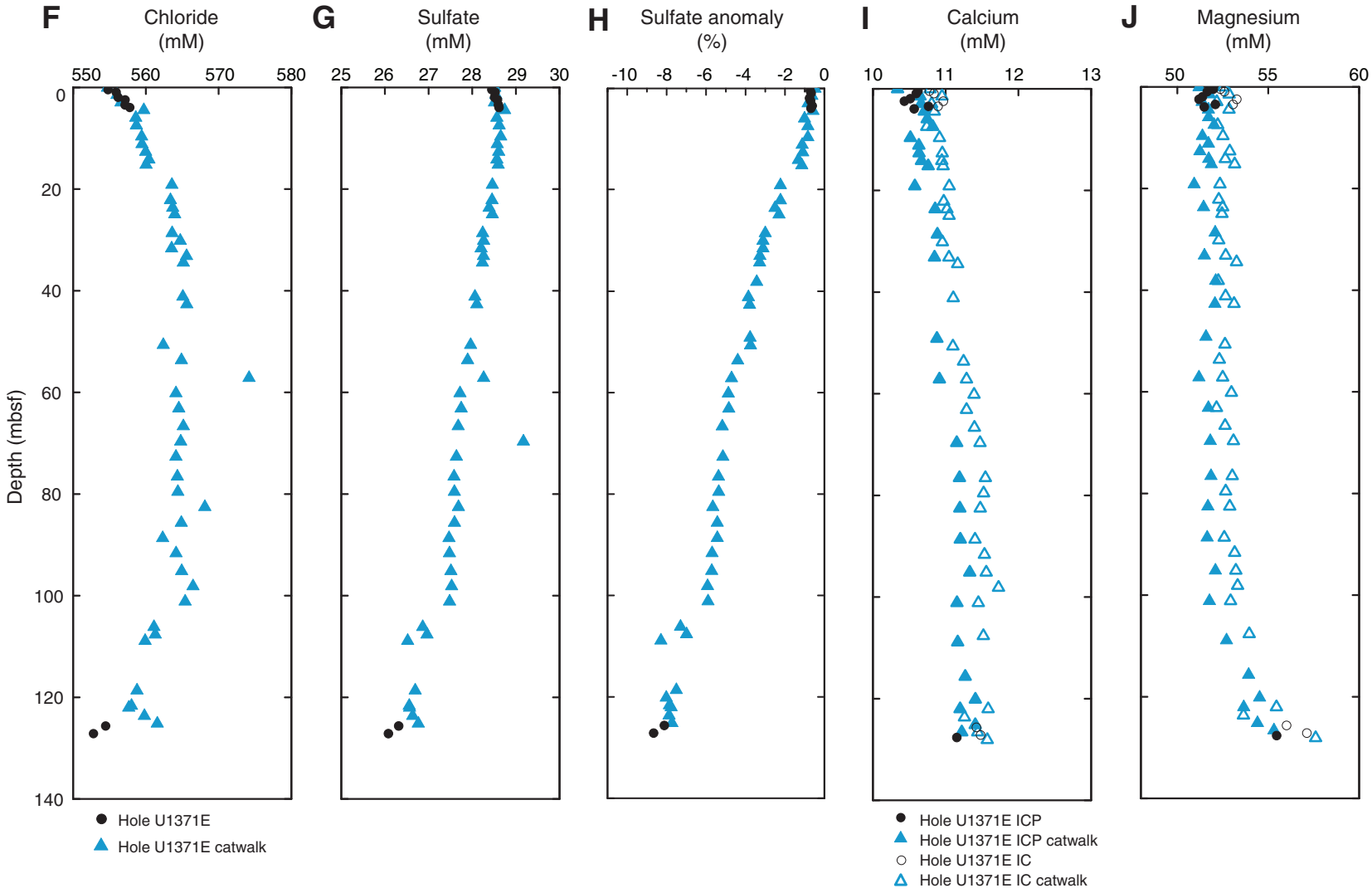

Figure F35 (continued). **K.** Sodium. **L.** Potassium. **M.** Iron. **N.** Manganese. **O.** Manganese with an expanded depth scale for the uppermost 20 mbsf.

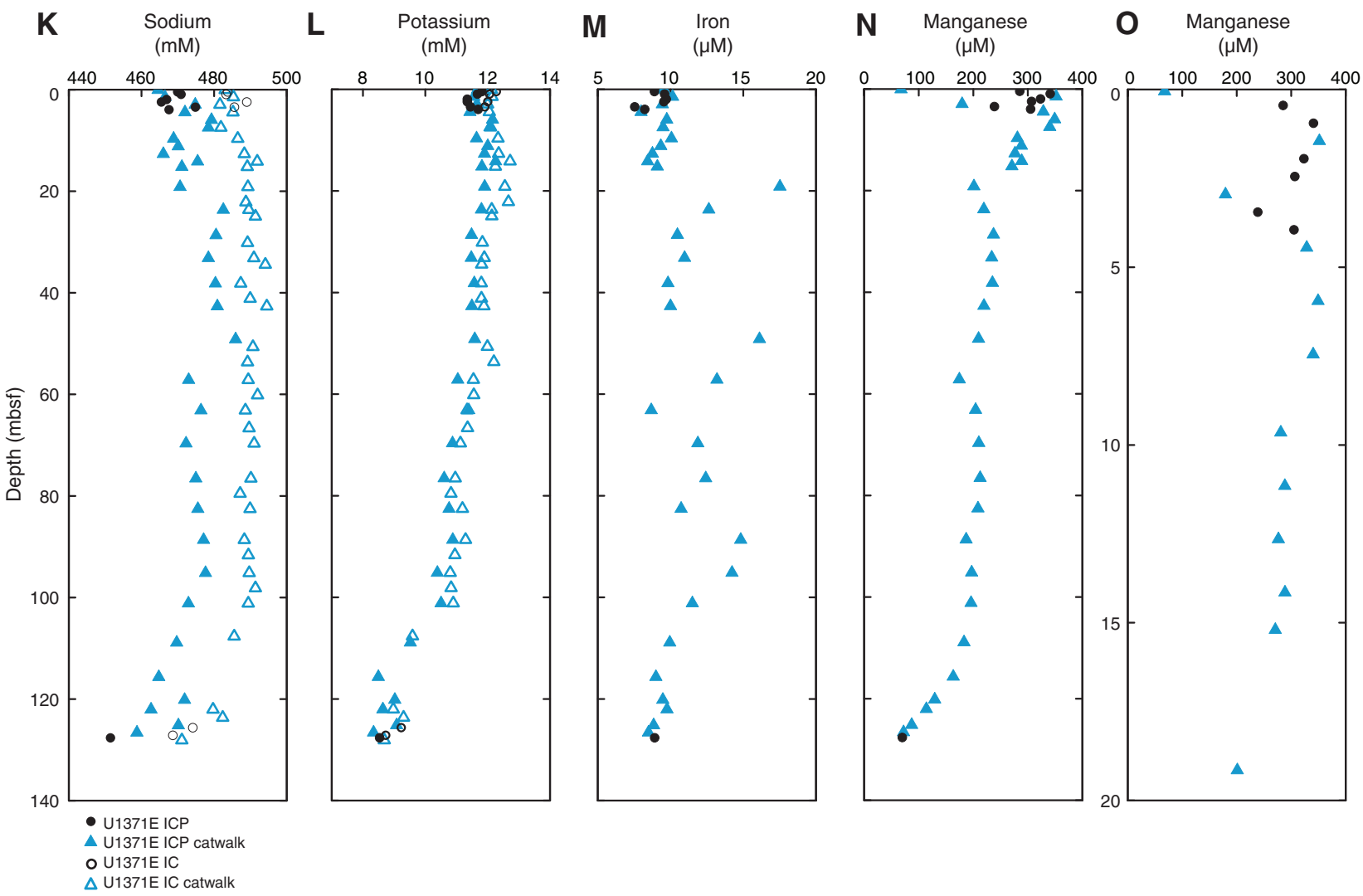

Figure F36. Solid-phase nitrogen and carbon content, Hole U1371E. **A.** Total nitrogen (TN). **B.** Total organic carbon (TOC). **C.** Total carbonate ($CaCO_3$).

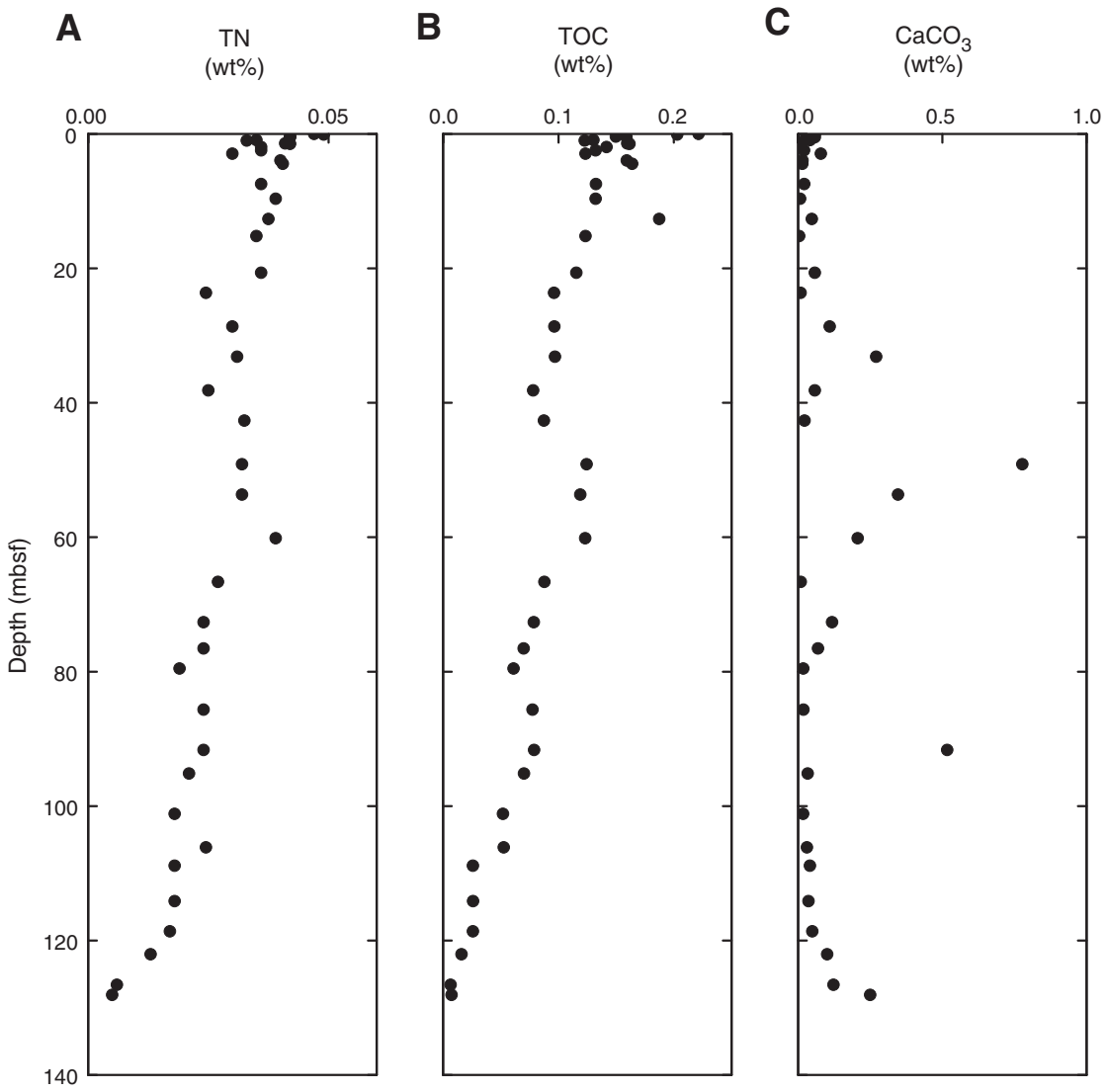

Figure F37. Plot of microbial cell abundance in Site U1371 sediment determined by epifluorescence microscopy. Only cell extracts were processed at this site. Direct counts below the blank were set to 10^2 cells/cm^3 in order to present them in the graph. See **"Microbiology"** in the "Methods" chapter (Expedition 329 Scientists, 2011a) for a detailed description of the blank and minimum detection limit (MDL) calculation. Red line = MDL, solid circles = microbial cell abundances above the MDL, open circles = counts below MDL.

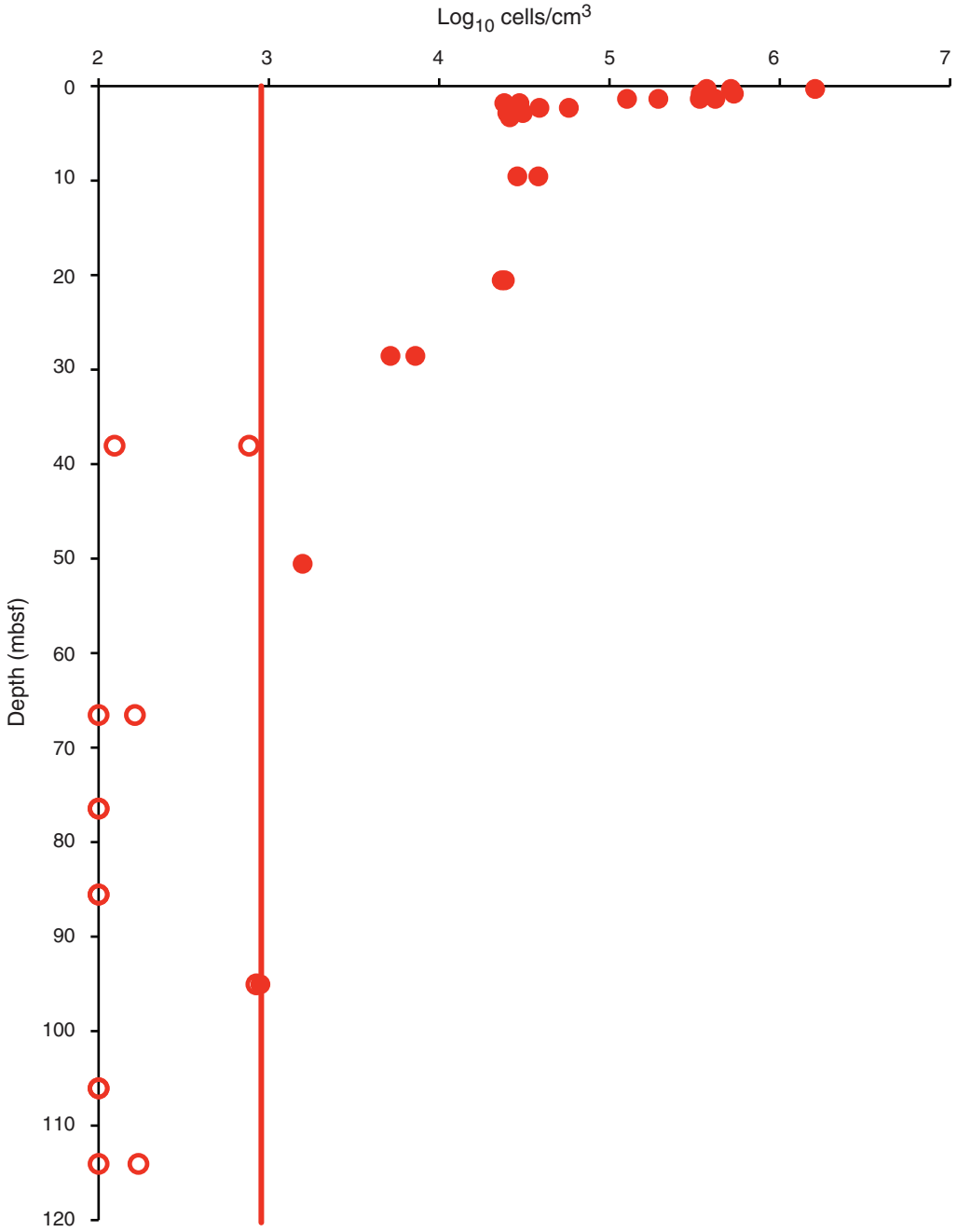

Table T1. Operations summary, Site U1371. (Continued on next three pages.)

Hole U1371A
Latitude: 45°57.8492′S
Longitude: 163°11.0513′W
Time on hole (h): 14.75
Seafloor (drill pipe measurement below rig floor, m DRF): 5316.0
Distance between rig floor and sea level (m): 11.2
Water depth (drill pipe measurement from sea level, mbsl): 5304.8 (tagged depth)
Total penetration (drilling depth below seafloor, m DSF): 123.5 (washdown to basement; basement contact established at 5438.5 mbrf; drilled 1 m into basement for verification)
Total length of cored section (m): NA
Total core recovered (m): NA
Core recovery (%): NA
Total number of cores: NA

Hole U1371B
Latitude: 45°57.8509′S
Longitude: 163°11.0673′W (20 m west of Hole U1371A)
Time on hole (h): 3.25
Seafloor (drill pipe measurement below rig floor, m DRF): 5316.4
Distance between rig floor and sea level (m): 11.2
Water depth (drill pipe measurement from sea level, mbsl): 5305.1
Total penetration (drilling depth below seafloor, m DSF): 8.1
Total length of cored section (m): 8.1
Total core recovered (m): 8.16
Core recovery (%): 100.6
Total number of cores: 1 (hole terminated because of poor core quality)

Hole U1371C
Latitude: 45°57.8404′S
Longitude: 163°11.0684′W (20 m north of Hole U1371B)
Time on hole (h): 1.75
Seafloor (drill pipe measurement below rig floor, m DRF): 5312.0
Distance between rig floor and sea level (m): 11.2
Water depth (drill pipe measurement from sea level, mbsl): 5300.8 (APC calculated)
Total penetration (drilling depth below seafloor, m DSF): 9.5
Total length of cored section (m): 9.5
Total core recovered (m): 9.85
Core recovery (%): 103.5
Total number of cores: 1 (hole terminated after Core 1H came up completely full)

Hole U1371D
Latitude: 45°57.8394′S
Longitude: 163°11.0512′W (20 m east of Hole U1371C)
Time on hole (h): 32.75
Seafloor (drill pipe measurement below rig floor, m DRF): 5311.1
Distance between rig floor and sea level (m): 11.2
Water depth (drill pipe measurement from sea level, mbsl): 5299.9
Total penetration (drilling depth below seafloor, m DSF): 126.0
Total length of cored section (m): 126.0
Total core recovered (m): 126.87
Core recovery (%): 100.7
Total number of cores: 14

Table T1 (continued). (Continued on next page.)

Hole U1371E
Latitude: 45°57.8397′S
Longitude: 163°11.0365′W (20 m east of Hole U1371D)
Time on hole (h): 21.5
Seafloor (drill pipe measurement below rig floor, m DRF): 5310.2
Distance between rig floor and sea level (m): 11.2
Water depth (drill pipe measurement from sea level, mbsl): 5298.9
Total penetration (drilling depth below seafloor, m DSF): 128.2
Total length of cored section (m): 128.2
Total core recovered (m): 118.16
Core recovery (%): 92.2
Total number of cores: 14

Hole U1371F
Latitude: 45°57.8502′S
Longitude: 163°11.0369′W (20 m south of Hole U1371E)
Time on hole (h): 20
Seafloor (drill pipe measurement below rig floor, m DRF): 5308.3
Distance between rig floor and sea level (m): 11.2
Water depth (drill pipe measurement from sea level, mbsl): 5297.0
Total penetration (drilling depth below seafloor, m DSF): 130.6
Total length of cored section (m): 130.6
Total core recovered (m): 118.44
Core recovery (%): 90.7
Total number of cores: 14

Hole U1371G
Latitude: 45°57.8637′S
Longitude: 163°11.0360′W (20 m south of Hole U1371F)
Time on hole (h): 2.75
Seafloor (drill pipe measurement below rig floor, m DRF): 5314.1
Distance between rig floor and sea level (m): 11.2
Water depth (drill pipe measurement from sea level, mbsl): 5302.7
Total penetration (drilling depth below seafloor, m DSF): 1.4
Total length of cored section (m): 1.4
Total core recovered (m): 1.37
Core recovery (%): 97.9
Total number of cores: 1

Hole U1371H
Latitude: 45°57.8648′S
Longitude: 163°11.0512′W (20 m south of Hole U1371F)
Time on hole (h): 16
Seafloor (drill pipe measurement below rig floor, m DRF): 5310.3
Distance between rig floor and sea level (m): 11.2
Water depth (drill pipe measurement from sea level, mbsl): 5298.9
Total penetration (drilling depth below seafloor, m DSF): 6.2
Total length of cored section (m): 6.2
Total core recovered (m): 6.19
Core recovery (%): 99.8
Total number of cores: 1

Table T1 (continued). (Continued on next page.)

Core	Date (2010)	Time (h)	Depth DSF (m) Top of cored interval	Depth DSF (m) Bottom of cored interval	Interval advanced (m)	Depth CSF (m) Top of cored interval	Depth CSF (m) Bottom of cored interval	Length of core recovered (m)	Recovery (%)	Sections (*N*)	Coring shoe type	Orientation	Remarks
329-U1371A-													
11	3 Dec	0900				*****Drilled from 0.0 to 123.5 m DSF*****							Basement tagged at 122.5 mbsf
329-U1371B-													
1H	3 Dec	1330	0.0	8.1	8.1	0.0	8.15	8.15	101	7	Non-mag core barrel	Y	Disturbed mudline core
329-U1371C-													
1H	3 Dec	1520	0.0	9.5	9.5	0.0	9.83	9.83	103	8	Non-mag core barrel	Y	No mudline - reshoot Hole D
329-U1371D-													
1H	3 Dec	1710	0.0	7.4	7.4	0.0	7.41	7.41	100	6	Non-mag core barrel	Y	High heave
2H	3 Dec	1840	7.4	16.9	9.5	7.4	15.40	8.00	84	7	Non-mag core barrel	Y	High heave
3H	3 Dec	2015	16.9	26.4	9.5	16.9	26.72	9.82	103	8	Non-mag core barrel	Y	High heave
4H	3 Dec	2205	26.4	35.9	9.5	26.4	34.83	8.43	89	7	Non-mag core barrel	Y	High heave
5H	4 Dec	0005	35.9	45.4	9.5	35.9	43.88	7.98	84	7	Non-mag core barrel	Y	High heave
6H	4 Dec	0630	45.4	54.9	9.5	45.4	54.43	9.03	95	8	Non-mag core barrel	Y	
7H	4 Dec	0950	54.9	64.4	9.5	54.9	64.49	9.59	101	8	Non-mag core barrel	Y	
8H	4 Dec	1150	64.4	73.9	9.5	64.4	73.15	8.75	92	7	Non-mag core barrel	Y	
9H	4 Dec	1340	73.9	83.4	9.5	73.9	83.61	9.71	102	8	Non-mag core barrel	Y	
10H	4 Dec	1535	83.4	92.9	9.5	83.4	92.88	9.48	100	8	Non-mag core barrel	Y	
11H	4 Dec	1720	92.9	102.4	9.5	92.9	102.42	9.52	100	8	Non-mag core barrel	Y	
12H	4 Dec	1900	102.4	111.9	9.5	102.4	111.78	9.38	99	8	STD		
13H	4 Dec	2040	111.9	121.4	9.5	111.9	121.60	9.70	102	8	STD		
14H	4 Dec	2215	121.4	126.0	4.6	121.4	131.47	10.07	219	8	STD		
329-U1371E-													
1H	5 Dec	0245	0.0	8.2	8.2	0.0	8.26	8.26	101	7	Non-mag core barrel		
2H	5 Dec	0410	8.2	17.7	9.5	8.2	15.51	7.31	77	6	Non-mag core barrel		
3H	5 Dec	0525	17.7	27.2	9.5	17.7	25.65	7.95	84	7	Non-mag core barrel		
4H	5 Dec	0635	27.2	36.7	9.5	27.2	35.29	8.09	85	7	Non-mag core barrel		
5H	5 Dec	0805	36.7	46.2	9.5	36.7	43.52	6.82	72	6	Non-mag core barrel		
6H	5 Dec	0920	46.2	55.7	9.5	46.2	55.54	9.34	98	8	Non-mag core barrel		
7H	5 Dec	1045	55.7	65.2	9.5	55.7	64.79	9.09	96	7	Non-mag core barrel		
8H	5 Dec	1215	65.2	74.7	9.5	65.2	74.24	9.04	95	7	Non-mag core barrel		
9H	5 Dec	1325	74.7	84.2	9.5	74.7	84.01	9.31	98	8	Non-mag core barrel		
10H	5 Dec	1440	84.2	93.7	9.5	84.2	93.86	9.66	102	8	Non-mag core barrel		
11H	5 Dec	1550	93.7	103.2	9.5	93.7	102.84	9.14	96	7	Non-mag core barrel		
12H	5 Dec	1720	103.2	112.7	9.5	103.2	109.21	6.01	63	5	Non-mag core barrel		
13H	5 Dec	1835	112.7	122.2	9.5	112.7	122.38	9.68	102	8	STD		
14H	5 Dec	2005	122.2	128.2	6.0	122.2	130.66	8.46	141	7	STD		
329-U1371F-													
1H	6 Dec	2235	0.0	9.2	9.2	0.0	9.18	9.18	100	8	Non-mag core barrel		
2H	6 Dec	2340	9.2	18.7	9.5	9.2	17.45	8.25	87	7	Non-mag core barrel		
3H	6 Dec	0100	18.7	28.2	9.5	18.7	26.22	7.52	79	6	Non-mag core barrel		
4H	6 Dec	0220	28.2	37.7	9.5	28.2	35.13	6.93	73	6	Non-mag core barrel		
5H	6 Dec	0350	37.7	47.2	9.5	37.7	44.33	6.63	70	6	Non-mag core barrel		
6H	6 Dec	0505	47.2	56.7	9.5	47.2	54.51	7.31	77	6	Non-mag core barrel		
7H	6 Dec	0615	56.7	66.2	9.5	56.7	65.87	9.17	97	7	Non-mag core barrel		
8H	6 Dec	0740	66.2	75.7	9.5	66.2	74.19	7.99	84	7	Non-mag core barrel		
9H	6 Dec	0915	75.7	85.2	9.5	75.7	84.93	9.23	97	8	Non-mag core barrel		
10H	6 Dec	1030	85.2	94.7	9.5	85.2	94.90	9.70	102	8	Non-mag core barrel		

Table T1 (continued).

Core	Date (2010)	Time (h)	Depth DSF (m) Top of cored interval	Depth DSF (m) Bottom of cored interval	Interval advanced (m)	Depth CSF (m) Top of cored interval	Depth CSF (m) Bottom of cored interval	Length of core recovered (m)	Recovery (%)	Sections (*N*)	Coring shoe type	Orientation	Remarks
11H	6 Dec	1140	94.7	104.2	9.5	94.7	104.45	9.75	103	8	Non-mag core barrel		
12H	6 Dec	1250	104.2	113.7	9.5	104.2	113.87	9.67	102	8	Non-mag core barrel		
13H	6 Dec	1415	113.7	123.2	9.5	113.7	123.41	9.71	102	8	STD		
14H	6 Dec	1530	123.2	130.6	7.4	123.2	130.60	7.40	100	7	STD		
329-U1371G-													
1H	6 Dec	1825	0.0	1.4	1.4	0.0	1.37	1.37	98	2	Non-mag core barrel		
329-U1371H-													
1H	6 Dec	2135	0.0	6.2	6.2	0.0	6.19	6.19	100	6	Non-mag core barrel		
				Advanced total:	533.5			389.01	95	327			
				Total interval cored:	410.0								

NA = not applicable. DSF = drilling depth below seafloor, CSF = core depth below seafloor. H = APC core, 1 = drilled interval. Non-mag = nonmagnetic, STD = standard. Time is UTC.

Table T2. Tabular listing of ash and pumice layers, Hole U1371D.

Core, section, interval (cm)
329-U1371D-
2H-5, 20–22
2H-5, 124–125
2H-5, 132–135
2H-5, 142–144
2H-5, 146–147
3H-3, 52–57
3H-3, 62–63
3H-6, 1–3
3H-6, 61–64
3H-6, 70–72
4H-1, 84–85
4H-1, 104–106
4H-3, 66–68
4H-3, 104–107
5H-6, 9–10
7H-2, 18–21
11H-3, 45–58
11H-4, 85–87
11H-7, 0–32
11H-CC, 2–5
14H-1, 112–113

Table T3. Tabular listing of hardground layers, Hole U1371D.

Core, section, interval (cm)
329-U1371D-
2H-3, 132–135
7H-1, 65
7H-1, 136
7H-1, 140–142
7H-3, 115–116
11H-4, 85–87

Table T4. Electrical conductivity measurements of surface seawater, Site U1371. (Continued on next page.)

Measurement number	Electrical conductivity (mS/cm)	Temperature (°C)	Correction factor 20°C (mS/cm)	Seawater electrical conductivity at 20°C (mS/cm)
1	53.19	23.1	51.08	49.87
2	53.15	23.1	51.08	49.84
18	52.40	23.1	51.08	49.13
19	52.41	23.1	51.08	49.14
20	52.40	23.1	51.08	49.13
35	52.13	23.0	50.97	48.98
36	52.18	23.0	50.97	49.03
44	52.09	22.9	50.87	49.04
52	52.10	22.9	50.87	49.05
59	52.06	22.9	50.87	49.01
67	51.78	22.7	50.66	48.95
68	51.77	22.7	50.66	48.94
80	51.73	22.8	50.77	48.80
81	51.66	23.1	51.08	48.44
82	51.71	22.6	50.56	48.98
83	51.56	22.6	50.56	48.84
84	51.45	22.4	50.35	48.94
90	51.06	22.2	50.15	48.76
101	51.12	22.3	50.25	48.72
111	50.68	21.4	49.32	49.21
112	50.64	21.4	49.32	49.17
113	50.70	21.6	49.53	49.02
122	50.61	21.6	49.53	48.94
131	50.48	21.5	49.43	48.91
136	50.52	21.7	49.63	48.75
137	50.48	21.7	49.63	48.71
138	51.22	23.0	50.97	48.13
145	50.68	22.5	50.46	48.11
153	51.06	22.5	50.46	48.47
162	50.90	22.5	50.46	48.31
170	50.95	22.3	50.25	48.56
178	50.63	22.2	50.15	48.35
186	50.37	22.0	49.94	48.30
190	50.10	21.9	49.84	48.14
191	50.07	21.9	49.84	48.12
192	50.52	22.2	50.15	48.25
201	50.45	22.2	50.15	48.18
210	50.36	22.1	50.04	48.20
219	50.72	22.4	50.35	48.24
228	50.69	22.2	50.15	48.41
237	50.40	22.0	49.94	48.33
242	51.43	22.3	50.25	49.02
243	50.66	22.3	50.25	48.28
251	50.57	20.9	48.81	49.62
260	50.61	22.4	50.35	48.14
269	50.49	22.4	50.35	48.02
278	50.61	22.4	50.35	48.14
282	50.41	22.8	50.77	47.56
283	50.38	22.8	50.77	47.53
289	50.67	22.6	50.56	48.00
298	50.38	22.5	50.46	47.82
307	50.50	22.7	50.66	47.74
316	50.41	22.4	50.35	47.95
325	50.13	22.3	50.25	47.78
326	49.62	22.3	50.25	47.29
327	49.63	22.2	50.15	47.40
336	49.12	21.6	49.53	47.50
337	49.09	21.6	49.53	47.47
346	48.91	21.7	49.63	47.20
347	48.95	21.6	49.53	47.33
355	48.92	21.8	49.74	47.11
356	48.91	21.8	49.74	47.10
365	48.98	21.9	49.84	47.07
374	48.95	21.8	49.74	47.14
385	48.85	21.8	49.74	47.04
386	48.88	21.8	49.74	47.07
387	49.44	22.5	50.46	46.93
396	49.22	22.2	50.15	47.01

Table T4 (continued).

Measurement number	Electrical conductivity (mS/cm)	Temperature (°C)	Correction factor 20°C (mS/cm)	Seawater electrical conductivity at 20°C (mS/cm)
405	49.07	22.2	50.15	46.86
414	48.50	22.3	50.25	46.22
423	49.12	22.3	50.25	46.82
432	49.01	22.3	50.25	46.71
438	48.30	22.2	50.15	46.13
439	48.35	22.1	50.04	46.27
445	48.70	22.4	50.35	46.32
453	48.47	22.1	50.04	46.39
462	48.68	22.2	50.15	46.49
471	48.56	22.2	50.15	46.38
480	48.30	22.2	50.15	46.13
486	48.56	22.3	50.25	46.28
492	48.55	22.2	50.15	46.37
493	52.51	22.8	50.77	49.54
501	51.85	22.8	50.77	48.92
510	51.54	22.9	50.87	48.52
519	51.33	23.0	50.97	48.23
528	51.56	22.6	50.56	48.84
537	50.48	22.9	50.87	47.53
546	50.10	22.8	50.77	47.26
549	50.03	23.1	51.08	46.91
556	49.95	22.9	50.87	47.03
565	49.53	22.7	50.66	46.82
574	49.25	22.4	50.35	46.84
583	48.31	22.3	50.25	46.04
592	48.53	22.2	50.15	46.35
601	48.74	22.0	49.94	46.74
604	48.57	22.8	50.77	45.82
613	48.52	22.5	50.46	46.05
614	48.71	22.5	50.46	46.24
621	48.63	22.3	50.25	46.35
629	48.46	22.6	50.56	45.90
638	48.61	22.4	50.35	46.23
647	48.84	22.6	50.56	46.26
656	48.73	22.7	50.66	46.07
659	48.71	22.6	50.56	46.14
660	49.16	23.2	51.18	46.00
667	49.07	22.9	50.87	46.20
668	48.54	22.8	50.77	45.79
676	48.87	22.8	50.77	46.10
685	48.78	22.7	50.66	46.11
693	48.55	22.7	50.66	45.90
702	48.45	22.4	50.35	46.08
709	48.44	22.6	50.56	45.89
714	48.41	22.5	50.46	45.95
715	48.50	22.7	50.66	45.85
721	48.64	22.6	50.56	46.07
730	48.79	22.7	50.66	46.12
739	48.67	22.4	50.35	46.29
745	48.50	22.2	50.15	46.32

Table T5. Best-fitting parameters to measurements on surface seawater, Site U1371.

Measurement number (*N*)	Best fitting slope (mS/m/*N*)	*y*-intercept (mS/m)
1–493	–0.0065	49.54
494–565	–0.0394	68.84
566–745	–0.0024	47.77

Table T6. Formation factor measurements, Site U1371. (Continued on next nine pages.)

Core, section, interval (cm)	Depth (mbsf)	Measurement number	Temperature-corrected seawater conductivity (mS/cm)	Sediment temperature (°C)	Sediment electrical conductivity (mS/cm)	Correction factor at 20°C (mS/cm)	Sediment electrical conductivity at 20°C (mS/cm)	Drift-corrected sediment electrical conductivity at 20°C (mS/cm)	Formation factor
329-U1371D-									
1H-1, 5	0.05	3	49.52	22.50	24.05	50.46	22.83	22.84	2.17
1H-1, 15	0.15	4	49.51	22.50	26.55	50.46	25.20	25.21	1.96
1H-1, 25	0.25	5	49.50	22.50	26.35	50.46	25.01	25.03	1.98
1H-1, 35	0.35	6	49.50	22.50	27.67	50.46	26.26	26.28	1.88
1H-1, 45	0.45	7	49.49	22.40	29.28	50.35	27.85	27.87	1.78
1H-1, 55	0.55	8	49.48	22.40	28.46	50.35	27.07	27.10	1.83
1H-1, 65	0.65	9	49.48	22.40	30.43	50.35	28.94	28.98	1.71
1H-1, 77	0.77	10	49.47	22.40	28.28	50.35	26.90	26.93	1.84
1H-1, 86	0.86	11	49.46	22.40	29.69	50.35	28.24	28.28	1.75
1H-1, 95	0.95	12	49.46	22.40	29.19	50.35	27.76	27.81	1.78
1H-1, 105	1.05	13	49.45	22.40	29.23	50.35	27.80	27.85	1.78
1H-1, 115	1.15	14	49.45	22.30	28.85	50.25	27.50	27.55	1.79
1H-1, 125	1.25	15	49.44	22.30	29.96	50.25	28.55	28.61	1.73
1H-1, 135	1.35	16	49.43	22.30	29.14	50.25	27.77	27.83	1.78
1H-1, 146	1.46	17	49.43	22.30	27.48	50.25	26.19	26.25	1.88
1H-2, 10	1.60	21	49.40	22.30	28.54	50.25	27.20	27.28	1.81
1H-2, 20	1.70	22	49.39	22.20	27.22	50.15	26.00	26.07	1.89
1H-2, 30	1.80	23	49.39	22.20	29.03	50.15	27.73	27.81	1.78
1H-2, 40	1.90	24	49.38	22.20	27.39	50.15	26.16	26.24	1.88
1H-2, 50	2.00	25	49.37	22.20	29.24	50.15	27.93	28.02	1.76
1H-2, 60	2.10	26	49.37	22.10	30.96	50.04	29.63	29.73	1.66
1H-2, 70	2.20	27	49.36	22.10	31.59	50.04	30.23	30.34	1.63
1H-2, 80	2.30	28	49.35	22.10	27.27	50.04	26.10	26.19	1.88
1H-2, 90	2.40	29	49.35	22.00	27.53	49.94	26.40	26.50	1.86
1H-2, 100	2.50	30	49.34	22.00	28.63	49.94	27.46	27.56	1.79
1H-2, 110	2.60	31	49.34	22.00	28.95	49.94	27.76	27.88	1.77
1H-2, 120	2.70	32	49.33	21.90	27.92	49.84	26.83	26.94	1.83
1H-2, 130	2.80	33	49.32	21.90	28.83	49.84	27.70	27.82	1.77
1H-2, 140	2.90	34	49.32	21.90	28.62	49.84	27.50	27.63	1.79
1H-3, 10	3.11	37	49.30	21.80	28.00	49.74	26.96	27.09	1.82
1H-3, 20	3.21	38	49.29	21.80	27.54	49.74	26.52	26.65	1.85
1H-3, 30	3.31	39	49.28	21.90	29.02	49.84	27.89	28.03	1.76
1H-3, 40	3.41	40	49.28	21.90	28.66	49.84	27.54	27.69	1.78
1H-3, 50	3.51	41	49.27	21.90	30.07	49.84	28.90	29.05	1.70
1H-3, 60	3.61	42	49.26	21.90	28.96	49.84	27.83	27.98	1.76
1H-3, 70	3.71	43	49.26	21.90	28.80	49.84	27.68	27.83	1.77
1H-3, 80	3.81	45	49.24	22.00	29.14	49.94	27.94	28.11	1.75
1H-3, 90	3.91	46	49.24	22.00	28.97	49.94	27.78	27.95	1.76
1H-3, 100	4.01	47	49.23	22.00	28.67	49.94	27.49	27.66	1.78
1H-3, 110	4.11	48	49.23	22.00	28.76	49.94	27.58	27.75	1.77
1H-3, 120	4.21	49	49.22	22.00	27.19	49.94	26.07	26.24	1.88
1H-3, 130	4.31	50	49.21	22.00	26.05	49.94	24.98	25.15	1.96
1H-3, 140	4.41	51	49.21	22.00	28.63	49.94	27.46	27.64	1.78
1H-4, 10	4.61	53	49.19	21.70	28.21	49.63	27.22	27.41	1.79
1H-4, 20	4.71	54	49.19	21.70	29.32	49.63	28.29	28.49	1.73
1H-4, 30	4.81	55	49.18	21.70	27.70	49.63	26.73	26.92	1.83
1H-4, 50	5.01	56	49.17	21.70	29.53	49.63	28.50	28.70	1.71
1H-4, 60	5.11	57	49.17	21.70	28.31	49.63	27.32	27.52	1.79
1H-4, 70	5.21	58	49.16	21.70	28.35	49.63	27.36	27.56	1.78
1H-4, 80	5.31	60	49.15	21.60	30.11	49.53	29.11	29.34	1.67
1H-4, 90	5.41	61	49.14	21.60	29.77	49.53	28.79	29.02	1.69
1H-4, 110	5.61	62	49.13	21.60	28.66	49.53	27.71	27.94	1.76
1H-4, 110	5.61	63	49.13	21.60	28.12	49.53	27.19	27.41	1.79
1H-4, 120	5.71	64	49.12	21.60	26.67	49.53	25.79	26.00	1.89
1H-4, 130	5.81	65	49.11	21.60	29.04	49.53	28.08	28.32	1.73
1H-4, 140	5.91	66	49.11	21.60	29.38	49.53	28.41	28.65	1.71
1H-5, 10	6.10	69	49.09	21.60	28.47	49.53	27.53	27.78	1.77
1H-5, 20	6.20	70	49.08	21.60	27.88	49.53	26.96	27.21	1.80
1H-5, 30	6.30	71	49.08	21.50	30.07	49.43	29.14	29.41	1.67
1H-5, 40	6.40	72	49.07	21.50	29.19	49.43	28.28	28.55	1.72
1H-5, 50	6.50	73	49.06	21.50	29.23	49.43	28.32	28.59	1.72
1H-5, 60	6.60	74	49.06	21.50	29.87	49.43	28.94	29.22	1.68
1H-5, 76	6.76	75	49.05	21.50	29.25	49.43	28.34	28.62	1.71
1H-5, 90	6.90	76	49.04	21.50	29.67	49.43	28.75	29.04	1.69
1H-5, 100	7.00	77	49.04	21.50	29.02	49.43	28.12	28.40	1.73

Table T6 (continued). (Continued on next page.)

Core, section, interval (cm)	Depth (mbsf)	Measurement number	Temperature-corrected seawater conductivity (mS/cm)	Sediment temperature (°C)	Sediment electrical conductivity (mS/cm)	Correction factor at 20°C (mS/cm)	Sediment electrical conductivity at 20°C (mS/cm)	Drift-corrected sediment electrical conductivity at 20°C (mS/cm)	Formation factor
1H-5, 110	7.10	78	49.03	21.50	27.01	49.43	26.17	26.44	1.85
1H-5, 120	7.20	79	49.02	21.50	26.74	49.43	25.91	26.18	1.87
2H-1, 80	8.20	85	48.99	20.90	29.15	48.81	28.60	28.92	1.69
2H-1, 100	8.40	86	48.98	21.00	28.24	48.91	27.65	27.96	1.75
2H-1, 115	8.55	87	48.97	21.10	29.69	49.02	29.01	29.34	1.67
2H-1, 125	8.65	88	48.97	21.10	27.80	49.02	27.16	27.48	1.78
2H-1, 140	8.80	89	48.96	21.10	25.06	49.02	24.49	24.77	1.98
2H-2, 10	9.01	91	48.95	20.80	28.05	48.71	27.58	27.91	1.75
2H-2, 30	9.21	92	48.94	20.80	28.65	48.71	28.17	28.51	1.72
2H-2, 50	9.41	93	48.93	20.80	29.07	48.71	28.58	28.93	1.69
2H-2, 70	9.61	94	48.93	20.80	26.56	48.71	26.11	26.44	1.85
2H-2, 80	9.71	95	48.92	20.80	24.10	48.71	23.70	23.99	2.04
2H-2, 90	9.81	96	48.91	20.80	27.76	48.71	27.29	27.64	1.77
2H-2, 100	9.91	97	48.91	20.80	28.66	48.71	28.18	28.54	1.71
2H-2, 120	10.11	98	48.90	20.80	28.48	48.71	28.00	28.36	1.72
2H-2, 135	10.26	99	48.89	20.80	29.57	48.71	29.07	29.45	1.66
2H-2, 145	10.36	100	48.89	20.80	28.04	48.71	27.57	27.93	1.75
2H-3, 10	10.51	102	48.87	22.30	29.47	50.25	28.09	28.46	1.72
2H-3, 30	10.71	103	48.87	22.30	27.40	50.25	26.11	26.47	1.85
2H-3, 50	10.91	104	48.86	22.30	27.30	50.25	26.02	26.37	1.85
2H-3, 70	11.11	105	48.86	22.30	28.69	50.25	27.34	27.72	1.76
2H-3, 80	11.21	106	48.85	22.30	29.74	50.25	28.34	28.74	1.70
2H-3, 90	11.31	107	48.84	22.30	28.16	50.25	26.84	27.21	1.79
2H-3, 100	11.41	108	48.84	22.30	27.76	50.25	26.46	26.83	1.82
2H-3, 120	11.61	109	48.83	22.30	28.01	50.25	26.70	27.08	1.80
2H-3, 140	11.81	110	48.82	22.30	29.40	50.25	28.02	28.42	1.72
2H-4, 10	12.01	114	48.80	20.90	25.36	48.81	24.88	25.25	1.93
2H-4, 30	12.21	115	48.79	20.90	28.38	48.81	27.85	28.26	1.73
2H-4, 50	12.41	116	48.78	20.90	29.37	48.81	28.82	29.25	1.67
2H-4, 70	12.61	117	48.78	20.90	27.30	48.81	26.79	27.20	1.79
2H-4, 90	12.81	118	48.77	20.60	24.83	48.51	24.52	24.90	1.96
2H-4, 108	12.99	119	48.76	20.60	28.16	48.51	27.80	28.24	1.73
2H-4, 130	13.21	120	48.76	20.60	28.63	48.51	28.27	28.71	1.70
2H-4, 150	13.41	121	48.75	20.60	27.26	48.51	26.92	27.34	1.78
2H-5, 10	13.50	123	48.74	20.90	25.05	48.81	24.58	24.97	1.95
2H-5, 30	13.70	124	48.73	20.90	28.12	48.81	27.59	28.04	1.74
2H-5, 50	13.90	125	48.73	20.70	28.28	48.61	27.86	28.32	1.72
2H-5, 70	14.10	126	48.72	20.60	28.00	48.51	27.65	28.10	1.73
2H-5, 90	14.30	127	48.71	20.70	26.86	48.61	26.47	26.91	1.81
2H-5, 107	14.47	128	48.71	20.70	25.78	48.61	25.40	25.83	1.89
2H-5, 127	14.67	129	48.70	20.70	29.74	48.61	29.30	29.80	1.63
2H-5, 147	14.87	130	48.69	20.70	27.69	48.61	27.28	27.75	1.75
2H-6, 10	15.01	132	48.68	20.70	27.84	48.61	27.43	27.90	1.74
2H-6, 20	15.11	133	48.67	20.70	29.01	48.61	28.58	29.08	1.67
2H-6, 30	15.21	134	48.67	20.70	27.89	48.61	27.48	27.96	1.74
2H-6, 40	15.31	135	48.66	20.70	26.40	48.61	26.01	26.47	1.84
3H-1, 10	17.00	139	48.64	21.40	26.58	49.32	25.81	26.28	1.85
3H-1, 50	17.40	140	48.63	21.40	27.39	49.32	26.60	27.08	1.80
3H-1, 70	17.60	141	48.62	21.40	26.80	49.32	26.02	26.50	1.83
3H-1, 90	17.80	142	48.62	21.30	27.43	49.22	26.69	27.19	1.79
3H-1, 110	18.00	143	48.61	21.30	27.67	49.22	26.92	27.43	1.77
3H-1, 130	18.20	144	48.60	21.30	27.99	49.22	27.23	27.75	1.75
3H-2, 10	18.50	146	48.59	21.10	28.54	49.02	27.89	28.42	1.71
3H-2, 30	18.70	147	48.58	21.10	25.60	49.02	25.01	25.49	1.91
3H-2, 50	18.90	148	48.58	21.10	27.45	49.02	26.82	27.34	1.78
3H-2, 70	19.10	149	48.57	21.10	25.64	49.02	25.05	25.54	1.90
3H-2, 90	19.30	150	48.56	21.10	28.82	49.02	28.16	28.71	1.69
3H-2, 110	19.50	151	48.56	21.10	27.12	49.02	26.50	27.02	1.80
3H-2, 130	19.70	152	48.55	21.10	27.36	49.02	26.73	27.26	1.78
3H-3, 10	20.00	154	48.54	20.90	26.66	48.81	26.16	26.69	1.82
3H-3, 30	20.20	155	48.53	20.90	24.64	48.81	24.18	24.67	1.97
3H-3, 50	20.40	156	48.52	20.90	23.99	48.81	23.54	24.02	2.02
3H-3, 70	20.60	157	48.52	20.90	26.55	48.81	26.05	26.59	1.83
3H-3, 90	20.80	158	48.51	20.90	26.96	48.81	26.45	27.00	1.80
3H-3, 110	21.00	159	48.51	20.90	26.01	48.81	25.52	26.05	1.86
3H-3, 130	21.20	160	48.50	20.90	24.93	48.81	24.46	24.97	1.94

Table T6 (continued). (Continued on next page.)

Core, section, interval (cm)	Depth (mbsf)	Measurement number	Temperature-corrected seawater conductivity (mS/cm)	Sediment temperature (°C)	Sediment electrical conductivity (mS/cm)	Correction factor at 20°C (mS/cm)	Sediment electrical conductivity at 20°C (mS/cm)	Drift-corrected sediment electrical conductivity at 20°C (mS/cm)	Formation factor
3H-3, 145	21.35	161	48.49	20.90	22.92	48.81	22.49	22.96	2.11
3H-4, 10	21.51	163	48.48	21.10	25.01	49.02	24.44	24.96	1.94
3H-4, 30	21.71	164	48.47	21.10	25.06	49.02	24.49	25.01	1.94
3H-4, 50	21.91	165	48.47	21.10	25.91	49.02	25.32	25.86	1.87
3H-4, 70	22.11	166	48.46	21.10	25.19	49.02	24.61	25.15	1.93
3H-4, 90	22.31	167	48.45	21.10	23.92	49.02	23.37	23.88	2.03
3H-4, 110	22.51	168	48.45	21.10	26.08	49.02	25.48	26.04	1.86
3H-4, 130	22.71	169	48.44	21.10	24.56	49.02	24.00	24.53	1.97
3H-5, 10	23.01	171	48.43	21.30	27.49	49.22	26.75	27.35	1.77
3H-5, 30	23.21	172	48.42	21.30	26.36	49.22	25.65	26.23	1.85
3H-5, 50	23.41	173	48.41	21.30	27.82	49.22	27.07	27.68	1.75
3H-5, 70	23.61	174	48.41	21.30	25.60	49.22	24.91	25.48	1.90
3H-5, 90	23.81	175	48.40	21.30	23.96	49.22	23.31	23.85	2.03
3H-5, 110	24.01	176	48.40	21.20	25.77	49.12	25.13	25.71	1.88
3H-5, 130	24.21	177	48.39	21.30	26.39	49.22	25.68	26.27	1.84
3H-6, 10	24.52	179	48.38	21.10	26.40	49.02	25.79	26.40	1.83
3H-6, 30	24.72	180	48.37	21.10	27.46	49.02	26.83	27.46	1.76
3H-6, 50	24.92	181	48.36	21.10	24.36	49.02	23.80	24.37	1.98
3H-6, 70	25.12	182	48.36	21.10	26.40	49.02	25.79	26.41	1.83
3H-6, 90	25.32	183	48.35	21.10	22.76	49.02	22.24	22.77	2.12
3H-6, 110	25.52	184	48.34	21.10	26.86	49.02	26.24	26.88	1.80
3H-6, 130	25.72	185	48.34	21.10	25.70	49.02	25.11	25.72	1.88
3H-7, 10	26.02	187	48.32	21.00	23.75	48.91	23.25	23.82	2.03
3H-7, 30	26.22	188	48.32	21.00	24.24	48.91	23.73	24.32	1.99
3H-7, 50	26.42	189	48.31	21.00	25.75	48.91	25.21	25.84	1.87
4H-1, 15	26.55	193	48.29	21.70	28.04	49.63	27.06	27.74	1.74
4H-1, 30	26.70	194	48.28	21.70	24.60	49.63	23.74	24.34	1.98
4H-1, 50	26.90	195	48.27	21.50	25.50	49.43	24.71	25.34	1.91
4H-1, 70	27.10	196	48.27	21.50	26.69	49.43	25.86	26.52	1.82
4H-1, 90	27.30	197	48.26	21.50	26.93	49.43	26.09	26.77	1.80
4H-1, 110	27.50	198	48.25	21.60	25.42	49.53	24.58	25.22	1.91
4H-1, 130	27.70	199	48.25	21.60	25.77	49.53	24.92	25.57	1.89
4H-1, 145	27.85	200	48.24	21.60	24.72	49.53	23.90	24.53	1.97
4H-2, 10	28.00	202	48.23	21.70	24.29	49.63	23.44	24.06	2.00
4H-2, 30	28.20	203	48.22	21.70	27.00	49.63	26.05	26.75	1.80
4H-2, 50	28.40	204	48.21	21.70	27.19	49.63	26.24	26.94	1.79
4H-2, 70	28.60	205	48.21	21.70	26.05	49.63	25.14	25.81	1.87
4H-2, 90	28.80	206	48.20	21.70	26.18	49.63	25.26	25.94	1.86
4H-2, 110	29.00	207	48.19	21.70	26.85	49.63	25.91	26.61	1.81
4H-2, 130	29.20	208	48.19	21.70	23.48	49.63	22.66	23.27	2.07
4H-2, 145	29.35	209	48.18	21.70	24.22	49.63	23.37	24.01	2.01
4H-3, 10	29.50	211	48.17	21.60	26.35	49.53	25.48	26.18	1.84
4H-3, 30	29.70	212	48.16	21.60	25.37	49.53	24.53	25.21	1.91
4H-3, 50	29.90	213	48.16	21.50	25.06	49.43	24.28	24.96	1.93
4H-3, 70	30.10	214	48.15	21.50	21.06	49.43	20.41	20.98	2.30
4H-3, 90	30.30	215	48.14	21.50	26.60	49.43	25.77	26.50	1.82
4H-3, 110	30.50	216	48.14	21.50	25.57	49.43	24.78	25.48	1.89
4H-3, 130	30.70	217	48.13	21.50	24.05	49.43	23.30	23.97	2.01
4H-3, 145	30.85	218	48.12	21.50	26.29	49.43	25.47	26.20	1.84
4H-4, 10	31.01	220	48.11	21.60	27.51	49.53	26.60	27.37	1.76
4H-4, 30	31.21	221	48.10	21.60	27.10	49.53	26.20	26.96	1.78
4H-4, 50	31.41	222	48.10	21.50	26.27	49.43	25.45	26.19	1.84
4H-4, 70	31.61	223	48.09	21.50	25.56	49.43	24.77	25.49	1.89
4H-4, 90	31.81	224	48.08	21.50	26.63	49.43	25.80	26.56	1.81
4H-4, 110	32.01	225	48.08	21.50	24.29	49.43	23.54	24.23	1.98
4H-4, 130	32.21	226	48.07	21.50	24.83	49.43	24.06	24.77	1.94
4H-4, 145	32.36	227	48.06	21.50	24.66	49.43	23.89	24.60	1.95
4H-5, 10	32.51	229	48.05	21.40	25.73	49.32	24.98	25.73	1.87
4H-5, 30	32.71	230	48.05	21.40	25.97	49.32	25.22	25.98	1.85
4H-5, 50	32.91	231	48.04	21.40	27.15	49.32	26.36	27.16	1.77
4H-5, 70	33.11	232	48.03	21.20	25.94	49.12	25.29	26.06	1.84
4H-5, 90	33.31	233	48.03	21.20	24.85	49.12	24.23	24.97	1.92
4H-5, 110	33.51	234	48.02	21.20	25.07	49.12	24.44	25.19	1.91
4H-5, 130	33.71	235	48.01	21.20	24.63	49.12	24.02	24.75	1.94
4H-5, 145	33.86	236	48.01	21.20	25.73	49.12	25.09	25.86	1.86
4H-6, 10	34.01	238	47.99	21.30	26.41	49.22	25.70	26.50	1.81

Table T6 (continued). (Continued on next page.)

Core, section, interval (cm)	Depth (mbsf)	Measurement number	Temperature-corrected seawater conductivity (mS/cm)	Sediment temperature (°C)	Sediment electrical conductivity (mS/cm)	Correction factor at 20°C (mS/cm)	Sediment electrical conductivity at 20°C (mS/cm)	Drift-corrected sediment electrical conductivity at 20°C (mS/cm)	Formation factor
4H-6, 30	34.21	239	47.99	21.30	26.82	49.22	26.10	26.91	1.78
4H-6, 50	34.41	240	47.98	21.30	25.51	49.22	24.82	25.60	1.87
4H-6, 70	34.61	241	47.97	21.30	28.89	49.22	28.11	29.00	1.65
5H-2, 20	37.21	244	47.95	22.20	29.07	50.15	27.76	28.65	1.67
5H-2, 40	37.41	245	47.95	22.20	25.90	50.15	24.74	25.53	1.88
5H-2, 60	37.61	246	47.94	22.20	27.38	50.15	26.15	26.99	1.78
5H-2, 80	37.81	247	47.93	22.10	27.77	50.04	26.58	27.44	1.75
5H-2, 100	38.01	248	47.93	22.10	27.82	50.04	26.62	27.49	1.74
5H-2, 120	38.21	249	47.92	22.10	26.74	50.04	25.59	26.42	1.81
5H-2, 140	38.41	250	47.92	22.10	26.82	50.04	25.67	26.51	1.81
5H-3, 10	38.61	252	47.90	22.00	24.87	49.94	23.85	24.64	1.94
5H-3, 30	38.81	253	47.90	22.00	27.53	49.94	26.40	27.28	1.76
5H-3, 50	39.01	254	47.89	22.20	26.17	50.15	24.99	25.82	1.85
5H-3, 70	39.21	255	47.88	22.20	25.77	50.15	24.61	25.43	1.88
5H-3, 90	39.41	256	47.88	22.20	27.23	50.15	26.01	26.88	1.78
5H-3, 110	39.61	257	47.87	22.20	26.51	50.15	25.32	26.17	1.83
5H-3, 130	39.81	258	47.86	22.20	25.46	50.15	24.32	25.14	1.90
5H-3, 145	39.96	259	47.86	22.20	25.52	50.15	24.37	25.20	1.90
5H-4, 10	40.11	261	47.84	22.10	23.96	50.04	22.93	23.71	2.02
5H-4, 30	40.31	262	47.84	22.10	26.64	50.04	25.49	26.37	1.81
5H-4, 50	40.51	263	47.83	22.10	26.12	50.04	25.00	25.86	1.85
5H-4, 70	40.71	264	47.82	22.00	26.20	49.94	25.13	25.99	1.84
5H-4, 90	40.91	265	47.82	22.00	26.24	49.94	25.16	26.04	1.84
5H-4, 110	41.11	266	47.81	22.00	26.09	49.94	25.02	25.89	1.85
5H-4, 130	41.31	267	47.81	22.00	24.52	49.94	23.51	24.34	1.96
5H-4, 145	41.46	268	47.80	22.00	25.09	49.94	24.06	24.90	1.92
5H-5, 15	41.66	270	47.79	21.80	27.36	49.74	26.35	27.28	1.75
5H-5, 30	41.81	271	47.78	21.80	27.72	49.74	26.69	27.64	1.73
5H-5, 50	42.01	272	47.77	21.80	26.74	49.74	25.75	26.67	1.79
5H-5, 70	42.21	273	47.77	21.70	26.72	49.63	25.78	26.70	1.79
5H-5, 90	42.41	274	47.76	21.70	25.54	49.63	24.64	25.53	1.87
5H-5, 110	42.61	275	47.75	21.70	26.28	49.63	25.36	26.27	1.82
5H-5, 130	42.81	276	47.75	21.60	26.01	49.53	25.15	26.06	1.83
5H-5, 145	42.96	277	47.74	21.60	25.80	49.53	24.95	25.85	1.85
5H-6, 10	43.12	279	47.73	21.70	20.77	49.63	20.04	20.77	2.30
5H-6, 30	43.32	280	47.72	21.60	24.15	49.53	23.35	24.21	1.97
5H-6, 50	43.52	281	47.71	21.60	25.53	49.53	24.69	25.59	1.86
6H-2, 60	47.52	284	47.70	22.00	30.99	49.94	29.72	30.82	1.55
6H-2, 80	47.72	285	47.69	22.00	28.15	49.94	27.00	28.00	1.70
6H-2, 100	47.92	286	47.68	22.00	23.61	49.94	22.64	23.49	2.03
6H-2, 123	48.15	287	47.68	22.00	18.85	49.94	18.08	18.76	2.54
6H-2, 140	48.32	288	47.67	22.00	27.35	49.94	26.23	27.22	1.75
6H-3, 15	48.55	290	47.66	21.70	27.95	49.63	26.97	27.99	1.70
6H-3, 30	48.70	291	47.65	21.70	27.87	49.63	26.89	27.92	1.71
6H-3, 50	48.90	292	47.64	21.70	26.70	49.63	25.76	26.75	1.78
6H-3, 70	49.10	293	47.64	21.60	27.23	49.53	26.33	27.34	1.74
6H-3, 90	49.30	294	47.63	21.60	29.04	49.53	28.08	29.16	1.63
6H-3, 110	49.50	295	47.62	21.70	26.51	49.63	25.58	26.57	1.79
6H-3, 130	49.70	296	47.62	21.60	26.69	49.53	25.81	26.81	1.78
6H-4, 145	51.36	297	47.61	21.60	27.06	49.53	26.17	27.18	1.75
6H-4, 10	50.01	299	47.60	21.70	25.54	49.63	24.64	25.61	1.86
6H-4, 30	50.21	300	47.59	21.70	25.94	49.63	25.03	26.01	1.83
6H-4, 50	50.41	301	47.58	21.70	25.72	49.63	24.82	25.80	1.84
6H-4, 70	50.61	302	47.58	21.70	26.44	49.63	25.51	26.52	1.79
6H-4, 90	50.81	303	47.57	21.70	26.11	49.63	25.19	26.19	1.82
6H-4, 110	51.01	304	47.57	21.70	24.90	49.63	24.03	24.98	1.90
6H-4, 130	51.21	305	47.56	21.70	24.40	49.63	23.54	24.48	1.94
6H-4, 145	51.36	306	47.55	21.70	24.84	49.63	23.97	24.93	1.91
6H-5, 10	51.51	308	47.54	21.80	26.59	49.74	25.61	26.64	1.78
6H-5, 30	51.71	309	47.53	21.80	24.31	49.74	23.41	24.36	1.95
6H-5, 50	51.91	310	47.53	21.80	25.75	49.74	24.80	25.80	1.84
6H-5, 70	52.11	311	47.52	21.80	25.16	49.74	24.23	25.21	1.88
6H-5, 90	52.31	312	47.51	21.80	25.39	49.74	24.45	25.45	1.87
6H-5, 110	52.51	313	47.51	21.80	23.81	49.74	22.93	23.87	1.99
6H-5, 130	52.71	314	47.50	21.80	24.03	49.74	23.14	24.09	1.97
6H-5, 145	52.86	315	47.49	21.80	24.18	49.74	23.28	24.24	1.96

Table T6 (continued). (Continued on next page.)

Core, section, interval (cm)	Depth (mbsf)	Measurement number	Temperature-corrected seawater conductivity (mS/cm)	Sediment temperature (°C)	Sediment electrical conductivity (mS/cm)	Correction factor at 20°C (mS/cm)	Sediment electrical conductivity at 20°C (mS/cm)	Drift-corrected sediment electrical conductivity at 20°C (mS/cm)	Formation factor
6H-6, 10	53.01	317	47.48	21.50	25.45	49.43	24.66	25.68	1.85
6H-6, 30	53.21	318	47.47	21.40	25.35	49.32	24.61	25.64	1.85
6H-6, 50	53.41	319	47.47	21.40	24.05	49.32	23.35	24.33	1.95
6H-6, 70	53.61	320	47.46	21.40	24.51	49.32	23.80	24.80	1.91
6H-6, 85	53.76	321	47.46	21.40	26.41	49.32	25.64	26.72	1.78
6H-7, 10	55.00	322	47.45	21.30	26.69	49.22	25.97	27.06	1.75
6H-7, 30	55.20	323	47.44	21.30	28.01	49.22	27.25	28.41	1.67
6H-7, 45	55.40	324	47.44	21.30	28.12	49.22	27.36	28.52	1.66
7H-1, 10	55.60	328	47.41	21.40	27.77	49.32	26.96	28.12	1.69
7H-1, 30	55.80	329	47.40	21.40	26.51	49.32	25.74	26.85	1.77
7H-1, 50	56.00	330	47.40	21.40	24.51	49.32	23.80	24.83	1.91
7H-1, 70	56.20	331	47.39	21.40	23.41	49.32	22.73	23.72	2.00
7H-1, 90	56.37	332	47.38	21.50	23.91	49.43	23.17	24.17	1.96
7H-1, 110	56.52	333	47.38	21.50	22.95	49.43	22.24	23.21	2.04
7H-1, 130	56.72	334	47.37	21.50	24.12	49.43	23.37	24.39	1.94
7H-1, 147	56.92	335	47.36	21.40	23.54	49.32	22.86	23.86	1.99
7H-2, 10	57.12	338	47.35	20.80	21.41	48.71	21.05	21.98	2.15
7H-2, 30	57.30	339	47.34	20.80	24.80	48.71	24.38	25.47	1.86
7H-2, 50	57.51	340	47.33	20.80	22.20	48.71	21.83	22.80	2.08
7H-2, 70	57.72	341	47.33	21.10	21.78	49.02	21.28	22.23	2.13
7H-2, 88	57.90	342	47.32	21.10	23.80	49.02	23.25	24.30	1.95
7H-2, 109	58.05	343	47.31	21.10	21.05	49.02	20.57	21.49	2.20
7H-2, 130	58.25	344	47.31	21.10	21.64	49.02	21.14	22.10	2.14
7H-2, 148	58.45	345	47.30	21.10	24.13	49.02	23.58	24.64	1.92
7H-3, 15	58.65	348	47.28	20.90	24.45	48.81	23.99	25.08	1.89
7H-3, 35	58.85	349	47.27	20.90	23.31	48.81	22.87	23.92	1.98
7H-3, 55	59.05	350	47.27	20.90	23.03	48.81	22.60	23.63	2.00
7H-3, 75	59.25	351	47.26	21.00	23.76	48.91	23.26	24.33	1.94
7H-3, 95	59.45	352	47.25	21.00	22.50	48.91	22.03	23.05	2.05
7H-3, 115	59.65	353	47.25	21.00	21.40	48.91	20.95	21.92	2.16
7H-3, 135	59.85	354	47.24	21.00	25.56	48.91	25.03	26.19	1.80
7H-4, 5	60.05	357	47.22	20.70	24.59	48.61	24.23	25.36	1.86
7H-4, 25	60.23	358	47.22	20.70	24.36	48.61	24.00	25.13	1.88
7H-4, 45	60.45	359	47.21	20.70	24.33	48.61	23.97	25.10	1.88
7H-4, 65	60.65	360	47.20	20.70	23.00	48.61	22.66	23.73	1.99
7H-4, 83	60.85	361	47.20	20.60	24.76	48.51	24.45	25.60	1.84
7H-4, 105	61.02	362	47.19	20.60	22.90	48.51	22.61	23.68	1.99
7H-4, 125	61.22	363	47.18	20.60	23.05	48.51	22.76	23.84	1.98
7H-4, 145	61.42	364	47.18	20.60	21.36	48.51	21.09	22.10	2.14
7H-5, 10	61.62	366	47.16	20.50	22.53	48.40	22.29	23.36	2.02
7H-5, 30	61.82	367	47.16	20.50	22.98	48.40	22.74	23.83	1.98
7H-5, 50	62.02	368	47.15	20.50	20.71	48.40	20.49	21.48	2.20
7H-5, 70	62.22	369	47.14	20.60	20.67	48.51	20.41	21.39	2.20
7H-5, 90	62.40	370	47.14	20.50	30.00	48.40	29.68	31.12	1.51
7H-5, 110	62.56	371	47.13	20.50	23.22	48.40	22.98	24.09	1.96
7H-5, 130	62.76	372	47.12	20.50	22.03	48.40	21.80	22.86	2.06
7H-5, 148	62.85	373	47.12	20.50	22.83	48.40	22.59	23.69	1.99
7H-6, 15	62.96	375	47.11	20.60	20.68	48.51	20.42	21.42	2.20
7H-6, 35	63.16	376	47.10	20.60	22.41	48.51	22.13	23.22	2.03
7H-6, 44	63.36	377	47.09	20.60	23.85	48.51	23.55	24.71	1.91
7H-6, 55	63.56	378	47.09	20.60	23.15	48.51	22.86	23.99	1.96
7H-6, 75	63.76	379	47.08	20.60	22.71	48.51	22.42	23.54	2.00
7H-6, 95	63.96	380	47.07	20.60	23.37	48.51	23.08	24.22	1.94
7H-6, 115	64.29	381	47.07	20.60	22.61	48.51	22.32	23.44	2.01
7H-6, 135	64.50	382	47.06	20.60	23.65	48.51	23.35	24.52	1.92
7H-7, 5	64.70	383	47.05	20.70	21.76	48.61	21.44	22.51	2.09
7H-7, 38	64.90	384	47.05	20.80	23.30	48.71	22.91	24.06	1.96
8H-1, 10	65.10	388	47.02	21.70	23.82	49.63	22.99	24.15	1.95
8H-1, 30	65.30	389	47.01	21.70	21.05	49.63	20.31	21.35	2.20
8H-1, 50	65.50	390	47.01	21.60	21.65	49.53	20.93	22.00	2.14
8H-1, 70	65.70	391	47.00	21.60	23.28	49.53	22.51	23.66	1.99
8H-1, 90	65.85	392	47.00	21.60	23.60	49.53	22.82	23.99	1.96
8H-1, 110	66.00	393	46.99	21.50	22.62	49.43	21.92	23.05	2.04
8H-1, 130	66.20	394	46.98	21.50	23.32	49.43	22.60	23.76	1.98
8H-1, 145	66.40	395	46.98	21.50	24.36	49.43	23.60	24.82	1.89
8H-2, 10	66.60	397	46.96	21.30	24.70	49.22	24.03	25.28	1.86

Table T6 (continued). (Continued on next page.)

Core, section, interval (cm)	Depth (mbsf)	Measurement number	Temperature-corrected seawater conductivity (mS/cm)	Sediment temperature (°C)	Sediment electrical conductivity (mS/cm)	Correction factor at 20°C (mS/cm)	Sediment electrical conductivity at 20°C (mS/cm)	Drift-corrected sediment electrical conductivity at 20°C (mS/cm)	Formation factor
8H-2, 30	66.80	398	46.96	21.30	22.92	49.22	22.30	23.46	2.00
8H-2, 50	67.00	399	46.95	21.20	24.14	49.12	23.54	24.77	1.90
8H-2, 70	67.20	400	46.94	21.20	23.12	49.12	22.54	23.72	1.98
8H-2, 90	67.35	401	46.94	21.20	21.75	49.12	21.21	22.32	2.10
8H-2, 110	67.50	402	46.93	21.20	23.83	49.12	23.24	24.46	1.92
8H-2, 130	67.70	403	46.92	21.20	21.46	49.12	20.92	22.03	2.13
8H-2, 145	67.90	404	46.92	21.20	17.36	49.12	16.93	17.82	2.63
8H-3, 10	68.10	406	46.90	21.20	23.90	49.12	23.30	24.54	1.91
8H-3, 30	68.30	407	46.90	21.20	26.05	49.12	25.40	26.75	1.75
8H-3, 50	68.50	408	46.89	21.20	24.63	49.12	24.02	25.30	1.85
8H-3, 70	68.70	409	46.88	21.20	21.67	49.12	21.13	22.26	2.11
8H-3, 90	68.85	410	46.88	21.20	22.83	49.12	22.26	23.45	2.00
8H-3, 110	69.00	411	46.87	21.20	24.14	49.12	23.54	24.80	1.89
8H-3, 130	69.20	412	46.87	21.20	23.54	49.12	22.95	24.19	1.94
8H-3, 145	69.40	413	46.86	21.20	25.30	49.12	24.67	26.00	1.80
8H-4, 10	69.60	415	46.85	21.20	24.16	49.12	23.56	24.84	1.89
8H-4, 30	69.80	416	46.84	21.20	23.55	49.12	22.96	24.21	1.93
8H-4, 50	70.00	417	46.83	21.20	22.06	49.12	21.51	22.68	2.06
8H-4, 70	70.20	418	46.83	21.20	25.28	49.12	24.65	26.00	1.80
8H-4, 90	70.35	419	46.82	21.20	24.74	49.12	24.12	25.45	1.84
8H-4, 110	70.50	420	46.81	21.20	24.56	49.12	23.95	25.26	1.85
8H-4, 130	70.70	421	46.81	21.20	23.85	49.12	23.25	24.54	1.91
8H-4, 145	70.90	422	46.80	21.20	24.72	49.12	24.10	25.43	1.84
8H-5, 10	71.10	424	46.79	21.20	25.22	49.12	24.59	25.95	1.80
8H-5, 30	71.30	425	46.78	21.20	24.24	49.12	23.63	24.95	1.88
8H-5, 50	71.50	426	46.77	21.20	20.15	49.12	19.65	20.74	2.26
8H-5, 70	71.70	427	46.77	21.20	23.59	49.12	23.00	24.29	1.93
8H-5, 90	71.85	428	46.76	21.20	22.92	49.12	22.35	23.60	1.98
8H-5, 110	72.00	429	46.76	21.20	22.45	49.12	21.89	23.12	2.02
8H-5, 130	72.20	430	46.75	21.30	23.56	49.22	22.92	24.21	1.93
8H-5, 145	72.40	431	46.74	21.30	23.00	49.22	22.38	23.64	1.98
8H-6, 10	72.60	433	46.73	21.10	23.52	49.02	22.98	24.28	1.92
8H-6, 30	72.80	434	46.72	21.10	22.90	49.02	22.37	23.65	1.98
8H-6, 50	74.60	435	46.72	21.10	22.70	49.02	22.18	23.44	1.99
8H-6, 70	74.80	436	46.71	21.10	21.51	49.02	21.02	22.22	2.10
8H-6, 90	75.00	437	46.70	21.10	23.21	49.02	22.68	23.97	1.95
9H-1, 70	75.20	440	46.68	21.40	23.16	49.32	22.49	23.78	1.96
9H-1, 90	75.35	441	46.68	21.40	23.74	49.32	23.05	24.38	1.91
9H-1, 110	75.50	442	46.67	21.40	23.30	49.32	22.62	23.93	1.95
9H-1, 130	75.70	443	46.66	21.40	22.30	49.32	21.65	22.91	2.04
9H-1, 145	75.90	444	46.66	21.40	22.34	49.32	21.69	22.95	2.03
9H-2, 10	76.10	446	46.64	21.20	24.65	49.12	24.03	25.44	1.83
9H-2, 30	76.30	447	46.64	21.20	23.25	49.12	22.67	24.00	1.94
9H-2, 50	76.60	448	46.63	21.20	24.49	49.12	23.88	25.28	1.84
9H-2, 70	76.80	449	46.63	21.20	22.89	49.12	22.32	23.63	1.97
9H-2, 90	77.01	450	46.62	21.20	21.92	49.12	21.37	22.63	2.06
9H-2, 120	77.21	451	46.61	21.20	25.09	49.12	24.46	25.91	1.80
9H-2, 140	77.41	452	46.61	21.20	22.95	49.12	22.38	23.70	1.97
9H-3, 10	77.61	454	46.59	21.50	22.76	49.43	22.05	23.36	1.99
9H-3, 30	77.81	455	46.59	21.50	19.91	49.43	19.29	20.44	2.28
9H-3, 50	78.01	456	46.58	21.50	23.65	49.43	22.92	24.28	1.92
9H-3, 70	78.21	457	46.57	21.50	22.40	49.43	21.70	23.00	2.02
9H-3, 90	78.36	458	46.57	21.40	21.49	49.32	20.87	22.12	2.11
9H-3, 110	78.51	459	46.56	21.40	21.43	49.32	20.81	22.06	2.11
9H-3, 130	78.71	460	46.55	21.40	21.23	49.32	20.61	21.85	2.13
9H-3, 145	78.91	461	46.55	21.40	22.91	49.32	22.25	23.59	1.97
9H-4, 10	79.11	463	46.53	21.40	24.72	49.32	24.00	25.46	1.83
9H-4, 30	79.31	464	46.53	21.40	22.83	49.32	22.17	23.51	1.98
9H-4, 50	79.51	465	46.52	21.40	22.30	49.32	21.65	22.97	2.03
9H-4, 70	79.71	466	46.52	21.30	22.85	49.22	22.23	23.59	1.97
9H-4, 90	79.86	467	46.51	21.30	23.45	49.22	22.82	24.21	1.92
9H-4, 110	80.01	468	46.50	21.30	23.27	49.22	22.64	24.03	1.94
9H-4, 130	80.21	469	46.50	21.30	22.42	49.22	21.81	23.15	2.01
9H-4, 145	80.41	470	46.49	21.30	22.34	49.22	21.74	23.07	2.01
9H-5, 10	80.61	472	46.48	21.20	22.93	49.12	22.36	23.74	1.96
9H-5, 30	80.81	473	46.47	21.20	23.74	49.12	23.15	24.58	1.89

Table T6 (continued). (Continued on next page.)

Core, section, interval (cm)	Depth (mbsf)	Measurement number	Temperature-corrected seawater conductivity (mS/cm)	Sediment temperature (°C)	Sediment electrical conductivity (mS/cm)	Correction factor at 20°C (mS/cm)	Sediment electrical conductivity at 20°C (mS/cm)	Drift-corrected sediment electrical conductivity at 20°C (mS/cm)	Formation factor
9H-5, 50	81.01	474	46.46	21.20	22.07	49.12	21.52	22.85	2.03
9H-5, 70	81.21	475	46.46	21.20	22.44	49.12	21.88	23.24	2.00
9H-5, 90	81.36	476	46.45	21.20	22.19	49.12	21.64	22.98	2.02
9H-5, 110	81.51	477	46.44	21.10	22.54	49.02	22.02	23.40	1.98
9H-5, 130	81.71	478	46.44	21.10	23.42	49.02	22.88	24.31	1.91
9H-5, 145	81.91	479	46.43	21.10	22.82	49.02	22.30	23.69	1.96
9H-6, 10	82.11	481	46.42	21.30	22.42	49.22	21.81	23.19	2.00
9H-6, 30	82.31	482	46.41	21.30	23.26	49.22	22.63	24.06	1.93
9H-6, 50	82.45	483	46.41	21.30	23.41	49.22	22.78	24.22	1.92
9H-6, 70	82.80	484	46.40	21.30	19.83	49.22	19.29	20.52	2.26
9H-6, 90	83.01	485	46.39	21.20	22.80	49.12	22.23	23.64	1.96
9H-7, 5	83.20	487	46.38	21.00	23.20	48.91	22.72	24.16	1.92
9H-7, 40	83.35	488	46.37	21.00	18.82	48.91	18.43	19.60	2.37
9H-7, 61	83.50	489	46.37	20.90	21.43	48.81	21.03	22.37	2.07
9H-7, 80	83.70	490	46.36	20.90	22.20	48.81	21.78	23.18	2.00
9H-7, 95	83.90	491	46.35	20.80	20.87	48.71	20.52	21.84	2.12
10H-1, 10	84.10	494	49.37	20.50	27.60	48.40	27.31	35.03	1.41
10H-1, 30	84.30	495	49.33	20.50	24.25	48.40	23.99	30.80	1.60
10H-1, 50	84.50	496	49.29	20.50	21.69	48.40	21.46	27.56	1.79
10H-1, 70	84.70	497	49.25	20.50	25.40	48.40	25.13	32.28	1.53
10H-1, 90	85.01	498	49.21	20.50	24.63	48.40	24.37	31.32	1.57
10H-1, 110	85.21	499	49.17	20.60	24.65	48.51	24.34	31.29	1.57
10H-1, 130	85.41	500	49.13	20.60	24.09	48.51	23.79	30.60	1.61
10H-2, 10	85.61	502	49.05	20.70	25.90	48.61	25.52	32.86	1.49
10H-2, 30	85.81	503	49.01	20.70	22.57	48.61	22.24	28.64	1.71
10H-2, 50	86.01	504	48.98	20.90	21.46	48.81	21.06	27.13	1.81
10H-2, 70	86.21	505	48.94	20.90	23.47	48.81	23.03	29.69	1.65
10H-2, 90	86.36	506	48.90	20.90	23.49	48.81	23.05	29.73	1.64
10H-2, 110	86.51	507	48.86	20.90	24.56	48.81	24.10	31.09	1.57
10H-2, 130	86.71	508	48.82	20.90	24.47	48.81	24.01	30.99	1.58
10H-2, 145	86.91	509	48.78	20.90	25.10	48.81	24.63	31.81	1.53
10H-3, 10	87.11	511	48.70	21.40	24.44	49.32	23.73	30.67	1.59
10H-3, 30	87.31	512	48.66	21.40	25.06	49.32	24.33	31.47	1.55
10H-3, 50	87.51	513	48.62	21.40	25.21	49.32	24.48	31.67	1.54
10H-3, 70	87.71	514	48.58	21.40	24.89	49.32	24.17	31.28	1.55
10H-3, 90	87.86	515	48.54	21.40	25.29	49.32	24.56	31.80	1.53
10H-3, 110	88.02	516	48.50	21.40	25.60	49.32	24.86	32.20	1.51
10H-3, 130	88.22	517	48.46	21.40	25.18	49.32	24.45	31.69	1.53
10H-3, 145	88.42	518	48.42	21.40	24.32	49.32	23.61	30.62	1.58
10H-4, 10	88.62	520	48.34	21.50	25.00	49.43	24.22	31.44	1.54
10H-4, 30	88.82	521	48.31	21.50	23.64	49.43	22.91	29.74	1.62
10H-4, 50	89.02	522	48.27	21.30	24.47	49.22	23.81	30.93	1.56
10H-4, 70	89.22	523	48.23	21.30	23.24	49.22	22.61	29.38	1.64
10H-4, 90	89.37	524	48.19	21.30	23.80	49.22	23.16	30.11	1.60
10H-4, 110	89.52	525	48.15	21.30	23.49	49.22	22.86	29.73	1.62
10H-4, 130	89.72	526	48.11	21.30	24.44	49.22	23.78	30.94	1.55
10H-4, 145	89.92	527	48.07	21.30	24.20	49.22	23.55	30.65	1.57
10H-5, 10	90.12	529	47.99	21.40	23.92	49.32	23.23	30.26	1.59
10H-5, 30	90.32	530	47.95	21.40	24.11	49.32	23.41	30.52	1.57
10H-5, 50	90.52	531	47.91	21.40	24.43	49.32	23.72	30.93	1.55
10H-5, 70	90.72	532	47.87	21.30	24.57	49.22	23.91	31.19	1.53
10H-5, 90	90.87	533	47.83	21.30	24.08	49.22	23.43	30.58	1.56
10H-5, 110	91.02	534	47.79	21.30	25.81	49.22	25.11	32.79	1.46
10H-5, 130	91.22	535	47.75	21.30	24.83	49.22	24.16	31.56	1.51
10H-5, 145	91.42	536	47.71	21.30	26.26	49.22	25.55	33.39	1.43
10H-6, 10	91.62	538	47.64	21.20	25.54	49.12	24.90	32.57	1.46
10H-6, 30	91.82	539	47.60	21.20	24.57	49.12	23.96	31.35	1.52
10H-6, 50	92.02	540	47.56	21.20	23.57	49.12	22.98	30.09	1.58
10H-6, 70	92.22	541	47.52	21.20	23.56	49.12	22.97	30.09	1.58
10H-6, 90	92.37	542	47.48	21.20	23.80	49.12	23.21	30.41	1.56
10H-6, 110	92.50	543	47.44	21.20	23.68	49.12	23.09	30.27	1.57
10H-6, 130	92.65	544	47.40	21.10	23.50	49.02	22.96	30.11	1.57
10H-6, 145	93.40	545	47.36	21.20	18.48	49.12	18.02	23.64	2.00
10H-7, 10	93.60	547	47.28	21.40	26.39	49.32	25.62	33.65	1.41
10H-7, 25	93.80	548	47.24	21.40	25.47	49.32	24.73	32.49	1.45
11H-1, 50	94.00	550	47.16	21.40	26.87	49.32	26.09	34.31	1.37

Table T6 (continued). (Continued on next page.)

Core, section, interval (cm)	Depth (mbsf)	Measurement number	Temperature-corrected seawater conductivity (mS/cm)	Sediment temperature (°C)	Sediment electrical conductivity (mS/cm)	Correction factor at 20°C (mS/cm)	Sediment electrical conductivity at 20°C (mS/cm)	Drift-corrected sediment electrical conductivity at 20°C (mS/cm)	Formation factor
11H-1, 70	94.20	551	47.12	21.40	25.40	49.32	24.66	32.44	1.45
11H-1, 90	94.35	552	47.08	21.20	24.83	49.12	24.21	31.86	1.48
11H-1, 110	94.56	553	47.04	21.10	25.12	49.02	24.54	32.32	1.46
11H-1, 130	94.71	554	47.00	21.10	25.16	49.02	24.58	32.38	1.45
11H-1, 145	94.91	555	46.96	21.10	24.97	49.02	24.40	32.15	1.46
11H-2, 15	95.10	557	46.89	21.00	26.13	48.91	25.58	33.74	1.39
11H-2, 30	95.31	558	46.85	21.00	25.20	48.91	24.67	32.56	1.44
11H-2, 50	95.51	559	46.81	21.00	25.81	48.91	25.27	33.36	1.40
11H-2, 69	95.71	560	46.77	20.90	25.63	48.81	25.15	33.21	1.41
11H-2, 90	95.86	561	46.73	20.90	25.47	48.81	24.99	33.02	1.42
11H-2, 110	96.01	562	46.69	20.90	22.97	48.81	22.54	29.79	1.57
11H-2, 130	96.21	563	46.65	20.90	23.44	48.81	23.00	30.41	1.53
11H-2, 145	96.41	564	46.61	20.90	23.46	48.81	23.02	30.45	1.53
11H-3, 10	96.61	566	46.39	21.10	23.87	49.02	23.32	24.00	1.93
11H-3, 30	96.81	567	46.38	21.00	21.76	48.91	21.31	21.92	2.12
11H-3, 50	97.01	568	46.38	21.00	25.21	48.91	24.68	25.40	1.83
11H-3, 70	97.21	569	46.38	21.00	19.62	48.91	19.21	19.77	2.35
11H-3, 90	97.36	570	46.38	21.10	23.34	49.02	22.80	23.47	1.98
11H-3, 110	97.51	571	46.37	21.10	23.95	49.02	23.40	24.08	1.93
11H-3, 130	97.71	572	46.37	21.10	23.07	49.02	22.54	23.20	2.00
11H-3, 145	97.91	573	46.37	21.10	22.94	49.02	22.41	23.07	2.01
11H-4, 10	98.11	575	46.36	20.90	20.55	48.81	20.16	20.76	2.23
11H-4, 30	98.31	576	46.36	20.90	22.99	48.81	22.56	23.22	2.00
11H-4, 50	98.51	577	46.36	20.90	22.87	48.81	22.44	23.10	2.01
11H-4, 70	98.71	578	46.36	20.90	23.06	48.81	22.63	23.29	1.99
11H-4, 90	98.86	579	46.36	20.90	21.50	48.81	21.10	21.72	2.13
11H-4, 110	99.01	580	46.35	21.00	21.81	48.91	21.35	21.99	2.11
11H-4, 130	99.21	581	46.35	21.00	21.14	48.91	20.70	21.31	2.17
11H-4, 145	99.41	582	46.35	21.00	21.98	48.91	21.52	22.16	2.09
11H-5, 10	99.61	584	46.34	21.20	19.90	49.12	19.40	19.98	2.32
11H-5, 30	99.81	585	46.34	21.20	21.53	49.12	20.99	21.62	2.14
11H-5, 50	100.01	586	46.34	21.10	21.80	49.02	21.30	21.94	2.11
11H-5, 70	100.21	587	46.34	21.10	20.83	49.02	20.35	20.96	2.21
11H-5, 90	100.36	588	46.33	21.10	20.57	49.02	20.10	20.70	2.24
11H-5, 110	100.51	589	46.33	21.10	21.00	49.02	20.52	21.14	2.19
11H-5, 130	100.71	590	46.33	21.10	20.07	49.02	19.61	20.20	2.29
11H-5, 145	100.91	591	46.33	21.10	19.74	49.02	19.29	19.87	2.33
11H-6, 10	101.11	593	46.32	21.40	20.12	49.32	19.54	20.13	2.30
11H-6, 30	101.31	594	46.32	21.30	19.93	49.22	19.39	19.98	2.32
11H-6, 50	101.51	595	46.32	21.30	21.65	49.22	21.07	21.71	2.13
11H-6, 70	101.71	596	46.31	21.30	21.52	49.22	20.94	21.58	2.15
11H-6, 90	101.86	597	46.31	21.30	21.49	49.22	20.91	21.55	2.15
11H-6, 110	102.03	598	46.31	21.30	21.85	49.22	21.26	21.91	2.11
11H-6, 130	102.18	599	46.31	21.30	21.01	49.22	20.44	21.07	2.20
11H-6, 145	102.50	600	46.30	21.30	19.74	49.22	19.21	19.80	2.34
11H-7, 10	102.70	602	46.30	21.00	20.60	48.91	20.17	20.79	2.23
11H-7, 25	102.90	603	46.30	21.00	17.93	48.91	17.56	18.10	2.56
12H-1, 10	103.10	605	46.29	20.40	23.56	48.30	23.36	24.08	1.92
12H-1, 30	103.30	606	46.29	20.40	20.85	48.30	20.67	21.31	2.17
12H-1, 50	103.50	607	46.29	20.40	23.27	48.30	23.07	23.79	1.95
12H-1, 70	103.70	608	46.28	20.40	23.21	48.30	23.01	23.73	1.95
12H-1, 90	103.85	609	46.28	20.50	25.08	48.40	24.82	25.59	1.81
12H-1, 110	104.00	610	46.28	20.50	23.56	48.40	23.31	24.04	1.93
12H-1, 130	104.20	611	46.28	20.50	24.17	48.40	23.92	24.66	1.88
12H-1, 145	104.40	612	46.27	20.50	23.34	48.40	23.09	23.82	1.94
12H-2, 10	105.00	615	46.27	21.20	23.17	49.12	22.59	23.30	1.99
12H-2, 30	105.20	616	46.26	21.20	21.53	49.12	20.99	21.65	2.14
12H-2, 50	105.35	617	46.26	21.20	18.70	49.12	18.23	18.81	2.46
12H-2, 110	105.50	618	46.26	21.20	16.57	49.12	16.16	16.67	2.78
12H-2, 130	105.70	619	46.26	21.20	14.93	49.12	14.56	15.02	3.08
12H-2, 145	105.90	620	46.26	21.20	16.08	49.12	15.68	16.18	2.86
12H-3, 10	106.10	622	46.25	21.00	16.67	48.91	16.32	16.84	2.75
12H-3, 30	106.30	623	46.25	21.00	15.82	48.91	15.49	15.98	2.89
12H-3, 50	106.50	624	46.25	21.00	15.19	48.91	14.87	15.35	3.01
12H-3, 70	106.65	625	46.24	21.00	15.07	48.91	14.76	15.23	3.04
12H-3, 90	106.78	626	46.24	21.10	13.87	49.02	13.55	13.99	3.31

Table T6 (continued). (Continued on next page.)

Core, section, interval (cm)	Depth (mbsf)	Measurement number	Temperature-corrected seawater conductivity (mS/cm)	Sediment temperature (°C)	Sediment electrical conductivity (mS/cm)	Correction factor at 20°C (mS/cm)	Sediment electrical conductivity at 20°C (mS/cm)	Drift-corrected sediment electrical conductivity at 20°C (mS/cm)	Formation factor
12H-3, 110	106.98	627	46.24	21.10	13.87	49.02	13.55	13.99	3.31
12H-3, 125	107.18	628	46.24	21.10	14.46	49.02	14.13	14.58	3.17
12H-4, 10	107.38	630	46.23	21.20	14.97	49.12	14.60	15.07	3.07
12H-4, 30	107.58	631	46.23	21.20	14.15	49.12	13.80	14.24	3.25
12H-4, 50	107.78	632	46.23	21.20	13.26	49.12	12.93	13.35	3.46
12H-4, 70	107.98	633	46.22	21.20	13.85	49.12	13.50	13.94	3.32
12H-4, 90	108.13	634	46.22	21.20	13.10	49.12	12.77	13.19	3.51
12H-4, 110	108.28	635	46.22	21.20	13.16	49.12	12.83	13.25	3.49
12H-4, 130	108.48	636	46.22	21.20	13.21	49.12	12.88	13.30	3.48
12H-4, 145	108.68	637	46.21	21.20	13.55	49.12	13.21	13.64	3.39
12H-5, 10	108.88	639	46.21	21.20	14.03	49.12	13.68	14.13	3.27
12H-5, 30	109.08	640	46.21	21.20	13.68	49.12	13.34	13.77	3.35
12H-5, 50	109.28	641	46.20	21.20	13.10	49.12	12.77	13.19	3.50
12H-5, 70	109.48	642	46.20	21.20	12.73	49.12	12.41	12.82	3.60
12H-5, 90	109.63	643	46.20	21.20	12.93	49.12	12.61	13.02	3.55
12H-5, 110	109.78	644	46.20	21.20	12.29	49.12	11.98	12.38	3.73
12H-5, 130	109.98	645	46.19	21.20	12.75	49.12	12.43	12.84	3.60
12H-5, 145	110.18	646	46.19	21.20	12.48	49.12	12.17	12.57	3.67
12H-6, 10	110.38	648	46.19	21.20	13.33	49.12	13.00	13.43	3.44
12H-6, 30	110.58	649	46.18	21.20	12.79	49.12	12.47	12.88	3.58
12H-6, 50	110.78	650	46.18	21.20	12.68	49.12	12.36	12.77	3.62
12H-6, 70	110.98	651	46.18	21.20	12.18	49.12	11.88	12.27	3.76
12H-6, 90	111.13	652	46.18	21.20	11.94	49.12	11.64	12.03	3.84
12H-6, 110	111.29	653	46.17	21.20	11.92	49.12	11.62	12.01	3.84
12H-6, 130	111.49	654	46.17	21.20	12.21	49.12	11.91	12.30	3.75
12H-6, 145	112.30	655	46.17	21.20	9.91	49.12	9.66	9.99	4.62
12H-7, 10	112.50	657	46.16	20.90	10.68	48.81	10.48	10.83	4.26
12H-7, 30	112.70	658	46.16	20.90	12.68	48.81	12.44	12.86	3.59
13H-1, 40	112.90	661	46.15	21.70	18.54	49.63	17.89	18.49	2.50
13H-1, 60	113.10	662	46.15	21.70	18.24	49.63	17.60	18.20	2.54
13H-1, 80	113.37	663	46.15	21.70	17.46	49.63	16.85	17.42	2.65
13H-1, 100	113.56	664	46.15	21.60	15.06	49.53	14.56	15.06	3.06
13H-1, 120	113.76	665	46.15	21.40	14.90	49.32	14.47	14.96	3.08
13H-1, 147	113.96	666	46.14	21.40	18.02	49.32	17.50	18.09	2.55
13H-2, 15	114.16	669	46.14	21.40	16.02	49.32	15.56	16.09	2.87
13H-2, 35	114.36	670	46.13	21.40	15.95	49.32	15.49	16.02	2.88
13H-2, 55	114.56	671	46.13	21.40	13.34	49.32	12.95	13.40	3.44
13H-2, 75	114.76	672	46.13	21.10	12.43	49.02	12.15	12.56	3.67
13H-2, 95	114.96	673	46.13	21.10	11.98	49.02	11.71	12.11	3.81
13H-2, 115	115.16	674	46.12	21.00	11.30	48.91	11.06	11.45	4.03
13H-2, 135	115.36	675	46.12	21.00	11.47	48.91	11.23	11.62	3.97
13H-3, 5	115.56	677	46.12	21.00	13.31	48.91	13.03	13.48	3.42
13H-3, 25	115.76	678	46.11	21.00	11.75	48.91	11.50	11.90	3.87
13H-3, 45	115.96	679	46.11	21.00	11.31	48.91	11.07	11.46	4.02
13H-3, 65	116.16	680	46.11	21.00	11.30	48.91	11.06	11.45	4.03
13H-3, 85	116.36	681	46.11	21.00	11.61	48.91	11.37	11.76	3.92
13H-3, 105	116.56	682	46.10	20.80	11.93	48.71	11.73	12.14	3.80
13H-3, 125	116.76	683	46.10	20.90	11.20	48.81	10.99	11.37	4.05
13H-3, 145	116.96	684	46.10	20.90	11.50	48.81	11.28	11.68	3.95
13H-4, 15	117.16	686	46.09	21.20	12.24	49.12	11.93	12.35	3.73
13H-4, 35	117.36	687	46.09	21.20	11.93	49.12	11.63	12.04	3.83
13H-4, 55	117.56	688	46.09	21.20	11.47	49.12	11.18	11.58	3.98
13H-4, 75	117.76	689	46.09	21.20	11.21	49.12	10.93	11.32	4.07
13H-4, 95	117.96	690	46.08	20.90	11.35	48.81	11.14	11.53	4.00
13H-4, 115	118.16	691	46.08	20.90	11.13	48.81	10.92	11.31	4.08
13H-4, 135	118.36	692	46.08	20.90	11.92	48.81	11.70	12.11	3.81
13H-5, 5	118.56	694	46.07	21.00	12.81	48.91	12.54	12.99	3.55
13H-5, 25	118.76	695	46.07	21.00	12.59	48.91	12.33	12.77	3.61
13H-5, 45	118.96	696	46.07	21.00	11.74	48.91	11.49	11.90	3.87
13H-5, 65	119.16	697	46.07	20.80	12.41	48.71	12.20	12.64	3.65
13H-5, 85	119.36	698	46.06	20.80	12.07	48.71	11.87	12.29	3.75
13H-5, 105	119.51	699	46.06	20.80	12.20	48.71	12.00	12.42	3.71
13H-5, 125	119.71	700	46.06	20.70	12.22	48.61	12.04	12.47	3.69
13H-5, 145	119.91	701	46.06	20.70	11.91	48.61	11.73	12.16	3.79
13H-6, 10	120.11	703	46.05	21.10	11.55	49.02	11.29	11.69	3.94
13H-6, 30	120.31	704	46.05	21.10	12.25	49.02	11.97	12.40	3.71

Table T6 (continued).

Core, section, interval (cm)	Depth (mbsf)	Measurement number	Temperature-corrected seawater conductivity (mS/cm)	Sediment temperature (°C)	Sediment electrical conductivity (mS/cm)	Correction factor at 20°C (mS/cm)	Sediment electrical conductivity at 20°C (mS/cm)	Drift-corrected sediment electrical conductivity at 20°C (mS/cm)	Formation factor
13H-6, 50	120.51	705	46.05	21.10	12.23	49.02	11.95	12.38	3.72
13H-6, 70	120.72	706	46.04	21.10	13.53	49.02	13.22	13.70	3.36
13H-6, 90	120.92	707	46.04	20.80	12.83	48.71	12.61	13.07	3.52
13H-6, 110	121.12	708	46.04	20.80	13.29	48.71	13.07	13.54	3.40
13H-7, 10	121.30	710	46.04	21.00	13.22	48.91	12.94	13.41	3.43
13H-7, 30	122.10	711	46.03	21.00	13.30	48.91	13.02	13.50	3.41
13H-7, 50	122.30	712	46.03	21.00	13.48	48.91	13.20	13.68	3.37
13H-7, 68	122.50	713	46.03	21.10	13.80	49.02	13.48	13.98	3.29
14H-1, 70	122.70	716	46.02	21.50	14.22	49.43	13.78	14.28	3.22
14H-1, 90	122.85	717	46.02	21.50	13.54	49.43	13.12	13.60	3.38
14H-1, 110	123.00	718	46.02	21.50	14.03	49.43	13.59	14.09	3.26
14H-1, 130	123.20	719	46.01	21.50	12.50	49.43	12.11	12.56	3.66
14H-1, 145	123.40	720	46.01	21.50	12.05	49.43	11.68	12.11	3.80
14H-2, 10	123.60	722	46.01	21.20	12.34	49.12	12.03	12.48	3.69
14H-2, 30	123.80	723	46.00	21.20	11.73	49.12	11.44	11.86	3.88
14H-2, 50	124.00	724	46.00	21.20	11.49	49.12	11.20	11.62	3.96
14H-2, 70	124.20	725	46.00	21.20	11.20	49.12	10.92	11.33	4.06
14H-2, 90	124.35	726	46.00	21.20	11.83	49.12	11.53	11.96	3.84
14H-2, 110	124.51	727	45.99	21.20	11.13	49.12	10.85	11.26	4.09
14H-2, 130	124.71	728	45.99	21.20	11.00	49.12	10.73	11.12	4.13
14H-2, 145	124.91	729	45.99	21.20	11.19	49.12	10.91	11.32	4.06
14H-3, 10	125.11	731	45.98	21.20	11.93	49.12	11.63	12.07	3.81
14H-3, 30	125.31	732	45.98	21.20	11.36	49.12	11.08	11.49	4.00
14H-3, 50	125.51	733	45.98	21.20	10.58	49.12	10.32	10.70	4.30
14H-3, 70	125.71	734	45.98	21.20	10.39	49.12	10.13	10.51	4.37
14H-3, 90	125.86	735	45.97	21.20	10.62	49.12	10.35	10.74	4.28
14H-3, 110	126.01	736	45.97	21.20	10.42	49.12	10.16	10.54	4.36
14H-3, 130	126.21	737	45.97	21.20	10.82	49.12	10.55	10.95	4.20
14H-3, 145	126.41	738	45.97	21.20	10.10	49.12	9.85	10.22	4.50
14H-4, 10	126.61	740	45.96	21.10	12.52	49.02	12.23	12.70	3.62
14H-4, 30	126.81	741	45.96	21.10	11.95	49.02	11.68	12.12	3.79

Table T7. Summary of APCT-3 temperature measurements, Site U1371.

Core	Depth (mbsf)	BWT (°C)	Origin time (s)	Time delay (s)	Start fit (s)	End fit (s)	Measurement time (min)	Equilibrium temperature (°C)	Remark
329-U1371D-									
4H	35.9	1.11	8,618	246.6	275	587	5.22	4.18	
5H	45.4	1.09	11,393	198.3	205	684	7.93	4.75	2.5 m heave
6H	64.4	1.11	9,563	265.6	326	481	2.50	5.92	Fair
8H	73.9	1.11	37,437	381.0	381	622	3.95	7.00	Poor
10H	92.9	1.11	18,827	33.5	53	248	3.27	7.48	

BWT = bottom water temperature.

Table T8. Dissolved oxygen concentrations determined using electrodes, Holes U1371B–U1371D, U1371F, and U1371H. (Continued on next page.)

Core, section, interval (cm)	Depth (mbsf)	O_2 (μM) Electrode 1	O_2 (μM) Electrode 2
329-U1371B-			
1H-1, 10	0.10	75.06	
1H-1, 20	0.20	25.06	
1H-1, 30	0.30		11.39
1H-1, 40	0.40		4.00
1H-1, 50	0.50	6.03	
1H-1, 60	0.60	7.43	
1H-1, 70	0.70		3.92
1H-1, 80	0.80		1.61
1H-1, 90	0.90	0.64	
1H-1, 100	1.00	0.55	
1H-1, 110	1.10		0.73
1H-1, 120	1.20		0.45
1H-1, 130	1.30	0.42	
1H-2, 10	1.60	4.70	
1H-2, 20	1.70		7.43
1H-2, 30	1.80		3.60
1H-2, 40	1.90	3.03	
1H-2, 50	2.00	39.88	
1H-2, 60	2.10		6.36
1H-2, 70	2.20		4.08
1H-2, 80	2.30	1.83	
1H-2, 90	2.40	0.65	
1H-2, 100	2.50		0.71
1H-2, 110	2.60		0.14
1H-2, 120	2.70	0.14	
1H-2, 130	2.80	0.00	
1H-2, 140	2.90		0.00
329-U1371C-			
1H-1, 15	0.10	33.09	
1H-1, 30	0.20		14.39
1H-1, 45	0.30	2.88	
1H-1, 60	0.40		3.01
1H-1, 75	0.50		1.71
1H-1, 90	0.60	5.31	
1H-1, 105	0.70		1.61
1H-1, 120	0.80	1.75	
1H-1, 135	0.90		1.22
1H-2, 15	1.60	0.96	
1H-2, 30	1.70		0.95
1H-2, 45	1.80	1.18	
1H-2, 60	1.90		1.06
1H-2, 75	2.00	1.59	
1H-2, 90	2.10		0.62
1H-2, 105	2.20	1.48	
1H-2, 120	2.30		0.86
1H-2, 135	2.40	0.84	
329-U1371D-			
1H-1, 10	0.10	54.92	
1H-1, 20	0.20	82.63	
1H-1, 30	0.30	60.07	
1H-1, 40	0.40	12.45	
1H-1, 50	0.50	4.53	
1H-1, 60	0.60	2.84	
1H-1, 70	0.70	1.44	
1H-1, 80	0.80	1.63	
1H-1, 90	0.90	1.26	
1H-1, 100	1.00	2.46	
1H-1, 110	1.10	2.35	
1H-1, 120	1.20	1.28	
1H-1, 130	1.30	0.86	
1H-1, 140	1.40	0.88	
1H-2, 10	1.60		0.86
1H-2, 20	1.70	0.84	0.90
1H-2, 30	1.80	0.94	0.65
1H-2, 40	1.90	0.93	0.35
1H-2, 50	2.00	0.35	0.10
1H-2, 60	2.10	0.66	0.40
1H-2, 70	2.20		0.51
1H-2, 80	2.30		0.84
1H-2, 90	2.40		0.55
1H-2, 100	2.50	0.10	0.44
1H-2, 110	2.60	0.37	0.10
1H-2, 120	2.70	0.05	0.08
1H-2, 130	2.80		0.08
1H-2, 140	2.90		0.07
1H-3, 10	3.10		0.28
1H-3, 20	3.20		
1H-3, 30	3.30		
1H-3, 40	3.40		0.46
1H-3, 50	3.50		0.73
1H-3, 60	3.60		0.72
1H-3, 75	3.75		
1H-3, 80	3.80		0.40
1H-3, 90	3.90		0.36
1H-3, 100	4.00		0.04
1H-3, 110	4.10		
1H-3, 125	4.25	0.76	
1H-4, 25	4.75	0.13	
1H-4, 75	5.25	0.16	
1H-4, 125	5.75	0.65	
1H-5, 25	6.25	0.09	
1H-5, 70	6.70	0.13	
1H-5, 125	7.25	0.43	
2H-1, 30	7.70	0.40	
2H-2, 30	9.20		
2H-3, 30	10.70	0.03	
2H-4, 30	12.20		
2H-5, 30	13.70	0.02	
2H-6, 30	15.20		
3H-1, 30	17.20	0.03	
3H-2, 30	18.70		
3H-3, 30	20.20	0.08	
3H-4, 30	21.70		
3H-5, 30	23.20	0.05	
3H-6, 30	24.70		
4H-1, 30	26.70	2.97	0.04
4H-2, 30	28.20	0.71	0.61
4H-3, 30	29.70	0.40	0.00
4H-4, 30	31.20	0.47	3.03
4H-5, 30	32.40	6.01	6.12
5H-2, 30	37.30	6.01	6.12
5H-3, 30	38.80	0.27	0.00
5H-4, 30	40.30	0.26	1.25
6H-1, 30	45.70	0.85	4.95
6H-2, 30	47.20	0.75	0.54
6H-3, 30	48.70	0.00	0.00
6H-4, 30	50.20	0.80	0.53
6H-5, 30	51.70	0.04	0.57
6H-6, 30	53.20	1.27	0.19
7H-1, 30	55.20	0.29	0.00
7H-2, 30	56.70	0.00	0.13
7H-3, 30	58.20	0.05	0.00
7H-4, 30	59.70	0.00	0.00
7H-5, 30	61.20	0.00	0.30
7H-6, 30	62.70	0.00	0.00
8H-1, 30	64.70	0.08	0.00
8H-2, 30	66.20	0.35	0.00
8H-3, 30	67.70	0.27	0.00
8H-4, 30	64.70	0.00	0.00
8H-5, 30	70.70	0.00	0.00
8H-6, 30	72.20	0.00	0.00
9H-1, 30	74.20	0.00	0.00
9H-2, 30	75.70	0.01	0.06
9H-3, 30	77.20	0.06	0.09
9H-4, 30	74.20	0.00	0.00
9H-5, 30	74.20	0.00	0.00
9H-6, 30	74.20	0.00	0.00
10H-1, 30	83.70	0.00	0.00
10H-2, 30	85.20	0.00	0.00
10H-3, 30	86.70	0.02	0.00
10H-4, 30	88.20	0.02	0.00
10H-5, 30	89.70	0.02	0.00
10H-6, 30	91.20	0.00	0.00
11H-1, 30	93.20	0.00	0.00
11H-2, 30	94.70	2.06	0.00
11H-3, 30	96.20	1.03	1.17
11H-4, 30	97.70	1.18	0.00
11H-5, 30	99.21	0.00	0.12
11H-6, 30	100.71	0.00	0.00
12H-1, 30	102.70	3.31	1.21
12H-2, 30	104.20	0.00	0.06
12H-3, 30	105.70	3.59	2.94
12H-4, 30	106.98	0.00	0.00
12H-5, 30	108.48	1.03	1.05
12H-6, 30	109.98	0.00	
13H-1, 30	112.20	0.00	
13H-2, 30	109.98	0.00	
13H-3, 30	115.20	0.72	
13H-3, 60	115.50	1.43	
13H-3, 80	115.70	1.33	
13H-3, 100	115.90	2.02	
13H-3, 110	116.00	0.00	
13H-4, 30	116.70	9.46	
13H-4, 60	117.00	8.74	
13H-4, 70	117.10	3.37	
13H-4, 80	117.20	3.00	
13H-4, 100	117.40	2.90	
13H-4, 110	117.50	2.22	
13H-4, 120	117.60	2.48	
13H-4, 130	117.70	2.28	
13H-4, 140	117.80	17.18	
13H-5, 60	118.50	9.57	
13H-5, 90	118.80	13.76	
13H-5, 100	118.90	2.30	
13H-5, 130	119.20	5.61	
13H-6, 60	120.00	0.00	
13H-6, 100	120.40	0.00	
13H-7, 60	121.20	0.04	
13H-7, 100	121.60	0.00	
14H-1, 20	121.60	3.22	
14H-1, 90	122.30	2.96	
14H-1, 100	122.40	2.98	
14H-2, 15	123.05	3.22	
14H-2, 80	123.70	2.97	
14H-2, 90	123.80	2.50	
14H-2, 100	123.90	2.84	
14H-2, 110	124.00	1.52	
14H-2, 120	124.10	1.83	
14H-2, 130	124.20	2.44	
14H-2, 140	124.30	3.37	
14H-3, 10	124.50	2.67	
14H-3, 30	124.70	3.42	
14H-3, 40	124.80	2.31	
14H-3, 60	125.00	1.14	
14H-3, 70	125.10	3.18	
14H-3, 90	125.30	4.24	
14H-3, 100	125.40	3.61	
14H-3, 120	125.60	2.99	
14H-3, 130	125.70	3.99	

Table T8 (continued).

Core, section, interval (cm)	Depth (mbsf)	O_2 (μM) Electrode 1	O_2 (μM) Electrode 2
329-U1371F-			
11H-1, 30	95.00	0.30	0.14
11H-2, 30	96.50	1.05	0.88
11H-3, 30	98.00	0.59	0.56
11H-4, 30	99.50	0.24	0.93
11H-5, 30	101.00	0.00	0.70
11H-6, 30	102.50	0.69	0.49
11H-7, 30	104.00	0.36	0.30
12H-1, 30	104.50	0.82	0.24
12H-2, 30	106.00	0.00	0.83
12H-3, 30	107.50	0.00	0.00
12H-4, 30	109.00	0.15	1.61
12H-5, 30	110.20	0.78	0.32
12H-6, 30	112.00	1.05	1.05
12H-7, 30	113.50	1.94	1.63
13H-2, 30	114.28	3.95	4.92
13H-2, 110	115.08	6.53	5.57
13H-3, 30	115.78	2.67	3.45
13H-4, 30	117.28	7.84	3.86
13H-4, 50	117.48	3.14	
13H-4, 90	117.88	7.83	6.17
13H-4, 110	118.08	2.78	2.10
13H-4, 130	118.28	2.23	2.20
13H-5, 10	118.58	1.49	1.65
13H-5, 50	118.98	1.44	2.10
13H-5, 90	119.38	1.50	7.62
13H-5, 130	119.78	4.88	9.78
13H-6, 10	120.08	2.35	1.68
13H-6, 30	120.28	3.41	3.06
13H-6, 90	120.88	3.53	3.66
13H-6, 110	121.08	2.05	1.58
13H-6, 130	121.28	2.31	2.98
13H-7, 30	121.78	1.25	1.77
13H-7, 50	121.98	2.62	2.30
13H-7, 90	122.38	4.10	4.07
13H-7, 130	122.78	6.80	5.45
14H-1, 50	123.70	4.84	
14H-1, 90	124.10	6.74	3.71
14H-1, 110	124.30	8.44	10.78
14H-2, 50	125.20	18.41	9.23
14H-2, 90	125.60	2.55	4.18
14H-2, 110	125.80	5.36	
14H-2, 130	126.00	5.63	
14H-3, 30	126.50	12.14	9.67
14H-3, 50	126.70	9.30	8.39
14H-3, 70	126.90	11.26	14.15
14H-3, 90	127.10	8.10	7.10
14H-3, 110	127.30	6.61	11.35
14H-3, 130	127.50	5.80	13.61
14H-4, 30	128.00	9.32	
14H-4, 50	128.20	18.71	25.29
14H-4, 70	128.40	12.59	12.53
14H-4, 90	128.60	15.36	11.25
14H-6, 30	129.42	14.91	8.30
14H-6, 50	129.62	10.17	10.23
14H-6, 70	129.82	11.72	12.77
14H-6, 90	130.02	5.74	7.54
329-U1371H-			
1H-1, 15	0.15	60.59	
1H-1, 25	0.25	52.06	
1H-1, 35	0.35		46.13
1H-1, 45	0.45		37.95
1H-1, 55	0.55	20.54	
1H-1, 65	0.65	13.94	
1H-1, 75	0.75		7.43
1H-1, 85	0.85		6.23
1H-1, 95	0.95	4.12	
1H-1, 105	1.05	3.16	
1H-1, 115	1.15		1.73
1H-1, 125	1.25		1.43
1H-2, 15	1.65	34.60	
1H-2, 25	1.75	28.14	
1H-2, 35	1.85		39.27
1H-2, 45	1.95		32.35
1H-2, 55	2.05	25.64	
1H-2, 65	2.15	30.26	
1H-2, 75	2.25		28.41
1H-2, 85	2.35		36.07
1H-2, 95	2.45	26.00	
1H-2, 105	2.55	29.55	
1H-2, 115	2.65		26.20
1H-2, 125	2.75		27.81
1H-3, 20	3.20	17.93	
1H-3, 30	3.30		8.88
1H-3, 50	3.50		5.62
1H-3, 60	3.60	4.07	
1H-3, 75	3.75	3.51	
1H-3, 90	3.90		5.60
1H-3, 105	4.05		6.13
1H-3, 120	4.20	73.69	
1H-3, 135	4.35	72.70	
1H-4, 30	4.80		27.79
1H-4, 60	5.10		29.07
1H-4, 90	5.40	22.92	
1H-4, 20	5.70	20.12	
1H-4, 40	5.90	19.71	

Values reported below 0.1 μM should be considered as below the limit of detection.

Table T9. Dissolved oxygen concentrations determined using optodes, Holes U1371B–U1371D and U1371H.

Core, section, interval (cm)	Depth (mbsf)	O_2 (μM)
329-U1371B-		
1H-1, 15	0.15	12.98
1H-1, 45	0.45	0.68
1H-1, 55	0.55	2.54
1H-1, 67	0.67	0.00
1H-1, 75	0.75	0.00
1H-1, 85	0.85	0.00
1H-1, 105	1.05	0.00
329-U1371C-		
1H-1, 10	0.10	23.41
1H-1, 20	0.20	44.92
1H-1, 30	0.30	12.65
1H-1, 50	0.50	3.75
1H-1, 65	0.65	4.45
1H-1, 95	0.95	5.03
1H-1, 110	1.10	2.62
1H-1, 140	1.40	3.62
1H-2, 40	1.90	4.21
1H-2, 70	2.20	2.49
1H-2, 100	2.50	2.14
1H-2, 125	2.75	2.77
1H-3, 25	3.25	1.61
1H-3, 80	3.80	2.27
1H-3, 130	4.30	3.92
1H-4, 80	5.30	0.00
1H-4, 130	5.80	0.00
1H-5, 130	7.30	0.00
329-U1371D-		
1H-1, 5	0.05	177.20
1H-1, 7.5	0.08	130.40
1H-1, 12.5	0.13	104.20
1H-1, 15	0.15	85.74
1H-1, 25	0.25	58.31
1H-1, 35	0.35	41.60
1H-1, 45	0.45	6.18
1H-1, 55	0.55	1.09
1H-1, 65	0.65	0.53
1H-1, 75	0.75	2.48
1H-1, 85	0.85	0.35
1H-1, 95	0.95	0.22
1H-1, 105	1.05	0.74
1H-1, 115	1.15	0.29
1H-1, 125	1.25	0.23
1H-1, 134	1.34	0.30
1H-1, 135	1.35	1.88
1H-1, 145	1.45	1.02
1H-2, 25	1.75	2.45
1H-2, 35	1.85	2.19
1H-2, 55	2.05	3.94
1H-2, 75	2.25	0.62
1H-2, 95	2.45	2.72
1H-2, 105	2.55	3.74
1H-2, 115	2.65	4.08
1H-2, 135	2.85	3.97
1H-3, 55	3.55	0.85
1H-3, 85	3.85	0.57
1H-3, 105	4.05	1.31
1H-4, 80	5.30	0.61
1H-4, 130	5.80	0.86
1H-5, 40	6.40	0.00
2H-1, 120	8.60	0.97
2H-3, 40	10.80	0.00
2H-3, 85	11.25	0.00
2H-4, 80	12.70	0.00
2H-5, 80	14.20	0.00
3H-2, 120	19.60	0.00
3H-4, 80	22.20	0.00
3H-6, 80	25.20	0.00
4H-1, 80	27.20	0.00
4H-3, 80	30.20	0.00
4H-4, 80	31.70	0.00
4H-5, 80	33.20	0.00
5H-3, 80	40.80	0.00
6H-5, 130	42.80	0.00
6H-6, 50	43.50	0.00
13H-3, 45	115.35	0.77
13H-3, 125	116.15	0.78
13H-4, 45	116.85	1.39
13H-5, 35	118.25	0.27
13H-5, 95	118.85	0.83
13H-6, 35	119.75	0.68
13H-6, 95	120.35	0.22
13H-7, 15	120.75	0.00
13H-7, 45	121.05	0.55
14H-2, 25	123.15	0.36
14H-2, 55	123.45	0.00
14H-2, 85	123.75	1.86
14H-2, 105	123.95	0.00
14H-2, 125	124.15	1.00
14H-3, 15	124.55	1.32
14H-3, 25	124.65	0.56
14H-3, 35	124.75	1.69
14H-3, 45	124.85	1.43
14H-3, 55	124.95	1.00
329-U1371H-		
1H-1, 5	0.05	111.65
1H-1, 10	0.10	77.41
1H-1, 20	0.20	54.52
1H-1, 30	0.30	45.23
1H-1, 40	0.40	35.04
1H-1, 50	0.50	25.94
1H-1, 60	0.60	15.63
1H-1, 70	0.70	7.63
1H-1, 80	0.80	1.33
1H-1, 90	0.90	0.00
1H-1, 100	1.00	0.00
1H-1, 110	1.10	0.00
1H-1, 120	1.20	0.00
1H-1, 130	1.30	0.00
1H-2, 20	1.70	0.00
1H-2, 80	2.30	0.00
1H-2, 105	2.55	0.00
1H-3, 70	3.70	0.00
1H-3, 110	4.10	0.00
1H-4, 40	4.90	0.00
1H-4, 50	5.00	0.00
1H-5, 20	6.20	0.00
1H-5, 25	6.25	0.00

Values reported below 0.4 μM should be considered as below the limit of detection.

Table T10. Redox potential determined using needle electrodes, Site U1371.

Core, section, interval (cm)	Depth (mbsf)	Redox potential (mV)
329-U1371D-		
1H-1, 70	0.70	199
1H-2, 70	2.20	199
1H-3, 70	3.70	173
1H-4, 70	5.20	161
1H-5, 68	6.68	153
2H-1, 70	8.10	8
2H-2, 70	9.60	–20
2H-3, 70	11.10	69
2H-4, 70	12.60	22
2H-5, 70	14.10	–139
3H-1, 70	17.60	–208
3H-2, 70	19.10	–168
3H-3, 70	20.60	–152
3H-4, 70	22.10	–35
3H-5, 70	23.60	–131
3H-6, 70	25.10	–132
3H-7, 30	26.20	–42
4H-1, 30	26.70	–106
4H-1, 70	27.10	–95
4H-1, 125	27.65	–72
4H-2, 70	28.60	–56
4H-3, 70	30.10	–38
4H-4, 70	31.60	–109
4H-5, 70	33.10	12
5H-2, 70	37.70	46
5H-3, 70	39.20	65
5H-4, 70	40.70	–28
5H-5, 70	42.20	–41
6H-1, 25	45.65	–90
6H-1, 75	46.15	–120
6H-1, 125	46.65	–451
6H-2, 25	47.15	–210
6H-2, 75	47.65	–144
6H-2, 125	48.15	–144
6H-3, 25	48.65	–198
6H-3, 75	49.15	–280
6H-3, 125	49.65	–309
6H-4, 25	50.15	–240
6H-4, 75	50.65	–288
6H-4, 125	51.15	–319
6H-5, 25	51.65	–308
6H-5, 75	52.15	–309
6H-5, 125	52.65	–326
7H-1, 75	55.65	–135
7H-2, 75	57.15	–154
7H-3, 75	58.65	–170
7H-4, 75	60.15	–144
7H-5, 75	61.65	–88
7H-6, 75	63.15	10
8H-1, 75	65.15	–132
8H-2, 75	66.65	–115
8H-3, 75	68.15	–96
8H-4, 75	69.65	–168
8H-5, 75	71.15	–184
8H-6, 75	72.65	–280
9H-1, 75	74.65	–39
9H-2, 75	76.15	–90
9H-3, 75	77.65	–148
9H-4, 75	79.15	–44
9H-5, 75	80.65	–138
9H-6, 50	81.90	–60
9H-7, 75	83.15	–134
10H-1, 75	84.15	–143
10H-2, 75	85.65	–275
10H-3, 75	87.15	–343
10H-4, 75	88.65	–554
10H-5, 75	90.15	–446
10H-6, 75	91.65	–550
11H-1, 75	93.65	–195
11H-2, 75	95.15	–193
11H-3, 75	96.65	–202
11H-4, 75	98.15	–511
11H-5, 75	99.66	–539
11H-6, 75	101.16	–500
12H-1, 75	103.15	–128
12H-2, 100	104.90	–85
12H-3, 75	106.15	–19
12H-4, 75	107.43	–14
12H-5, 75	108.93	–18
12H-6, 75	110.43	37
13H-1, 75	112.65	145
13H-2, 75	114.15	138
13H-3, 75	115.65	135
13H-4, 75	117.15	139
13H-5, 75	118.65	177
13H-6, 75	120.15	174
13H-7, 75	121.35	212
14H-1, 75	122.15	194
14H-2, 75	123.65	203
14H-3, 50	124.90	238
14H-4, 75	126.65	237
329-U1371F-		
11H-1, 70	95.40	–144
11H-2, 70	96.90	–244
11H-3, 70	98.40	–264
11H-4, 70	99.90	–198
11H-5, 70	101.40	–79
11H-6, 90	103.10	31
12H-1, 70	104.90	–32
12H-2, 70	106.40	–80
12H-3, 70	107.90	–82
12H-4, 70	109.40	–97
12H-5, 70	110.90	–21
12H-6, 30	112.00	–9
13H-2, 70	114.68	68
13H-3, 70	116.18	29
13H-4, 70	117.68	25
13H-5, 70	119.18	57
13H-6, 70	120.68	116
13H-7, 70	122.18	124
14H-1, 70	123.90	200
14H-2, 70	125.40	129
14H-3, 70	126.90	190
14H-4, 70	128.40	193
14H-5, 70	129.72	134

Table T11. Dissolved hydrogen measured by the headspace gas method, Site U1371.

Core, section	Depth (mbsf)	H_2 (nM)	Catwalk sampling
329-U1371E-			
1H-1	0.30	10.4	No
1H-1	0.80	1.7	No
1H-1	1.40	1.7	Yes
1H-2	1.80	1.5	No
1H-2	2.30	BD	No
1H-2	2.90	BD	Yes
1H-3	3.30	BD	No
1H-3	3.80	1.5	Yes
1H-3	4.30	1.8	Yes
1H-4	5.90	BD	Yes
1H-5	7.40	2.8	Yes
1H-6	8.00	3.1	Yes
2H-1	9.60	BD	Yes
2H-2	11.10	1.9	Yes
2H-3	12.60	2.2	Yes
2H-4	14.10	1.4	Yes
2H-5	15.10	1.8	Yes
3H-2	20.60	BD	Yes
3H-3	22.00	BD	Yes
3H-4	23.60	BD	Yes
3H-5	24.90	BD	Yes
3H-6	25.40	BD	Yes
4H-1	28.60	BD	Yes
4H-2	30.10	BD	Yes
4H-3	31.60	BD	Yes
4H-4	33.10	BD	Yes
4H-5	34.40	BD	Yes
5H-1	38.10	1.4	Yes
5H-2	39.60	1.6	Yes
5H-3	41.10	1.5	Yes
5H-4	42.60	1.4	Yes
5H-5	43.30	1.7	Yes
6H-3	50.60	7.6	Yes
6H-5	53.60	2.5	Yes
7H-1	57.10	BD	Yes
7H-3	60.00	BD	Yes
7H-5	63.10	2.0	Yes
8H-1	66.60	BD	Yes
8H-3	69.60	BD	Yes
8H-5	72.60	BD	Yes
9H-2	76.50	1.4	Yes
9H-4	79.50	BD	Yes
9H-6	82.50	BD	Yes
10H-1	85.60	2.0	Yes
10H-3	88.60	BD	Yes
10H-5	91.60	BD	Yes
11H-1	95.10	BD	Yes
11H-3	98.00	BD	Yes
11H-5	101.10	BD	Yes
12H-2	106.10	BD	Yes
12H-3	107.50	BD	Yes
12H-4	108.80	BD	Yes
13H-1	114.10	BD	Yes
13H-2	115.60	BD	Yes
13H-3	117.00	BD	Yes
13H-4	118.60	BD	Yes
13H-5	120.10	BD	Yes
13H-6	121.60	BD	Yes
13H-7	121.90	BD	Yes
14H-1	123.60	BD	Yes
14H-2	125.10	1.5	Yes
14H-3	125.50	4.3	Yes
14H-3	126.00	1.7	Yes
14H-3	126.50	4.1	Yes
14H-4	127.00	1.6	Yes
14H-4	127.50	1.8	No
14H-4	128.00	5.4	Yes
14H-5	128.50	2.1	Yes
14H-5	129.00	1.4	Yes
14H-5	129.50	2.1	No
14H-6	130.20	BD	Yes

BD = below detection (<1.4 nM).

Table T12. Interstitial fluid chemistry in Rhizon samples, Site U1371.

Core, section, interval (cm)	Depth (mbsf)	NO_3 (μM)	NH_4 (μM)
329-U1371B-			
1H-1, 20–22	0.21	BD	ND
1H-1, 40–42	0.41	BD	ND
329-U1371E-			
1H-1, 10–20	0.15	15.8	0.35
1H-1, 50–60	0.55	2.5	0.16
1H-1, 100–110	1.05	BD	4.05
1H-2, 0–10	1.55	ND	8.56
1H-2, 50–60	2.05	ND	12.52
1H-2, 100–110	2.55	ND	15.24
1H-3, 0–10	3.05	ND	18.29
1H-3, 50–60	3.55	ND	20.67
1H-3, 100–110	4.05	ND	22.78
1H-4, 60–70	5.15	BD	27.18
1H-5, 60–70	6.65	ND	30.72
2H-1, 70–80	8.95	ND	34.77
2H-2, 60–70	10.35	ND	30.06
2H-3, 60–70	11.85	ND	34.39
2H-4, 60–70	13.35	BD	35.10
2H-5, 60–70	14.85	ND	38.59
3H-2, 60–70	19.85	ND	44.10
3H-3, 60–70	21.35	BD	41.00
3H-4, 60–70	22.85	ND	44.17
3H-5, 60–70	24.35	ND	44.27
3H-6, 20–30	25.25	BD	48.54
4H-1, 60–70	27.85	ND	60.24
4H-2, 60–70	29.35	ND	48.06
4H-3, 60–70	30.85	BD	55.87
4H-4, 60–70	32.35	ND	50.83
4H-5, 60–70	33.85	ND	46.59
4H-6, 20–30	34.75	ND	51.85
5H-1, 60–70	37.35	ND	51.26
5H-3, 60–70	40.35	BD	51.05
5H-5, 0–10	42.75	ND	53.35
6H-4, 60–70	51.35	BD	51.81
7H-1, 60–70	56.35	ND	59.18
7H-3, 60–70	59.35	ND	55.64
7H-5, 60–70	62.35	BD	55.53
8H-1, 100–110	66.25	BD	58.33
8H-3, 60–70	68.85	ND	46.27
8H-5, 60–70	71.85	ND	47.73
9H-2, 60–70	75.75	BD	47.51
9H-4, 60–70	78.75	ND	47.56
9H-6, 60–70	81.75	BD	44.15
10H-1, 60–70	84.85	ND	49.07
10H-3, 70–80	87.95	ND	40.21
10H-5, 60–70	90.85	BD	43.99
11H-1, 110–120	94.85	ND	44.01
11H-3, 60–70	97.35	ND	40.97
11H-6, 60–70	101.85	BD	ND
12H-2, 80–90	105.55	1.7	ND
12H-3, 70–80	106.95	3.2	ND
12H-4, 60–70	108.35	5.0	ND
13H-3, 60–70	116.35	2.0	ND
14H-1, 60–70	122.85	2.9	ND
329-U1371H-			
1H-1, 18–28	0.23	41.0	ND
1H-1, 31–41	0.36	36.9	ND
1H-1, 48–58	0.53	34.8	ND
1H-1, 61–71	0.66	33.5	ND
1H-1, 78–88	0.83	29.1	ND
1H-1, 108–118	1.13	22.8	ND
1H-1, 128–138	1.33	17.4	ND
1H-2, 8–18	1.63	11.7	ND
1H-2, 28–38	1.83	8.8	ND
1H-2, 48–58	2.03	6.7	ND
1H-2, 68–78	2.23	4.1	ND
1H-2, 98–108	2.53	2.1	ND
1H-2, 128–138	2.83	BD	ND
1H-3, 13–23	3.18	BD	ND
1H-3, 43–53	3.48	BD	ND
1H-3, 68–78	3.73	BD	ND
1H-3, 128–138	4.33	BD	ND
1H-4, 8–18	4.63	BD	ND
1H-4, 33–43	4.88	BD	ND
1H-4, 63–73	5.18	BD	ND
1H-4, 93–103	5.48	4.4	ND
1H-5, 23–33	5.78	BD	ND

BD = below detection, ND = not determined.

Table T13. Interstitial fluid chemistry, Site U1371. (Continued on next page.)

Core, section, interval (cm)	Depth (mbsf)	pH ISE	Alkalinity (mM) TITRAUTO	DIC (mM) OI-IC	Cl (mM) M-IC	SO_4 (mM) M-IC	SO_4 (%) Calc. anom.	P (µM) Spec.	Si (µM) Spec.	Ca (mM) Dx-IC	Mg (mM) Dx-IC	Na (mM) Dx-IC	K (mM) Dx-IC	Ca (mM) ICPAES	Mg (mM) ICPAES	Na (mM) ICPAES	K (mM) ICPAES	Fe (µM) ICPAES	Mn (µM) ICPAES	Catwalk sampling
329-U1371E-																				
1H-1, 0–10	0.05	7.79	3.014	2.894	554.72	28.52	–0.47	9.93	533	10.8	52.4	483.8	12.3	10.3	51.2	465	11.7	9.5	67.7	Yes
1H-1, 40–50	0.45	7.88	3.065	2.964	554.81	28.45	–0.72	13.55	542	10.8	52.6	483.3	12.1	10.6	52.0	470	11.8	8.9	285	No
1H-1, 90–100	0.95	7.90	3.158	3.076	555.93	28.52	–0.67	18.32	530	—	—	—	—	10.6	51.7	471	11.7	9.6	341	No
1H-1, 140–150	1.45	7.79	3.232	3.099	556.04	28.54	–0.63	22.64	602	11.0	53.3	489.0	12.0	10.6	51.8	466	11.6	10.2	352	Yes
1H-2, 40–50	1.95	7.90	3.161	3.041	556.18	28.51	–0.75	21.45	572	10.9	53.1	485.6	11.9	10.5	51.4	467	11.4	9.7	323	No
1H-2, 90–100	2.45	7.89	3.168	3.051	557.16	28.58	–0.70	22.11	536	—	—	—	—	10.4	51.2	465	11.3	9.5	307	No
1H-2, 140–150	2.95	7.78	3.164	3.064	556.59	28.51	–0.83	22.34	598	11.4	56.0	474.1	9.2	10.7	51.4	475	11.7	9.4	179	Yes
1H-3, 40–50	3.45	7.89	3.215	3.023	557.15	28.60	–0.62	25.97	568	—	—	—	—	10.8	52.1	475	11.5	7.5	239	No
1H-3, 90–100	3.95	7.86	3.215	3.096	557.80	28.62	–0.68	27.17	597	11.5	57.1	468.7	8.7	10.6	51.5	468	11.7	8.2	305	No
1H-3, 140–150	4.45	7.80	3.137	3.044	559.71	28.74	–0.58	24.37	583	—	—	—	—	10.7	51.7	472	11.4	8.0	328	Yes
1H-4, 140–150	5.95	7.77	3.102	3.072	558.63	28.57	–1.00	24.44	674	10.8	52.5	483.1	12.1	10.7	51.7	479	12.2	9.7	349	Yes
1H-5, 140–150	7.45	7.78	3.043	2.994	558.70	28.62	–0.83	26.94	674	11.0	52.9	485.3	12.1	10.8	52.0	478	12.1	9.5	340	Yes
2H-1, 140–150	9.65	7.75	3.006	2.950	559.42	28.65	–0.83	26.76	667	10.8	52.2	481.6	12.0	10.5	51.4	469	11.6	10.1	281	Yes
2H-2, 140–150	11.15	7.73	2.993	2.942	559.48	28.57	–1.13	26.56	703	10.8	52.8	485.2	12.1	10.6	51.7	470	12.0	9.3	288	Yes
2H-3, 140–150	12.65	7.82	3.053	3.012	559.98	28.61	–1.10	26.84	668	—	—	—	—	10.6	51.2	466	11.9	8.8	277	Yes
2H-4, 140–150	14.15	7.83	3.031	2.950	560.43	28.57	–1.32	21.52	746	10.7	52.2	481.9	12.1	10.7	51.7	475	12.3	8.4	289	Yes
2H-5, 95–105	15.20	7.74	2.979	2.935	560.03	28.60	–1.14	25.99	759	10.9	52.5	486.5	12.3	10.8	51.9	471	11.8	9.1	271	Yes
3H-1, 140–150	19.15	7.74	3.008	2.879	563.58	28.46	–2.23	18.15	724	—	—	—	—	10.6	50.9	471	11.9	17.5	201	Yes
3H-2, 140–150	20.65	—	—	ND	—	—	—	—	—	11.0	52.9	488.3	12.4	—	—	—	—	—	—	Yes
3H-3, 140–150	22.15	7.89	3.094	2.927	563.39	28.45	–2.23	18.95	750	10.9	52.6	491.9	12.7	—	—	—	—	—	—	Yes
3H-4, 140–150	23.65	7.85	2.982	2.946	563.69	28.39	–2.51	21.73	691	11.0	53.2	489.1	12.3	10.9	51.4	483	11.8	12.6	219	Yes
3H-5, 120–130	24.95	7.87	3.001	2.876	563.97	28.46	–2.30	19.67	672	11.0	52.3	489.3	12.6	—	—	—	—	—	—	Yes
4H-1, 140–150	28.65	7.76	2.792	2.790	563.61	28.24	–3.00	19.19	725	—	—	—	—	10.9	52.1	481	11.5	10.5	237	Yes
4H-2, 140–150	30.15	7.76	2.816	2.799	564.74	28.26	–3.11	17.74	661	11.0	52.3	488.8	12.7	—	—	—	—	—	—	Yes
4H-3, 140–150	31.65	7.77	2.720	2.744	563.55	28.20	–3.11	17.65	698	11.0	52.5	489.6	12.1	—	—	—	—	—	—	Yes
4H-4, 140–150	33.15	7.74	2.727	2.790	565.60	28.26	–3.27	14.6	719	11.0	52.5	491.4	12.1	10.8	51.5	478	11.5	11.0	234	Yes
4H-5, 120–130	34.45	7.69	2.745	2.734	565.16	28.23	–3.28	14.12	682	—	—	—	—	—	—	—	—	—	—	Yes
5H-1, 140–150	38.15	7.71	2.688	2.753	—	—	–3.43	14.03	734	11.0	52.3	489.2	11.8	11.1	52.1	480	11.6	9.8	235	Yes
5H-3, 140–150	41.15	7.72	2.662	2.673	565.09	28.06	–3.85	13.45	719	—	—	—	—	—	—	—	—	—	—	Yes
5H-4, 140–150	42.65	7.75	2.701	2.684	565.63	28.11	–3.80	11.66	771	11.0	52.7	490.9	11.9	11.0	52.1	481	11.5	10.0	220	Yes
6H-2, 140–150	49.15	7.77	2.635	2.601	—	—	–3.77	12.33	741	11.2	53.3	494.1	11.8	10.9	51.6	486	11.6	16.1	210	Yes
6H-3, 140–150	50.65	6.86	2.620	2.544	562.40	27.96	–3.74	9.86	734	—	52.3	487.3	11.8	—	—	—	—	—	—	Yes
6H-5, 140–150	53.65	7.90	2.743	2.604	564.89	27.90	–4.40	8.55	725	11.1	52.7	489.9	11.8	—	—	—	—	—	—	Yes
7H-1, 140–150	57.15	7.88	2.660	2.566	574.18	28.26	–4.71	7.33	712	—	53.1	494.5	11.9	10.9	51.2	473	11.0	13.2	175	Yes
7H-3, 140–150	60.15	7.78	2.568	2.555	564.13	27.72	–4.87	7.4	756	—	—	—	—	—	—	—	—	—	—	Yes
7H-5, 140–150	63.15	7.72	2.515	2.569	564.53	27.75	–4.84	7.37	781	11.1	52.6	490.7	12.0	11.1	51.7	476	11.4	8.7	204	Yes
8H-1, 140–150	66.65	7.76	2.530	2.559	565.15	27.68	–5.18	7.37	—	11.2	52.3	489.2	12.2	—	—	—	—	—	—	Yes
8H-3, 140–150	69.65	7.71	2.467	2.553	564.80	29.17	—	7.02	769	11.3	52.5	489.4	11.5	11.2	51.8	472	10.9	11.9	210	Yes
8H-5, 140–150	72.65	7.72	2.463	2.511	564.14	27.64	–5.15	6.11	782	11.4	53.0	492.0	11.6	—	—	—	—	—	—	Yes
9H-2, 140–150	76.55	7.70	2.446	2.572	564.34	27.58	–5.37	5.71	753	11.3	52.2	488.6	11.3	11.2	51.9	475	10.6	12.4	213	Yes
9H-4, 140–150	79.55	7.67	2.375	2.528	564.40	27.59	–5.36	4.4	820	11.4	52.6	489.6	11.4	—	—	—	—	—	—	Yes
9H-6, 140–150	82.55	7.67	2.360	2.474	568.11	27.68	–5.66	5.35	811	11.5	53.1	491.0	11.1	11.2	51.7	476	10.8	10.7	209	Yes
10H-1, 140–150	85.65	7.74	2.368	2.448	564.88	27.59	–5.43	4.34	789	—	—	—	—	—	—	—	—	—	—	Yes
10H-3, 140–150	88.65	7.77	2.387	2.401	562.32	27.47	–5.43	3.41	852	11.5	53.0	490.1	11.0	11.2	51.6	477	10.9	14.8	187	Yes
10H-5, 140–150	91.65	7.75	2.381	2.444	564.15	27.48	–5.70	3.17	823	11.5	52.7	487.2	10.8							Yes
11H-1, 140–150	95.15	7.71	2.335	2.411	564.93	27.51	–5.72	3.12	844	11.5	52.9	489.9	11.2	11.3	52.1	478	10.4	14.2	197	Yes
11H-3, 140–150	98.15	7.69	2.323	2.424	566.49	27.53	–5.92	2.42	826	—	—	—	—	—	—	—	—	—	—	Yes
11H-5, 140–150	101.15	7.67	2.286	2.344	565.40	27.48	–5.90	2.67	816	11.4	52.6	488.3	11.3	11.2	51.8	473	10.5	11.5	196	Yes

Table T13 (continued).

Core, section, interval (cm)	Depth (mbsf)	pH ISE	Alkalinity (mM) TITRAUTO	DIC (mM) OI-IC	Cl (mM) M-IC	SO_4 (mM) M-IC	SO_4 (%) Calc. anom.	P (µM) Spec.	Si (µM) Spec.	Ca (mM) Dx-IC	Mg (mM) Dx-IC	Na (mM) Dx-IC	K (mM) Dx-IC	Ca (mM) ICPAES	Mg (mM) ICPAES	Na (mM) ICPAES	K (mM) ICPAES	Fe (µM) ICPAES	Mn (µM) ICPAES	Catwalk sampling
12H-2, 140–150	106.15	7.68	2.215	2.282	561.11	26.87	–7.30	1.96	709	11.5	53.2	489.4	10.9	—	—	—	—	—	—	Yes
12H-3, 140–150	107.65	7.66	2.244	2.296	561.30	26.97	–6.99	2.46	672	11.6	53.2	489.7	10.8	—	—	—	—	—	—	Yes
12H-4, 113–123	108.88	7.65	2.204	2.286	559.91	26.52	–8.29	2.17		11.7	53.3	491.4	10.8	11.2	52.7	470	9.5	10.0	183	Yes
13H-1, 140–150	114.15	7.69	2.161	2.193	—	—	—	—	—	11.4	52.9	489.4	10.9	—	—	—	—	—	—	Yes
13H-2, 140–150	115.65	7.66	2.174	2.217	—	—	—	—	—	—	—	—	—	11.3	53.9	465	8.5	9.0	163	Yes
13H-3, 140–150	117.15	7.70	2.219	ND	—	—	—	—	—	11.5	54.0	485.5	9.6	—	—	—	—	—	—	Yes
13H-4, 140–150	118.65	8.08	2.174	2.221	558.78	26.70	–7.51	—	—	—	—	—	—	—	—	—	—	—	—	Yes
13H-5, 140–150	120.15	8.08	2.201	2.254	—	—	–8.02	—	—	—	—	—	—	11.4	54.5	472	9.0	9.5	129	Yes
13H-6, 140–150	121.65	8.07	2.202	2.243	558.03	26.56	–7.86	—	—	—	—	—	—	—	—	—	—	—	—	Yes
13H-7, 29–39	122.04	7.70	2.245	2.282	557.66	26.57	–7.77	1.52	441	—	—	—	—	11.2	53.7	463	8.6	9.8	114	Yes
14H-1, 140–150	123.65	7.69	2.206	2.239	559.80	26.64	–7.88	1.25	413	—	—	—	—	—	—	—	—	—	—	Yes
14H-2, 140–150	125.15	—	—	ND	561.57	26.76	–7.73	—	—	—	—	—	—	11.4	54.4	470	9.1	8.8	87.0	Yes
14H-3, 40–50	125.65	7.75	2.214	2.226	554.49	26.32	–8.12	1.71	424	—	—	—	—	—	—	—	—	—	—	No
14H-3, 90–100	126.15	7.68	2.152	2.211	—	—	—	—	—	11.6	55.5	479.7	9.0	—	—	—	—	—	—	No
14H-3, 130–150	126.60	7.71	2.134	2.162	—	—	—	1.63	372	11.3	53.6	482.4	9.3	11.2	55.3	459	8.3	8.5	72.3	Yes
14H-4, 40–50	127.15	—	—	ND	552.80	26.08	–8.66	1.22	360	—	—	—	—	—	—	—	—	—	—	No
14H-4, 90–100	127.65	—	—	ND	—	—	—	1.64	370	11.4	—	—	—	11.2	55.5	451	8.5	8.9	70.1	No
14H-4, 130–150	128.10	7.67	2.032	2.081	—	—	—	1.53	383	11.6	57.6	471.1	8.7	—	—	—	—	—	—	Yes
14H-6, 56–66	130.31	7.68	2.054	2.100	—	—	—	—	—	—	—	—	—	—	—	—	—	—	—	Yes

ISE = ion-selective electrode, TITRAUTO = automated titration, IC = ion chromatography, OI-IC = OI analytical IC, M-IC = Metrohm IC, Calc. anom. = calculated anomaly, Spec. = spectrophotometry, ICPAES = inductively coupled plasma–atomic emission spectroscopy. — = no data.

Table T14. Solid-phase carbon and nitrogen, Site U1371.

Core, section, interval (cm)	Depth (mbsf)	TC (wt%)	TN (wt%)	TOC (wt%)	TIC (wt%)	$CaCO_3$ (wt%)
329-U1371E-						
1H-1, 0–2	0.01	0.25	0.047	0.22	0.01	0.06
1H-1, 8–10	0.09	0.22	0.049	0.20	BD	0.03
1H-1, 40–42	0.41	0.18	0.042	0.15	BD	0.03
1H-1, 48–50	0.49	0.18	0.042	0.16	0.01	0.06
1H-1, 90–92	0.91	0.13	0.035	0.13	0.01	0.04
1H-1, 98–100	0.99	0.13	0.033	0.12	BD	0.02
1H-1, 140–142	1.41	0.18	0.041	0.16	BD	0.01
1H-1, 148–150	1.49	0.18	0.042	0.16	BD	0.01
1H-2, 40–50	1.95	0.15	0.036	0.14	BD	0.01
1H-2, 90–100	2.45	0.14	0.036	0.13	BD	0.02
1H-2, 140–150	2.95	0.12	0.030	0.12	0.01	0.08
1H-3, 90–100	3.95	0.16	0.040	0.16	BD	0.02
1H-3, 140–150	4.45	0.18	0.041	0.16	BD	0.01
1H-5, 140–150	7.45	0.15	0.036	0.13	BD	0.02
2H-1, 140–150	9.65	0.14	0.039	0.13	BD	0.01
2H-3, 140–150	12.65	0.20	0.038	0.19	0.01	0.05
2H-5, 95–105	15.20	0.12	0.035	0.12	BD	0.00
3H-2, 140–150	20.65	0.13	0.036	0.12	0.01	0.06
3H-4, 140–150	23.65	0.10	0.025	0.10	BD	0.01
4H-1, 140–150	28.65	0.12	0.030	0.10	0.01	0.11
4H-4, 140–150	33.15	0.13	0.031	0.10	0.03	0.27
5H-1, 140–150	38.15	0.09	0.025	0.08	0.01	0.06
5H-4, 140–150	42.65	0.10	0.033	0.09	BD	0.02
6H-2, 140–150	49.15	0.21	0.032	0.12	0.09	0.78
6H-5, 140–150	53.65	0.17	0.032	0.12	0.04	0.35
7H-3, 140–150	60.15	0.15	0.039	0.12	0.02	0.21
8H-1, 140–150	66.65	0.10	0.027	0.09	BD	0.01
8H-5, 140–150	72.65	0.10	0.024	0.08	0.01	0.12
9H-2, 140–150	76.55	0.08	0.024	0.07	0.01	0.07
9H-4, 140–150	79.55	0.07	0.019	0.06	BD	0.02
10H-1, 140–150	85.65	0.09	0.024	0.08	BD	0.02
10H-5, 140–150	91.65	0.13	0.024	0.08	0.06	0.52
11H-1, 140–150	95.15	0.08	0.021	0.07	BD	0.03
11H-5, 140–150	101.15	0.04	0.018	0.05	BD	0.02
12H-2, 140–150	106.15	0.05	0.025	0.05	BD	0.03
12H-4, 113–123	108.88	0.03	0.018	0.03	BD	0.04
13H-1, 140–150	114.15	0.03	0.018	0.03	BD	0.04
13H-4, 140–150	118.65	0.03	0.017	0.03	0.01	0.05
13H-7, 29–39	122.04	0.03	0.013	0.02	0.01	0.10
14H-3, 130–150	126.60	0.03	0.006	0.01	0.01	0.12
14H-4, 130–150	128.10	0.03	0.005	0.01	0.03	0.25

TC = total carbon, TN = total nitrogen, TOC = total organic carbon, TIC = total inorganic carbon. BD = below detection.

Table T15. Cell counts by manual microscopy in sediment, Site U1371.

Core, section, interval (cm)	Depth (mbsf)	Cell count (log_{10} cells/cm^3) extracted			
		Count 1	Count 2	Count 3	Count 4
329-U1371E-					
1H-1, 30–40	0.30	5.6	6.2	5.7	5.8
1H-1, 80–90	0.80	5.7	5.5		
1H-1, 135–140	1.35	5.6	5.5	5.3	5.1
1H-2, 30–40	1.80	4.5	4.4		
1H-2, 80–90	2.30	4.8	4.6		
1H-2, 125–130	2.85	4.4	4.5		
1H-3, 30–40	3.30	4.4			
1H-3, 125–130	4.25				
1H-4, 135–140	5.85				
1H-5, 135–140	7.35				
1H-6, 52–57	8.02				
2H-1, 135–140	9.55	4.6	4.5		
2H-2, 135–140	11.05				
2H-3, 135–140	12.55				
2H-4, 135–140	14.05				
2H-5, 90–95	15.10				
3H-2, 135–140	20.55	4.4	4.4		
3H-3, 125–130	21.95				
3H-4, 135–140	23.55				
3H-5, 115–120	24.85				
3H-6, 41–46	25.41				
4H-1, 135–140	28.55	3.9	3.7		
4H-2, 135–140	30.05				
4H-3, 135–140	31.55				
4H-4, 135–140	33.05				
4H-5, 115–120	34.35				
5H-1, 135–140	38.05	2.9	2.1		
5H-2, 135–140	39.55				
5H-3, 135–140	41.05				
5H-4, 135–140	42.55				
5H-5, 60–65	43.30				
6H-3, 135–140	50.55	3.2			
6H-5, 135–140	53.55				
7H-1, 135–140	57.05				
7H-2, 135–140	58.55				
7H-3, 125–130	59.95				
7H-5, 135–140	63.05				
8H-1, 135–140	66.55	BD	2.2		
8H-3, 135–140	69.55				
8H-5, 135–140	72.55				
9H-2, 135–140	76.45	BD	0.5		
9H-2, 135–140	76.45	0.5			
9H-4, 135–140	79.45				
9H-6, 135–140	82.45				
10H-1, 135–140	85.55	BD	1.8		
10H-3, 135–140	88.55				
10H-5, 135–140	91.55				
11H-1, 135–140	95.05	3.0	2.9		
11H-3, 125–130	97.95				
11H-5, 135–140	101.05				
12H-2, 135–140	106.05	BD	BD		
12H-3, 125–130	107.45				
12H-4, 108–118	108.78				
13H-1, 135–140	114.05	BD	2.2		
13H-2, 135–140	115.55				
13H-3, 125–130	116.95				
13H-4, 135–140	118.55				
13H-5, 135–140	120.05				
13H-6, 135–140	121.55				
13H-7, 24–29	121.94				
14H-1, 135–140	123.55				
14H-2, 135–140	125.05				
14H-3, 30–40	125.50				
14H-3, 80–90	126.00				
14H-3, 125–130	126.45				
14H-4, 30–40	127.00				
14H-4, 80–90	127.50				
14H-4, 125–130	127.95				
14H-5, 30–40	128.50				
14H-5, 80–90	129.00				
14H-5, 125–130	129.45				
14H-6, 51–56	130.21				

BD = below detection. Blank cells = no count (will be counted postexpedition).

Table T16. Samples to be analyzed postexpedition for virus-like particle counts, Site U1371.

Core, section, interval (cm)	Depth (mbsf)
329-U1371E-	
1H-1, 30–40	0.30
1H-1, 80–90	0.80
1H-1, 135–140	1.35
1H-2, 70–80	2.20
1H-2, 70–80	2.20
1H-3, 30–40	3.30
1H-3, 80–90	3.80
1H-3, 125–130	4.25
1H-4, 135–140	5.85
1H-5, 135–140	7.35
1H-6, 52–57	8.02
2H-1, 135–140	9.55
2H-2, 135–140	11.05
2H-3, 135–140	12.55
2H-4, 135–140	14.05
2H-5, 90–95	15.10
3H-2, 135–140	20.55
3H-3, 125–130	21.95
3H-4, 135–140	23.55
3H-5, 115–120	24.85
3H-6, 41–46	25.41
4H-1, 135–140	28.55
4H-2, 135–140	30.05
4H-3, 135–140	31.55
4H-4, 135–140	33.05
4H-5, 115–120	34.35
5H-1, 135–140	38.05
5H-2, 135–140	39.55
5H-3, 135–140	41.05
5H-4, 135–140	42.55
5H-5, 60–65	43.30
6H-3, 135–140	50.55
6H-5, 135–140	53.55
7H-1, 135–140	57.05
7H-2, 135–140	58.55
7H-3, 125–130	59.95
7H-5, 135–140	63.05
8H-1, 135–140	66.55
8H-3, 135–140	69.55
8H-5, 135–140	72.55
9H-2, 135–140	76.45
9H-4, 135–140	79.45
9H-6, 135–140	82.45
10H-1, 135–140	85.55
10H-3, 135–140	88.55
10H-5, 135–140	91.55
11H-1, 135–140	95.05
11H-3, 125–130	97.95
11H-5, 135–140	101.05
12H-2, 135–140	106.05
12H-3, 125–130	107.45
12H-4, 108–113	108.78
13H-1, 135–140	114.05
13H-2, 135–140	115.55
13H-3, 125–130	116.95
13H-4, 135–140	118.55
13H-5, 135–140	120.05
13H-6, 135–140	121.55
13H-7, 24–29	121.94
14H-1, 135–140	123.55
14H-2, 135–140	125.05
14H-3, 30–40	125.50
14H-3, 80–90	126.00
14H-3, 125–130	126.45
14H-4, 30–40	127.00
14H-4, 80–90	127.50
14H-4, 125–130	127.95
14H-5, 30–40	128.50
14H-5, 80–90	129.00
14H-5, 125–130	129.45
14H-6, 51–56	130.21
329-U1371F-	
1H-1, 130–140	1.30
1H-2, 120–130	2.70
1H-4, 50–60	5.00
2H-2, 100–110	11.70
2H-4, 30–40	14.00
1H-1, 110–120	1.10
1H-3, 70–80	3.70
1H-5, 40–50	6.40
2H-2, 90–100	11.60

Table T17. List of samples and culture media used for onboard cultivation experiments, Site U1371.

Core, section	Media used for cultivation
329-U1371E-	
1H-1	Mmm1, Mmm2, SPG-ASW, SPG-JL, SLURRY
1H-2	SPG-JL, SLURRY
1H-3	Mmm1, Mmm2, SPG-ASW, SPG-JL, SLURRY
1H-4	SLURRY
1H-5	Mmm1, Mmm2, SPG-ASW, SLURRY
2H-2	Mmm1, SPG-ASW, SLURRY
2H-4	SLURRY
3H-2	SLURRY
3H-3	SPG-JL
3H-5	SLURRY
4H-5	SLURRY
5H-2	Mmm1, SPG-ASW
5H-3	SPG-JL
5H-4	SLURRY
5H-5	SLURRY
7H-2	SPG-JL
7H-5	SLURRY
8H-3	Mmm1, SPG-ASW
9H-3	SPG-JL
9H-6	SLURRY
11H-2	Mmm1, SPG-ASW, SPG-JL
12H-3	SLURRY
13H-3	SLURRY
329-U1371F-	
14H-1	SLURRY
14H-2	Mmm1, Mmm2, SPG-ASW
14H-3	SPG-JL
14H-3	SPG-JL
14H-4	SPG-JL, SLURRY

SLURRY = sediment stored anoxically in flushed serum bottles or in syringes kept in sterile foil bags. For more detailed information on the media, see **"Microbiology"** in the "Methods" chapter (Expedition 329 Scientists, 2011a).